ENGINEERING MODEL 8–CM THRUSTER SUBSYSTEM

B.G. Herron, J. Hyman, D.J. Hopper, W.S. Williamson, C.R. Dulgeroff, and C.R. Collett

Hughes Research Laboratories

3011 Malibu Canyon Road

Malibu, CA 90265

June 1978

NAS 3–18917

Final Report

20 June 1974 through 20 November 1976

Prepared for

NATIONAL AERONAUTICS AND SPACE ADMINISTRATION

Lewis Research Center

Cleveland, Ohio

TECHNICAL REPORT STANDARD TITLE PAGE

1. Report No.	2. Government Accession No.	3. Recipient's Catalog No
CR 135406		

4. Title and Subtitle
ENGINEERING MODEL 8-CM THRUSTER SUBSYSTEM

5. Report Date
June 1978

6. Performing Organization Code

7 Author(s) B.G. Herron, J. Hyman, D.J. Hopper, W.S. Williamson, C.R. Dulgeroff, and C.R. Collett

8. Performing Organization Report No.

9. Performing Organization Name and Address
Hughes Research Laboratories
3011 Malibu Canyon Road
Malibu, CA 93065

10. Work Unit No.

11. Contract or Grant No
NAS 3-18917

12. Sponsoring Agency Name and Address
NASA Lewis
Lewis Research Center
Cleveland, Ohio

13 Type of Report and Period Covered
Final Report
20 June 1974 - 20 November 1976

14 Sponsoring Agency Code

15. Supplementary Notes

16. Abstract

An Engineering Model (EM) 8-cm Ion Thruster Propulsion Subsystem has been developed for operation at a thrust level 5 mN (1.1 mlb) at a specific impulse I_{sp} = 2667 sec with a total system input power P_{in} = 165 W. The system dry mass is 15 kg with a mercury-propellant-reservoir capacity of 8.75 kg permitting uninterrupted operation for about 12,500 hr. The subsystem can be started from a dormant condition in a time less than or equal to 15 min. The thruster has a design lifetime of 20,000 hr with 10,000 startup cycles. A gimbal unit is included to provide a thrust vector deflection capability of ±10 degrees in any direction from the zero position. The EM subsystem development program included thruster optimization, power-supply circuit optimization and flight packaging, subsystem integration, and subsystem acceptance testing including a cyclic test of the total propulsion package.

17 Key Words (Selected by Author(s))	18 Distribution Statement
Space Auxiliary Propulsion Ion Propulsion Subsystem Electric Rocket SIT-8 EM 8-cm Ion Thruster Propulsion Subsystem	

19. Security Classif. (of this report)	20. Security Classif (of this page)	21. No of Pages	22 Price*
UNCLASSIFIED	UNCLASSIFIED	142	

*For sale by the Clearinghouse for Federal Scientific and Technical Information, Springfield, Virginia 22151.

TABLE OF CONTENTS

LIST OF ILLUSTRATIONS

SUMMARY

In June 1974, the Hughes Aircraft Company began a program to develop an Engineering Model (EM) 8-cm Ion Propulsion Subsystem for operation at a thrust level of 5 mN (1.1 mlb). The now-completed subsystem operates at a specific impulse I_{sp} = 2667 sec with a total system input power P_{in} = 165 W. The system dry mass is 15 kg with a mercury-propellant-reservoir capacity of 8.75 kg, permitting an uninterrupted operation of about 12,500 hr. The system can be started from a dormant condition in a time ≤15 min. The thruster has a design lifetime of 20,000 hr with 10,000 startup cycles. A gimbal unit is included to provide a trust vector deflection capability of ±10 deg in any azimuthal direction from the zero position. The EM subsystem development program included thruster optimization, power-supply circuit optimization and flight packaging, system integration, and system acceptance testing including a cyclic test of the total propulsion package.

The EM 8-cm Ion Thruster includes all elements necessary to generate 5 mN of reactive thrust when provided with liquid mercury from the propellant reservoir and appropriately conditioned electric power from the Power-Processor Unit. Critical subassemblies such as the Cathode-Isolator-Vaporizer (CIV) and Neutralizer-Isolator-Vaporizer (NIV) are little changed from the original designs developed earlier under the SIT-5 and SIT-8 ion thruster development programs. As compared with the SIT-8 prototype configuration, the EM Thruster differs mainly in structural design features and in the special treatment of discharge-chamber interior surfaces to minimize the effects of ion-bombardment erosion (sputtering) of discharge-chamber surfaces. Techniques have been developed to coat most of the cathode-potential surfaces with a plasma-sprayed layer of tantalum to reduce the sputter yield below the value anticipated for surfaces composed of iron or stainless steel. Under the present program, an extensive discharge-chamber optimization has retained performance gains demonstrated with the SIT-8 thruster by the use of ion-machined accel grids, while achieving a high level of discharge stability through small but important changes in critical discharge-chamber dimensions.

Power-supply and electronic-control development of the EM propulsion package derive also from an earlier contractual program (between HRL and NASA LeRC) to design, fabricate, and test a thermal vacuum breadboard (TVBB) power-processing unit capable of providing sustained operation of the SIT-8 thruster at a maximum thrust level of 9 mN (2 mlb) and a nominal thrust of 4.5 mN (1 mlb). The major thrust of the EM power-processor development has been to optimize system circuitry for operation at the 5 mN (1.1 mlb) thrust level (eliminating the 9 mN capability), and to package the electronic subsystem in a configuration suitable for space-flight operation. An outstanding feature of the EM power-processor flight packaging is the separation of power and control circuits into separate physical enclosures. This feature addresses the need for flexibility in the design of the control section to meet the functional and interface requirements of a particular spacecraft.

After completion of all thruster optimization, a new EM 8-cm thruster module (S/N 901) was fabricated and assembled for acceptance tests. Before testing, the thruster was characterized by measurements of the discharge-chamber magnetic field including generation of an iron-filing map. Both vaporizers were calibrated for flowrate as a function of vaporizer temperature. Thruster performance was characterized both for operation at a difference between anode and keeper voltages of 29 V and at a discharge voltage (V_D) of 40 V. Electron back-streaming from the ion beam was shown to occur for an accelerator voltage (V_A) less than 100 V whereas the nominal value is $V_A = -300$ V. Neutralizer-coupling characteristics were found to be satisfactory. An ExB-type ion-velocity analyzer was employed to characterize the ion beam at the two setpoints. The doubly charged ion fraction was 5% and 10% for operation at the two setpoints ($V_D - V_{DK}$) = 29 V and V_D = 40 V, respectively. The thruster showed remarkable stability for operation over a wide range of parametric variation about the nominal setpoints.

Subsystem integration began with interconnecting the thruster with the propellant reservoir and then filling the reservoir and integration testing of the EM thruster, gimbal, and propellant reservoir with the PPU. Finally, a 10-cycle thermal-vacuum test of the entire subsystem was completed. After correcting one system control-loop problem, thruster operation was stable and repeatable over a discharge range of $33 \text{ V} \leq V_D \leq 42 \text{ V}$. System convergence to within this commanded range from outside operating points was also investigated and found to occur smoothly. The performance of the EM 8-cm system during the thermal-vacuum cyclic test was very good. The only deviation from predicted performance was that a telemetry transductor failed twice. Post-test analysis identified the failure mode, and, subsequently, voltage suppression circuitry was incorporated in the PEU. After the system cyclic test was completed, it was discovered that, because of a mechanical mismatch between the pressurant chamber valve (of the propellant reservoir) and the filling system valve, some of the pressurant gas (80% nitrogen, 20% krypton) had leaked out, decreasing the total charge from 241 kPa (35 psia) to 103 kPa (15 psia). This error had no effect on subsequent tests, and the mismatch has since been corrected.

SECTION 1

INTRODUCTION

In June 1974, the Hughes Aircraft Company began a program, under contract to the NASA Lewis Research Center (NASA LeRC) to develop (with existing technology) an Engineering Model (EM) 8-cm Ion Thruster Propulsion Subsystem for operation at a thrust level of 5 mN (1.1 mlb). Specifications for the subsystem development were defined by Banks[1] to accommodate the requirements for north-south stationkeeping of geosynchronous spacecraft. In addition, a gimbal system was included to allow east-west stationkeeping, momentum-wheel dumping, and/or attitude control to be performed when the spacecraft is suitably configured. The north-south stationkeeping velocity requirement greatly exceeds the other requirements and represents the most probable use of the EM 8-cm thruster subsystem.

The successful development of this propulsion subsystem represents the culmination of 17 years of continuing research and development, which began in 1960 with invention of the electron-bombardment mercury-ion thruster by H.R. Kaufman[2] at NASA LeRC. The present EM 8-cm Ion Propulsion Subsystem includes all of the elements of a self-contained propulsion package, requiring for successful operation only electric power from the spacecraft bus and thrust-on commands from the spacecraft computer. The EM 8-cm Thruster Subsystem represents the first integration of a complete mercury ion-propulsion flight package in which the design is fully engineered for spacecraft-control applications.

As compared with the SIT-8 (8-cm Structurally Integrated Thruster) prototype configuration[3] (developed earlier at Hughes Research Laboratories (HRL)), the EM thruster differs mainly in structural design features and in the special treatment of the discharge-chamber interior surfaces to minimize the effects of ion-bombardment erosion (sputtering) of discharge-chamber surfaces. Techniques have been developed to coat most of the cathode-potential surfaces with a plasma-sprayed layer of tantalum to reduce the sputter yield below the value anticipated for

surfaces composed of iron or stainless steel.[4] Under the present program, an extensive program of discharge-chamber optimization has retained performance gains demonstrated with the SIT-8 thruster by the use of ion-machined accel grids,[5] while achieving a high level of discharge stability through small but important changes in critical discharge-chamber dimensions.

The now-completed EM propulsion subsystem represents the furthest advancement of a technology base that has been under continuous development throughout the present decade. Critical assemblies such as the Cathode-Isolator-Vaporizer (CIV) and Neutralizer-Isolator-Vaporizer (NIV) are little changed from the original designs developed for the 5-cm thruster, SIT-5 (Ref. 6). The SIT-5 first demonstrated the outstanding durability of these components in operation of a 10,000 hr life test carried out at NASA LeRC.[7] Later, these critical subassemblies were incorporated into the design of the Hughes-developed SIT-8 prototype configuration;[8,9] a similar 4.5-mN (1-mlb) configuration served to demonstrate even greater durability of these basic subassemblies as part of a separate 15,000 hr durability test also conducted at NASA LeRC.[10]

Power supply and electronic-control development of the EM propulsion package derive also from an earlier contractual program[11] (between HRL and NASA LeRC) to design, fabricate, and test a Thermal Vacuum Breadboard (TVBB) Power-Processing Unit (PPU). This unit is capable of providing sustained operation of the SIT-8 thruster at a maximum thrust level of 9 mN (2 mlb) and a nominal thrust of 4.5 mN (1 mlb). The major thrust of the EM power-processor development has been to optimize system circuitry for operation at the 5-mN (1.1-mlb) thrust level (eliminating the 9-mN capability) and to package the electronic subsystem in a configuration suitable for spaceflight operation. An outstanding feature of the EM power-processor flight packaging is the separation of power and control circuits into separate physical enclosures. This feature addresses the need for flexibility in the design of the control section to meet the functional and interface requirements of a particular spacecraft.

All other components of the propulsion package also have undergone earlier development and tests at HRL and NASA LeRC. Several alternative mechanical thrust vectoring systems were developed at HRL[3] and NASA LeRC[1] for comparative evaluation. Thruster component endurance tests were carried out at NASA LeRC, which established criteria for the specification of thruster material-coating procedures and identified advantageous thruster-operating setpoints.[1] Also, a pressurized (and sealed) mercury propellant reservoir (developed during the SIT-5 program[6]) was endurance tested for 14,000 hr with entirely satisfactory results.[1]

SECTION 2

SYSTEM HARDWARE

The EM 8-cm Ion Thruster Subsystem is composed of four major elements: an 8-cm electron bombardment mercury ion thruster, a propellant reservoir, a gimbal unit, and a PPU. Figure 1 shows the EM 8-cm Ion Thruster Subsystem in one of the many layout configurations possible with this set of free-standing elements. The reservoir is shown at the left in Figure 1 (next to the thruster, which is attached to the gimbal system). These are followed by the power-processor electronics unit (PEU) and the power-processor digital-interface unit (DIU).

Electrical integration is accomplished via a connector-terminated system harness which interconnects the system elements. Propellant integration consists of a stainless-steel feedline which runs between the propellant reservoir and the base of the gimbal unit.

The PPU is subdivided into two package, PEU and a DIU. The PEU contains nine programmable power supplies designed to satisfy the thruster's requirements. The DIU houses the command, control, data conversion, and protective circuitry necessary to interface with an external data command/subsystem and to implement automatic system operation.

Major system parameters which characterize the EM Subsystem are summarized in Table 1, and the weight breakdown for the system is presented in Table 2. A more detailed description of the four elements of the 8-cm EM Thruster Subsystem follows.

A. THRUSTER

The EM 8-cm Ion Thruster, shown in Figure 2, includes all elements necessary to generate 5 mN of reactive thrust when provided with liquid mercury (from the propellant reservoir) and appropriately conditioned electric power (from the PPU). A summary of thruster specifications is given in Table 3. Complete performance data taken during unit acceptance testing is presented in Section 3.

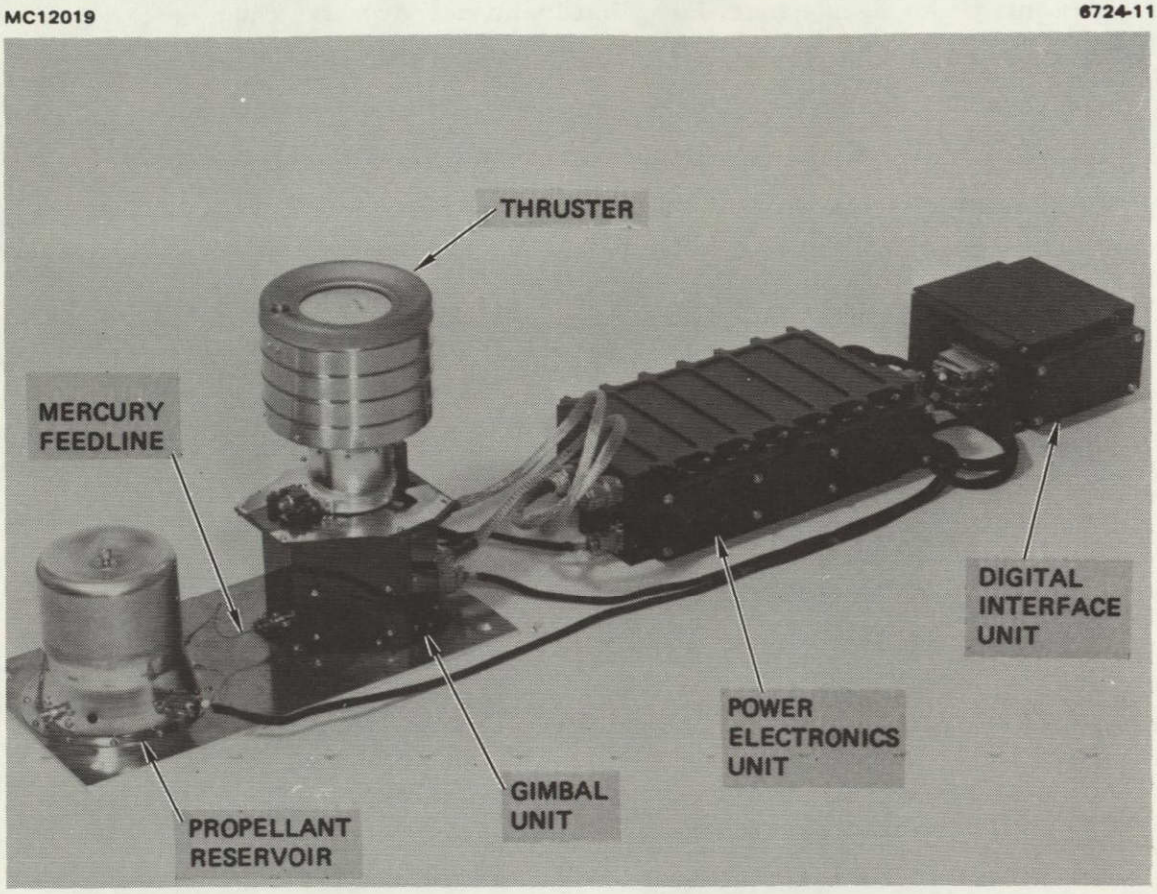

Figure 1. EM 8-cm ion thruster subsystem.

Table 1. EM 8-cm Ion Thruster Subsystem Summary Specifications

Parameter	Value
Thrust level	5 mN
Specific impulse	2667 sec
System input power at rated thrust[a]	165 W
System dry mass[b]	15 kg
Mercury propellant reservoir capacity	8.75 kg
Thruster vector deflection angle	10° any azimuth
Start-up time	≤15 min
Design lifetime	20,000 hr 10,000 cycles
Electrical interfaces	
Power	70 ± 20 Vdc (160 W) 28 ± 1 Vdc (5 W)
Command	16-bit, serial (0,5 V)
Thermal interfaces (mounting surface)	
PEU	-20 to +50°C
DIU	-20 to +50°C
Thruster-gimbal	-30 to +85°C
Propellant tank	-30 to +60°C

[a]Total input power from the main (70 V ± 20 V) and auxiliary (28 V) power bases to provide 119.5 W of conditioned power to this thruster.

[b]Does not include external power and signal harnesses necessary for integration into spacecraft.

5911

Table 2. Subsystem Dry Weight Summary

Item	Mass, kg
Thruster[a]	2.2
Gimbal unit	1.5
Propellant reservoir	1.2
Power processor[b]	10.1
TOTAL	15.0 (33 lb)

[a]Mass includes thruster input power harness between thruster and gimbal unit bulkhead.

[b]Interunit harnessing mass was not included since it is a function of system layout. Mass of practical minimum length harness estimated at 0.7 kg.

5911

Table 3. EM 8-cm Ion Thruster Summary Specifications

Thrust level	5 mN
Specific impulse	2667 sec
Power input	119.5 W
Mass[a]	2 kg
Size[b]	
Length	22.60 cm
Diameter of ground screen including ribs	17.03 cm
Diameter of gimbal adapter	7.59 cm
Design lifetime	20,000 hr 10,000 cycles

[a]Mass and size specifications include the entire structure, from the tip of the neutralizer cathode to the base of the gimbal adapter. The mass of all electrical wiring and connectors is included in the value given.

5911

M11782

Figure 2. EM 8-cm ion thruster.

1. Design Philosophy

Development of the EM 8-cm thruster is the culmination of a continuing technology evolution that began with design and analysis of the SIT-5 ion thruster.[12] Development of the SIT-5 was supported by a coordinated program of detailed thermal and structural design analysis, which was carried out in coordination with discharge-chamber optimization and component development. The thermally integrated CIV and NIV structures were first designed and tested under that program, and the entire thruster module was structurally and thermally integrated to ensure its structural integrity during booster launch and to ensure efficient and effective performance during spacecraft operation over its design lifetime of 10,000 hr.

The SIT-5 ion thruster that resulted from that initial development demonstrated outstanding performance[6] and durability.[7] This accomplishment served as impetus for a program of intensive component research (conducted principally at NASA LeRC[1]) and thruster development (conducted principally at Hughes[8,9]) which led to the development of the EM 8-cm thruster. The EM 8-cm thruster extends the capability of the SIT-5 configuration for operation at an increased thrust level, with greater efficiency, over a significantly longer period.

a. Thruster Durability

The 10,000 hr test of the SIT-5 thruster system (at NASA LeRC) was terminated at 9,700 hr because of the presence of a metal flake that fell over one of the beam-forming apertures of the screen electrode and disturbed the beam trajectory, causing it to impinge directly on elements of the electrostatic thrust-vectoring accel electrode. Direct impingement of a large part of the beamlet current quickly severed an accel element and caused it to fall into a position where it caused a short circuit between the screen and accel electrode, making further beam extraction impossible. John Power[13] of NASA LeRC has shown that the flakes form inside of the discharge chamber as a result of ion-bombardment sputtering of cathode-potential surfaces and that essentially all of the sputtered material is ultimately

deposited on the anode, from which it eventually flakes off. His studies have shown that the sputter-deposited film exhibits good adherence with the anode surface up to the point where film deposits are accumulated that are sufficiently thick to cause the interstitial layers to separate, at which time spalling and flake formation begin to occur.

The metal flake control techniques listed below were developed at NASA LeRC and HRL to prevent interruption of thruster operation by metal flake perturbations:

- Reduce discharge voltage to minimize ion-bombardment sputtering
- Use tantalum cover surfaces to reduce the ion-sputtering yield
- Roughen discharge-chamber surfaces (by grit blasting) to enhance adhesion where sputter deposition is known to occur
- Use a wire-mesh anode to prevent large-flake detachment
- Add a grid-clearing circuit to the PPU to vaporize flakes that cause short circuits.

These techniques concentrate on each stage of the problem: the ion-bombardment sputtering process, adherence of the anode films, and the neutralization of the metal flakes. All of the techniques have been incorporated to some extent in the design of the EM 8-cm thruster subsystem.

b. Thruster Performance

The initial goal identified for development of the subject thruster size was to achieve efficient operation at the 4.5 and 9.0 mN (1 and 2 mlb) thrust levels. To accommodate the maximum thrust requirement, an 8-cm beam diameter was chosen for this development by direct scaling from the Hughes 30-cm thruster which operates at a maximum thrust level of 135 mN (30 mlb).[14] At maximum thrust level, the beam-extraction system of either thruster would operate at an average beam-current density just below j_B = 3 mA/cm; long-term operation at higher levels has not yet been demonstrated.

Immediate mission goals have restricted initial optimization of the 8 cm thruster to the 4.5 mN (1 mlb) thrust level, and special techniques have been developed to ensure high operating efficiency at the lower beam-current value. The NASA-developed Small Hole Accel Grid (SHAG) beam-extraction system has been singularly effective in helping to attain design performance goals.[5] The SHAG system employs a high-transparency screen electrode to minimize discharge power,[15] while high propellant-utilization efficiency is achieved simultaneously with an accel electrode of low optical transparency which limits neutral-particle losses.[5] This combination has been found to be capable of well collimated beam-formation characteristics generating near parallel ion trajectories within a single beamlet. The screen-to-accel interelectrode gap was set at 0.635 mm, which was thought to be the smallest value consistent with high reliability.

Performance of the EM 8-cm Thruster was advanced significantly by a comprehensive program of discharge-chamber performance optimization. This program has dealt mainly with the need to combine stable current-voltage (I-V) characteristics with high performance efficiency. In an earlier design[3] (the SIT-8 configuration), stable operation was facilitated by using a variable magnetic baffle to shape the magnetic field in the vicinity of the cathode-cup polepiece. By shaping the magnetic field in the annulus separating the main and cathode plasmas, the variable baffle also facilitated ion-beam throttling by adjusting discharge impedance as required to maintain the desired value of beam current.

Since ion-beam throttling was not a goal of the subject development, the variable magnetic baffle was discarded to simplify the discharge-chamber configuration. The resulting SIT-8 configuration was capable of efficient performance; however, discharge characteristics were initially characterized by high-level oscillations in the discharge current and a tendency toward mode switching to a less efficient operating condition. Stable and efficient discharge-chamber characteristics were re-established in the EM 8-cm configuration by reducing the length of the discharge chamber (from the SIT-8 value) while preserving the

axial separation between the screen electrode, the lip of the cathode-cup polepieces, and the cathode tip. These modifications place the cathode tip 3.4 mm upstream from the saddle-point-zero of magnetic field, which occurs near the plane of the thruster endplate.

c. Design Innovation

Several unique design innovations included in the EM 8-cm Thruster were adopted on the basis of experience gained during the evolutionary developmental process. For example, experience gained during dynamic testing of the SIT-5 (Ref. 16) ion thruster led to the inclusion of the following mechanical features into the EM 8-cm design.

- All ceramics are in compression
- Uninsulated, braided, tantalum wire connects all thruster electrodes
- The ground screen is not perforated
- No spot welds are used.

In the shake test of the second SIT-5 configuration, two of the four thruster support insulators were fractured by dynamic forces. (However, the two remaining support insulators and the isolator ceramic continued to hold the thruster in place.) These insulators had failed under tension (ceramics under tension exhibit only one-tenth their strength in compression); this possibility is avoided in the EM 8-cm design by always clamping ceramics in pairs back-to-back.

Free standing uninsulated wire was used in the SIT-5 design to make electrical connection to thruster electrodes on the theory that ambient heating and metal sputter deposition would nullify the protection afforded by even the best of available insulations. The original single-strand nickle wires failed uniformly by fatigue fracture during dynamic testing of the SIT-5 module.[16] This led to the adoption of braided tantalum wire, which was chosen for its low electrical resistance, non-ferromagntic quality, high melting point, and high resistance to fatigue failure. The natural fatigue resistance of the tantalum itself is enhanced by braiding together numerous stands of thin

wire; this provides a higher degree of single-wire flexibility combined with the highly damped mechanical characteristics of the wire bundle.

Ground-screen tearing also occurred during the SIT-5 shake test along a path defined by perforations in the outer metal skin of the SIT-5 thrusters. Although this failure was traced to reduction in ground-screen-material thickness due to excessive electropolishing, this experience led Hughes to question the utility of these perforations (which have traditionally been used as a ground-screen material to facilitate the venting of liberated gases). Since the requirement for gas venting was judged to be minimal in the EM 8-cm thruster, an unperforated ground screen was used to enhance its structural strength. This change was also motivated by the anticipation that future system requirements might demand that a quasi-hermetic seal be used (by attachment of a downstream ground-screen cover) to protect sensitive interior surfaces (e.g., the cathode insert) from deleterious ambient environmental factors.

SIT-5 shake tests[16] also argue strongly against the use of spot welds as an attachment procedure. It was not so much the concern that a spot-weld might fail, but rather that the spot weld could weaken the element that it attempts to attach to the extent that small pieces of metal would be torn away and be free to fly against thruster surfaces. This possibility became apparent when a small iron sliver tore lose at a spotweld location from the magnet-retainer lug. The iron sliver was drawn by the magnetic field of the screen polepiece to a location where it established a dead short between the screen and accel beam-extraction electrodes. Although the spot weld continued to hold the magnet lug in place, the resulting sliver would have caused to total failure of an actual spaceflight mission.

A final design innovation introduced in the EM 8-cm design which bears special mention is the use of a high voltage (HV) pulse ignitor. This ignition method replaced the technique used in all earlier hollow-cathode thrusters of applying a steady-state dc voltage (in the range 250 V to 500 V) directly to the keeper electrodes. The HV pulse technique was developed by E.G. Wintuchky[17] at NASA LeRC, who demonstrated

rapid and reliable ignition of the hollow cathode discharges for both open and enclosed keeper cathodes. The HV pulse was generated by discharging a capacitor across the primary winding of a step-up transformer. The pulse was then applied to either an auxliary electrode or directly to the keeper. In the EM 8-cm thruster, a HV pulse is applied to the keeper electrodes to achieve ignition. All metal-to-metal separations from the HV pulse transmission line are maintained in excess of 1.59 mm to prevent unwanted arc-over.

2. Design Description

An isometric of the EM thruster and gimbal is shown in Figure 3. The discharge-chamber design consists of an outer-shell assembly formed by rolling thin, stainless-steel sheet stock to form a cylindrical section. Structural rigidity of this shell is provided by circular stiffening ribs and by flanged sleeves located at the two ends. Axial strength is provided by sections of cylindrical tubing which enclose eight rod-shaped permanent magnets mounted axially around the periphery. The tubes are brazed at both ends to a set of flanges, one of which serves as the interface between the endplate on the closed end of the discharge chamber, and the other as the mount for the beam-extraction system on the opposite end. A cylindrical anode fabricated from wire mesh sintered to a solid 3-mil stainless-steel back is supported within the shell by insulating supports totally shielded against sputtering. As with the thruster shell, stiffening ribs are used to maintain its circular cross section.

The beam-extraction system is fabricated in a dish-contoured shape to maintain structural rigidity against deformation, even though the electrode elements are of thin cross section. This permits using a high-perveance electrode pair in which the screen-to-accel separation is set to a small dimension. Without the dished geometry, electrode shorting might occur under operating conditions where thermal gradients would otherwise cause significant deformation.

The cathode-cup enclosure has been penetrated to provide propellant-diversion ports. These ports lower the neutral-particle density in the

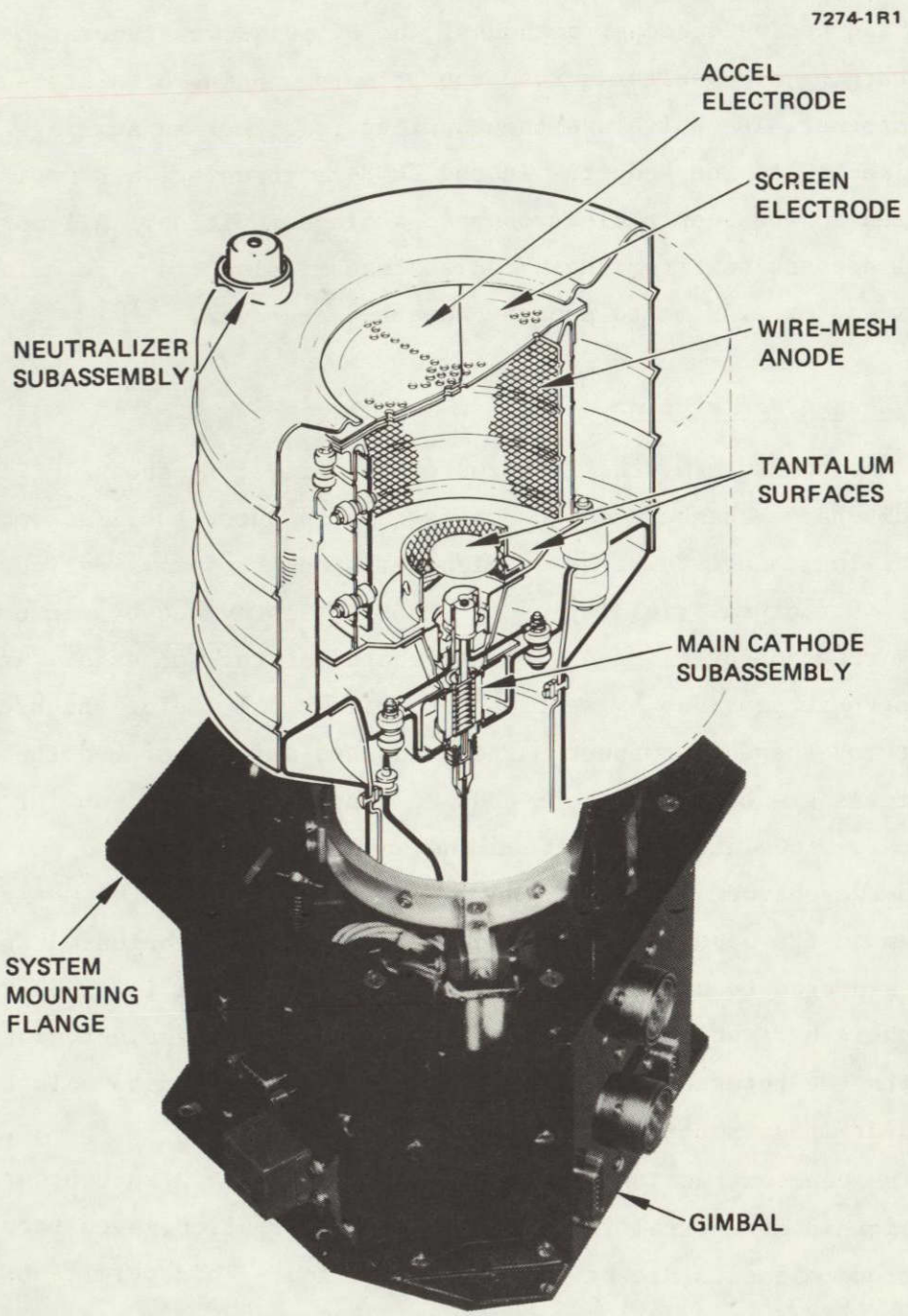

Figure 3. Isometric of EM 8-cm thruster and gimbal.

vicinity of the main cathode so as to adjust discharge-chamber impedance to the desired value.[8] The portholes are covered by a 49% transparent tantalum-wire mesh (0.008-cm wire diameter) that is brazed to the inside of the cathode cup; this mesh interrupts the continuity of plasma flow and restricts the transmission of electron current to the region of an annular gap between the electron baffle and the lip of the cathode-cup polepiece.

Two concentric sets of terminals are provided on the thruster-support flange for the various electrical connections. Connections between these terminals and the thruster components are made using short lengths of uninsulated wire. Sputter shielding is employed at both ends of these terminals to ensure that shorting cannot occur across insulating surfaces. All electrical connections internal to the ground-screen enclosure are designed to withstand the thermal environment (200°C to 300°C) typical of ion thruster operation. All electrical insulators are machined from alumina (Al_2O_3), and electrical wiring is generally fabricated from braided strands of tantalum wire terminated by nickel lugs.

The NIV subassembly is shown in Figure 4 with braided tantalum leads connecting NIV elements with a number of insulators located on the thruster-support flange. These wires are surrounded by a sufficiently large dynamic envelope to permit freedom of motion without the possibility of shorting to nearby surfaces. Other wires lead to a central ring of insulators surrounding the CIV subassembly. Since the required dynamic envelope cannot be provided at this location, the connecting wires are fabricated as the central element of coaxial conductor with swaged alumina insulation. The outer conductor is mechanically fastened to nearby thruster structural members.

The upstream surface of the thruster support plane is shown in Figure 5. This region lies outside the thermal enclosure surrounded by the ground screen; therefore, Teflon-insulated nickel wire can be used beyond this point. A bracket mounted parallel to the vaporizer element includes two insulators which support the delicate wires leading to the platinum-resistance thermometer. The thermometer senses the temperature of the vaporizer element. A similar configuration is used at the NIV location.

6704-33

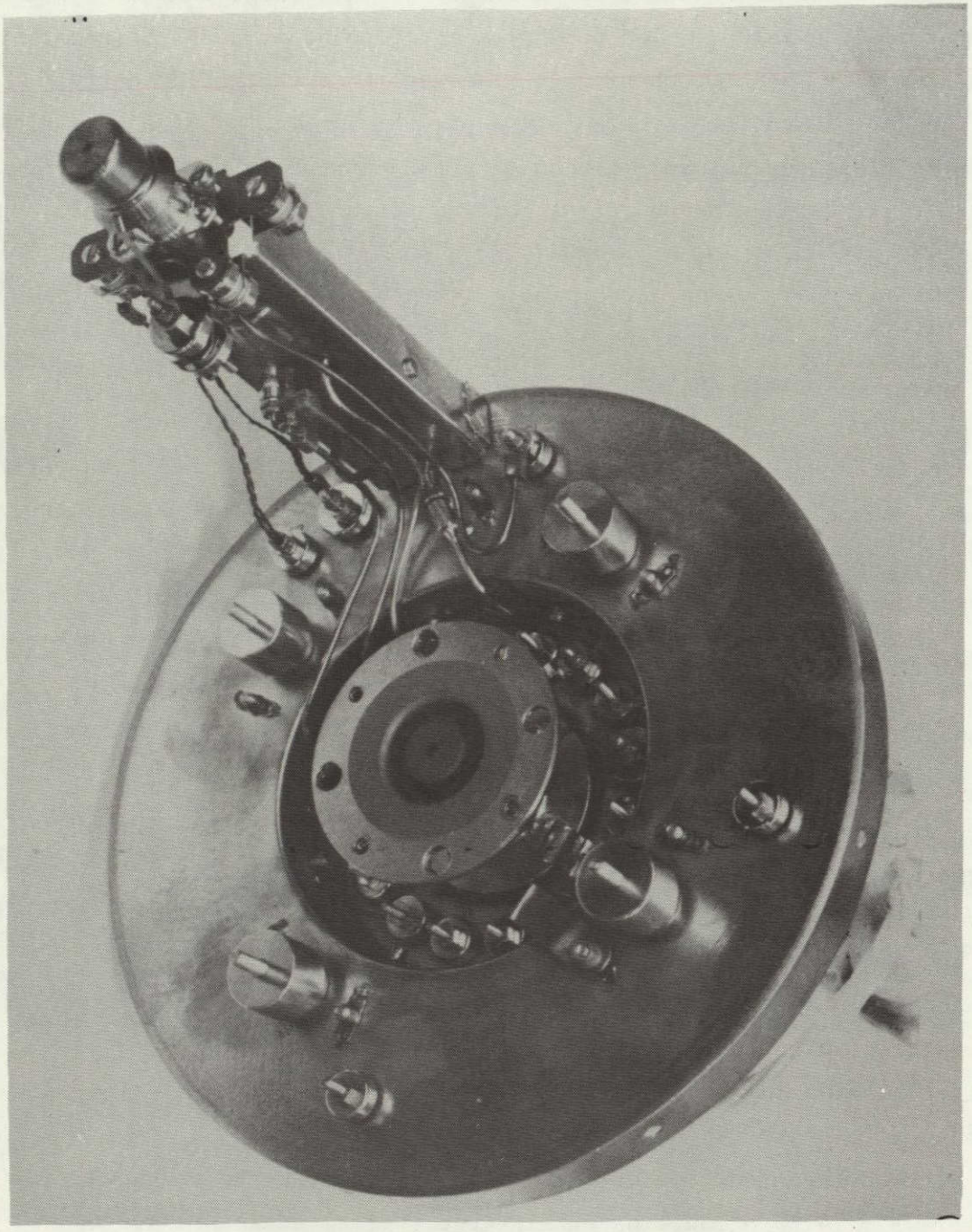

Figure 4. NIV electrical connections.

6704-34

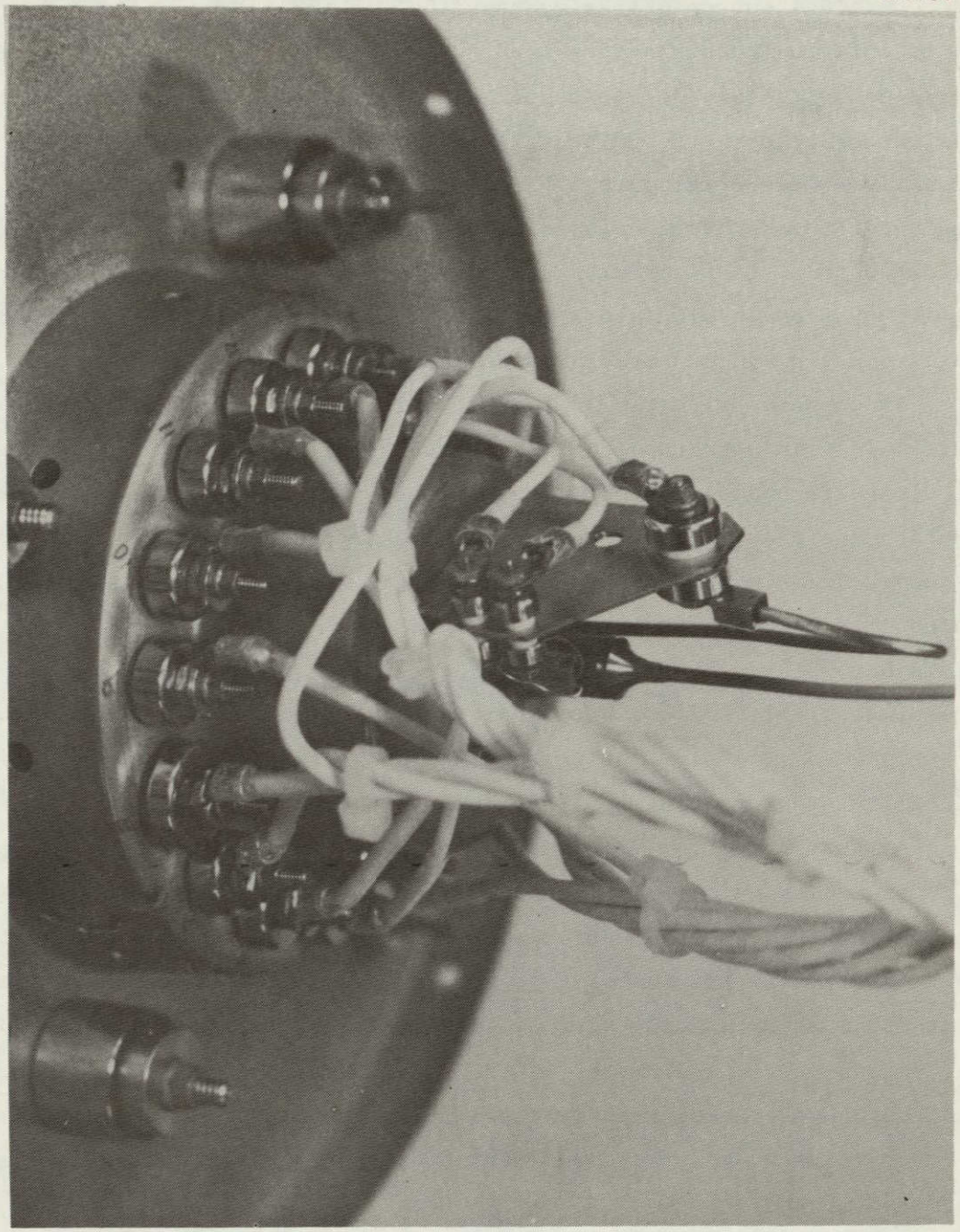

Figure 5. Upstream surface of thruster support flange showing vaporizer element of the CIV assembly.

Critical subassemblies such as the CIV and NIV are improved versions of the original designs developed for the SIT-5 (Ref. 6). The SIT-5 first demonstrated the outstanding durability of these components in operation during a 10,000 hr life test carried out at NASA LeRC.[7] More recently, these critical subassemblies have been incorporated into the design of the Hughes-developed SIT-8 prototype configuration;[9] a similar 4.5 mN (1 mlb) configuration served to demonstrate the even greater durability of these basic subassemblies as part of a separate 15,000 hr durability test also conducted at NASA LeRC.[10]

As compared with the prototype configuration, the EM Thruster differs mainly in structural design features and in the special treatment of discharge chamber interior surfaces to minimize the effects of ion-bombardment erosion (sputtering) of discharge chamber surfaces. Techniques have been developed to coat most of the cathode-potential surfaces with a plasma-sprayed layer of tantalum to reduce the sputter yield below the value anticipated for surfaces composed of iron or stainless steel.[4] Minor but significant discharge chamber dimensional changes were also made during the EM program to simultaneously optimize stability and performance. This work is discussed in Section 3.

Another variation from the prototype SIT-8 design is the present use of a beam-extraction system entirely machined chemically as opposed to an ion-machined accel electrode. The new electrodes are designed to operate with similar performance to the ion-machined set, since the center-to-center spacing of the beam-forming apertures is unchanged and the screen-aperture diameter is the same value as employed in the earlier design. Furthermore, the diameters of the chemically machined accel apertures are closely matched with the aperture diameters which result from ion machining.[3]

B. PROPELLANT RESERVOIR

The propellant reservoir is shown in Figure 6. This subsystem element includes fill valves for both the liquid propellant and the gas pressurant; a Resistoflex* fitting is provided for connecting the transmission line, which delivers liquid mercury to the thruster. The reservoir also includes an integral pressure transducer which serves as a gross indicator of propellant consumption during operation of the propulsion system; it also serves to give warning if a leak develops in the gas pressurant. A summary of specifications for the propellant reservoir is given in Table 4.

As shown in Figure 7, the reservoir structure consists of a balloon hemisphere, which is supported on its exterior by a perforated-metal hemisphere and clamped by a metal flange that joins it to a matching stainless-steel hemisphere (type 304L) at its equator. The mercury is stored in the spherical region between the two hemispheres and is held under pressure by a charge of gaseous nitrogen trapped between the bladder and an outer housing, which covers the upstream half of the spherical container. As the mercury is consumed, the bladder collapses and the gas expands to fill the void, with an attendant decrease in pressure. By making the volume of gas sufficiently large, this pressure drop is maintained within the limits permitted for satisfactory vaporizer operation. An amount of krypton (20%) is added to the nitrogen to permit inspection for leaks with a mass spectrometer detector.

The gas seal between the bladder and the flange is ensured by the same O-ring that seals the liquid within the spherical cavity. This O-ring is fabricated as an integral part of the bladder. The bladder is 0.089 cm thick molded from pure butyl rubber, which has a working temperature range from -50°C to +107°C. Nitrogen and krypton are used as the pressurizing agents because they are inert and do not liquify over the anticipated range of working temperatures. The bladder has

*"Resistoflex" is a tradename of Resistoflex Corp., Roseland, N.J.

M11795

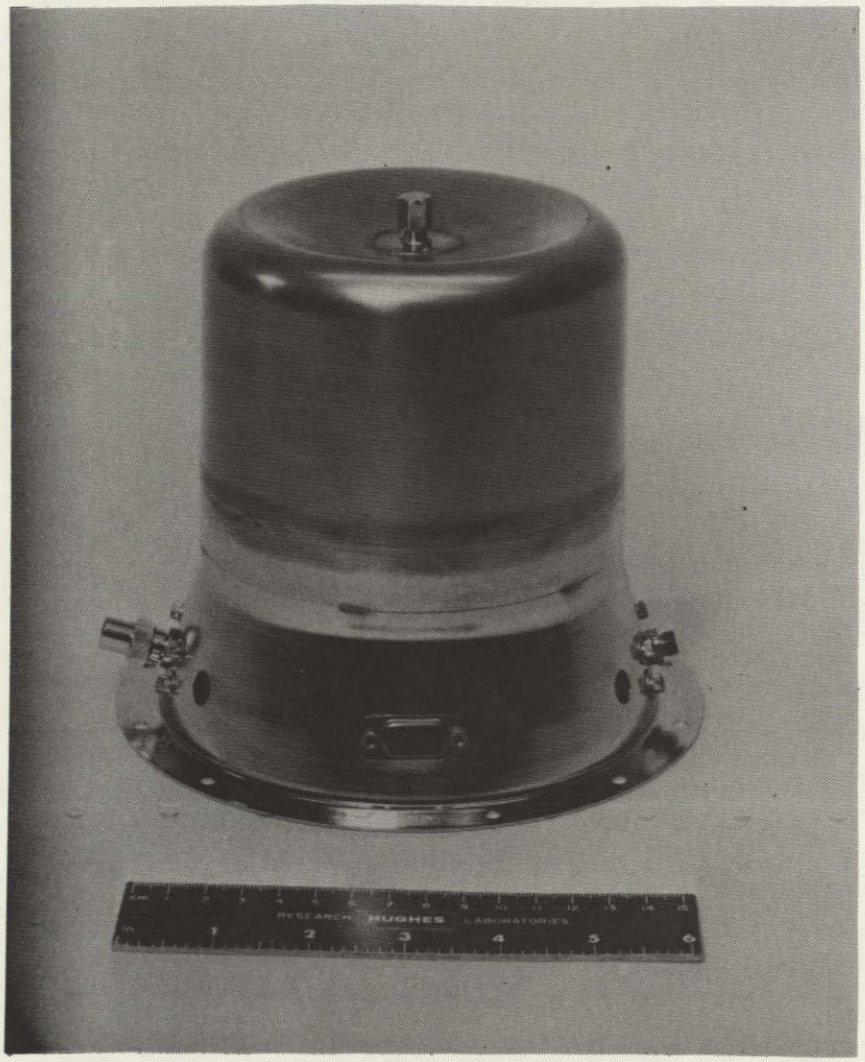

Figure 6. Mercury propellant reservoir.

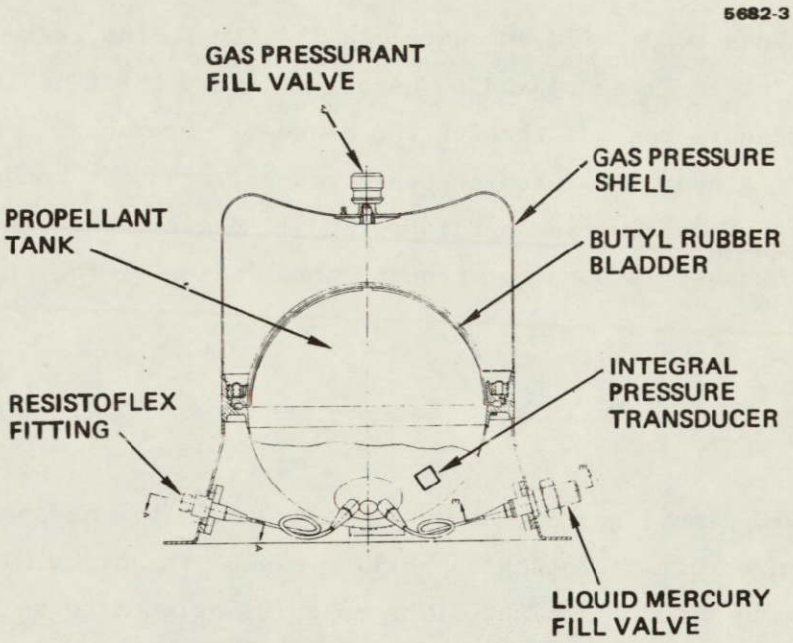

Figure 7. Propellant reservoir design.

Table 4. Propellant reservoir summary specifications

Parameter	Value
Filled mass	9.91 kg
Dry mass	1.16 kg
Propellant mass	8.75 kg
Drive pressure (80% nitrogen, 20% krypton)	241 kPa (35 psia)
Gas volume ratio (empty/full)	2
Overall height	16.29 cm
Overall diameter	18.42 cm
Bolt-circle diameter (twelve 0.422 cm diameter holes, equally spaced)	17.5 cm

5911

been designed to provide adequate flexibility to assure complete expulsion of the mercury and to be sufficiently thick to limit diffusion of the pressurizing gas through the bladder. Pressure in the mercury reservoir is monitored with a strain-gauge transducer bonded directly to the hemispherical surface. This method of pressure measurement was selected because it does not require penetration of the propellant reservoir.

C. GIMBAL UNIT

The EM gimbal unit is shown in Figure 8. This subsystem element provides a thrust vectoring capability of 10° in any azimuth about the normal to the mounting plane. The unit is designed to be mounted to an appropriately configured spacecraft structure from either its upper or lower flange. Standard electrical and propellant interconnections are incorporated in the design to simplify system integration. Gimbal unit summary specifications are given in Table 5.

Table 5. Gimbal unit summary specifications

Parameter	Value
Deflection in any azimuth	10°
Motor steps per degree deflection	2421
Time from $+10^{o}$ to -10^{o} deflection	120 sec
Motor drive power (max)	7 W
Mass[a]	1.50 kg
Size	
Base	14.41 cm x 15.15 cm
Height	13.48 cm

[a]Includes mass of internal propellant feedline and manifold.

5911

M11823

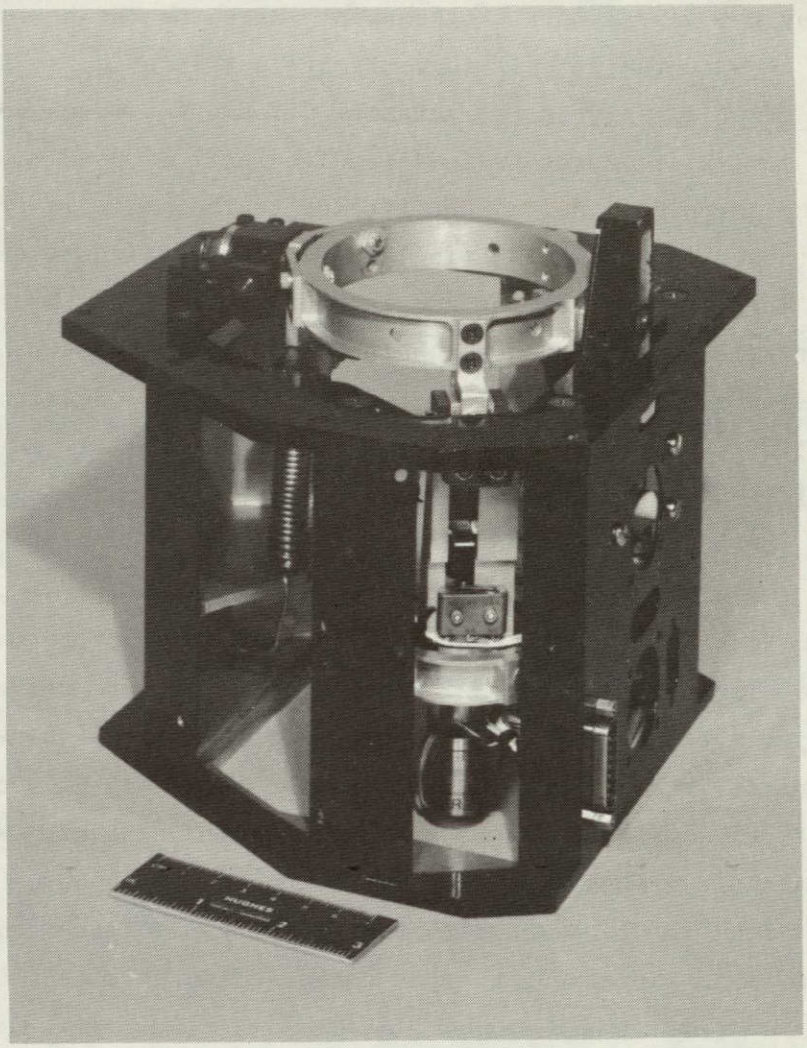

Figure 8. Gimbal unit with side panels removed.

Figure 9 shows selected details of the gimbal unit interior and the manner of integration with the thruster. The thruster is mechanically supported by the gimbal unit at the point where the thruster adapter column attaches to the gimbal ring. Propellant interfacing is achieved with independent lines from the thruster CIV and NIV which couple to the propellant manifold. A constrained feedline coil is used to route propellant from the gimbal unit input fitting to the manifold (which is rigidly attached to the gimbal ring) to facilitate flexure during gimbaling. Electrical interfacing consists of routing the thruster's connector-terminated flying power harness through the interior of the gimbal housing and mounting these connectors in hole locations provided in the wall of the structure.

Gimbaling action is achieved by pivoting the gimbal ring about the two-axis pivot support located on the top flange. Forces to position and retain the ring are derived from two screw actuators coupled to the ring with U-joints and the pivot support; together they form a three-point suspension for the ring. The screw actuators are driven by miniature stepper motors located near the base of the gimbal housing.

Differential motor drive causes rotation about one axis of the pivot support; coincident drive causes rotation about the other. Motor drive power signals are issued by circuitry in the power processor DIU as a result of system input commands that define the motor to be driven, the direction of motor rotation, and the number of motor steps.

The gimbal unit was developed by NASA LeRC under the direction of R.J. Zavesky.[1] Subsequent effort on the EM program consisted mainly of modifying and augmenting the basic design to provide for structural, propellant, and electrical integration with the EM 8-cm thruster.

D. POWER PROCESSOR

A power processor for operating an 8-cm thruster at the 5-mN level was earlier designed and developed for NASA LeRC under Contract NAS 3-18917. In adapting this design for the EM 8-cm thruster, the majority of the effort was divided into two areas: the power electronics and the development of a new DIU. In the power electronics area,

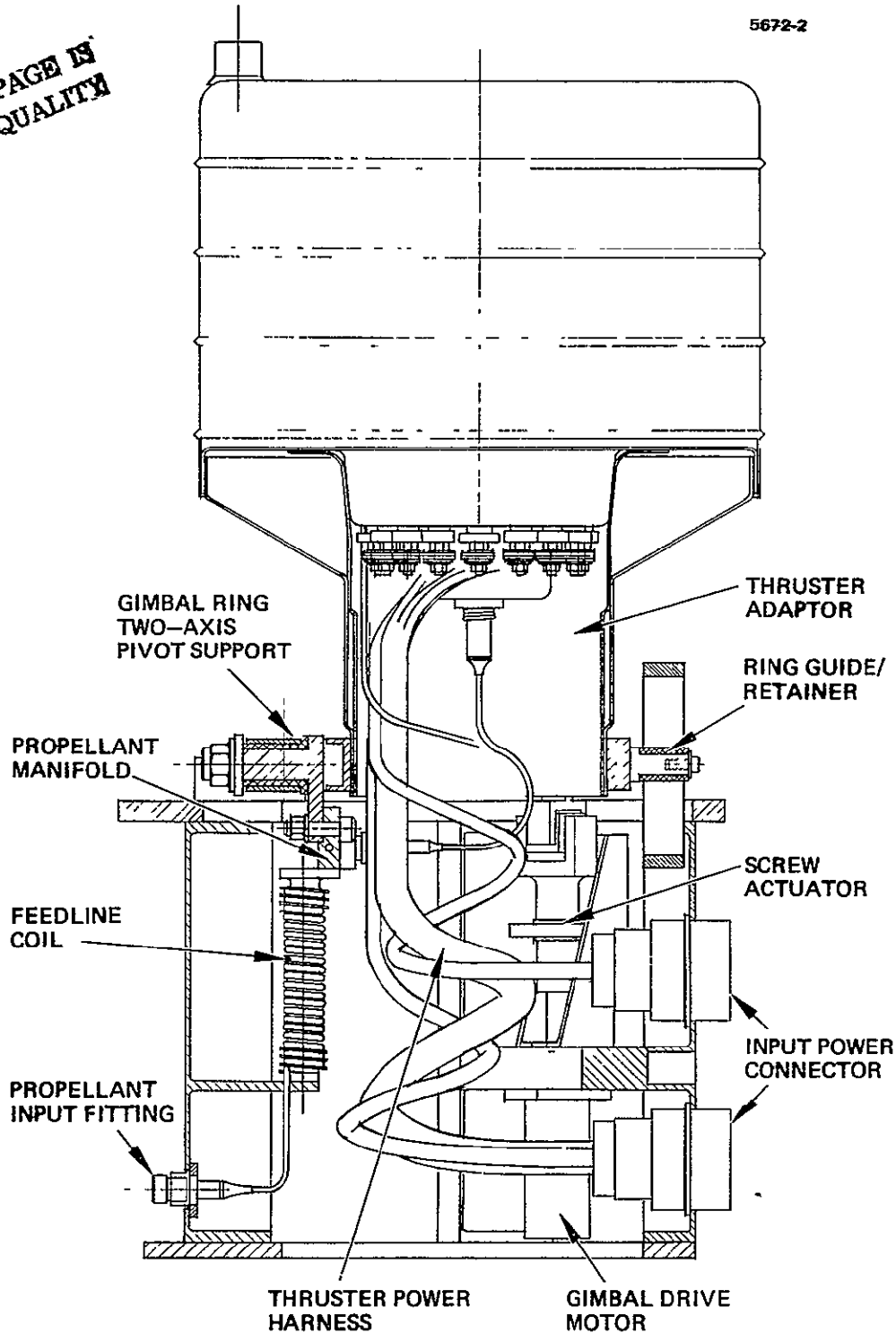

Figure 9. Gimbal unit drawing showing internal detail and interfacing with thruster.

the effort was devoted to defining power-supply requirements for operation at the nominal 5 mN thruster operation, and to redesigning the supplies for efficient operation at a thrust level reduced from that of the TVBB power processor, developed earlier under NASA Contract NAS 3-17780.[11] The specifications for the EM power processor are given in Table 6. Development of the new DIU was mandated by the requirement of the EM power processor to receive serial commands while the TVBB received parallel strobed commands.

The electrical interface with the spacecraft is at the DIU. The command signal lines and the +28 Vdc housekeeping power go no further than the DIU. However, the +70 Vdc bus passes through the DIU to the PEU. The 70 Vdc bus is used in the DIU for over-power and under-voltage detection as well as for generating bus current telemetry. The PEU receives 0 to 5 Vdc control signals from the DIU to set the output levels of the nine power supplies in the PEU.

1. Physical Properties of PPU Package

Table 7 is a compilation of the physical characteristics of the PPU package. The present package configuration (refer to Figure 11) was chosen to establish a satsifactory thermal design with the capability of mounting the unit either on the spacecraft shelf (typical communication satellite) or at the end of the solar-panel boom on a 3-axis oriented spacecraft. A satisfactory thermal design is one that maintains the component temperatures at levels consistent with high reliability of the individual components.

The bottom surfaces of the packages are machined so that they can be thermally mated to their mounting surface to provide thermal stabilization. The exterior is designed (using various thermal paint patterns) so that most of the internal heat will be radiated and a small amount conducted through the mechanical mounting interface. The internal structure was designed to maximize both electrical shielding and thermal conduction around dissipative components. The modules are identically machined designs; prior to drilling for component mounting, the modules are interchangeable. Mounting techniques are consistent with electronics fabricated for spaceflight launch and operation.

Table 6. 8-cm Thruster Power Processor Supply Specifications

Supply	Maximum Power	Nominal Power	Regulation Type & ±%	Output Reference Potential	Type Control Input
1. Discharge vaporizer	6 V at 3 A	5 V at 2 A	I, 5	Spacecraft	8 fixed setpoints and loop control with D/A variable reference
2. Discharge cathode heater	8V at 4 A	6 V at 3 A	I, 5	Screen	8 setpoints
3. Discharge keeper	25 V at 0.5 A	15 V at 0.36 A	I, 3	Screen	4 setpoints
4. Neutralizer vaporizer heater	4 V at 2 A	2 V at 1 A	I, 5	Spacecraft	Variable reference and loop control with D/A variable reference
5. Neutralizer cathode heater	8 V at 4 A	6 V at 3 A	I, 5	Neutralizer common	8 setpoints
6. Neutralizer keeper	25 V at 0.5 A	20 V at 0.36 A	I, 3	Neutralizer common	4 setpoints
7. Discharge	50 V at 1 A	40 V at 0.5 A	I, 3	Screen	D/A variable reference
8. Screen	1200 V at 0.090 A	1180 V at 0.072 A	V, 1	PPU common	Single setpoint
9. Accel	-500 V at 0.008 A	-300 V at 0.001 A	V, 1	PPU common	Single setpoint

5911

Table 7. Power Processor Physical Characteristics

Characteristics	PEU	DIU
Height	10.8 cm	10.8 cm
Width	20 cm	20 cm
Length	38.7 cm	20 cm
Mass	6.97 kg	3.15 kg

5911

2. PEU Description

A functional block diagram of the EM power processor is shown in Figure 10. The heater and keeper supplies, which are magnetic-amplifier controlled, operate from a 96 Vac power distribution bus. The 96 Vac power is created by an inverter that operates in conjunction with the line regulator. The line regulator provides regulated 48 Vdc power to the inverter from the unregulated solar cell bus. The screen and discharge supplies operate directly from the unregulated solar-cell bus. Both of these supplies employ pulsewidth modulation to achieve the desired regulation. The DIU, which furnishes the control signals to the various power supplies, provides the interface to the spacecraft.

The power processor is constructed as two separable units — a power electronics unit (PEU) and a digital interface unit (DIU). These units are shown in Figure 11. As the figure shows, both units are comprised of several modules that are bolted together. In the PEU, each module is an individual supply or a group of supplies. For example, one module is the screen supply and another is the combination of the line regulator, distribution inverter, and input filter. With this configuration, the individual modules may be tested and characterized before the PEU is assembled as a whole. Figure 12 is a photograph of one of the modules. As shown in the figure, the components are mounted between terminal strips and connected with point-to-point wiring. One of the modules of the DIU contains individual functions or groups of functions. This provides easier testing without requiring the entire DIU to be assembled. As shown in Figure 13(a), the electrical components are mounted to a printed circuit card which in turn is mounted to

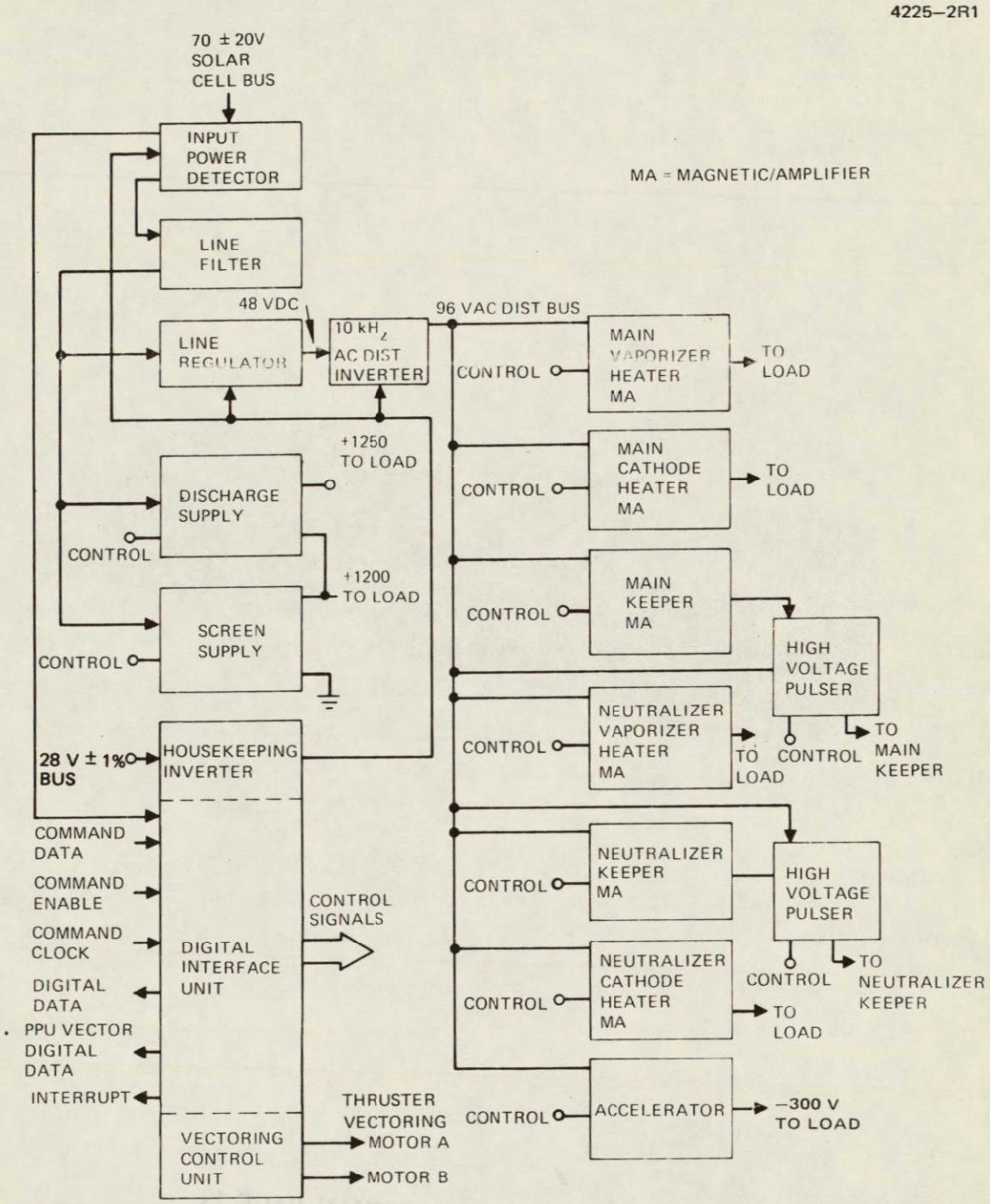

Figure 10. 8-cm ion thruster EM power processor functional block diagram.

M12017

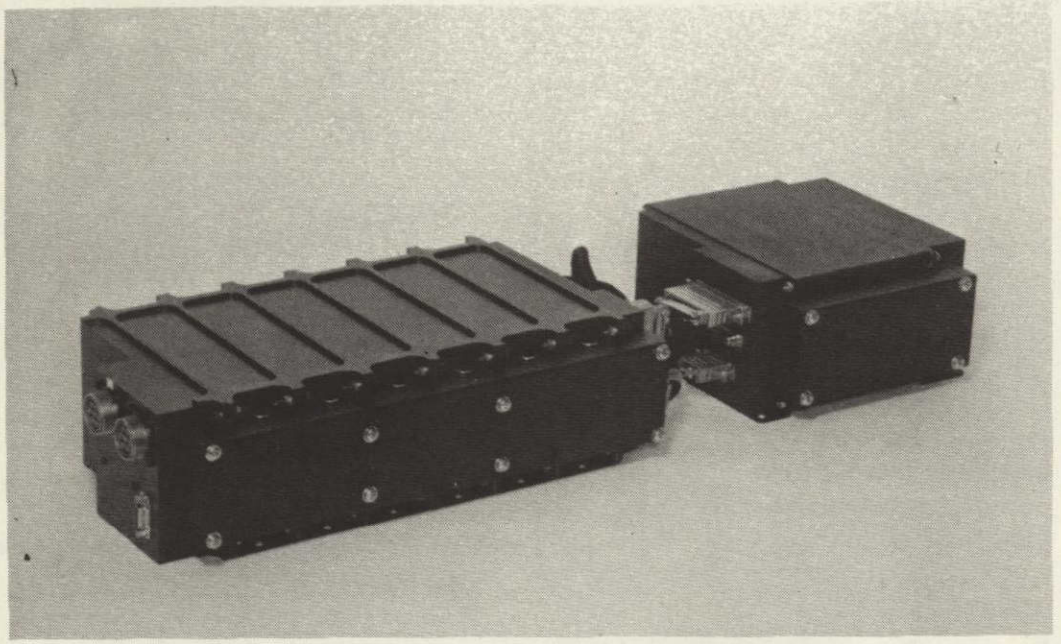

Figure 11. Power electronics unit and digital interface unit (left and right, respectively).

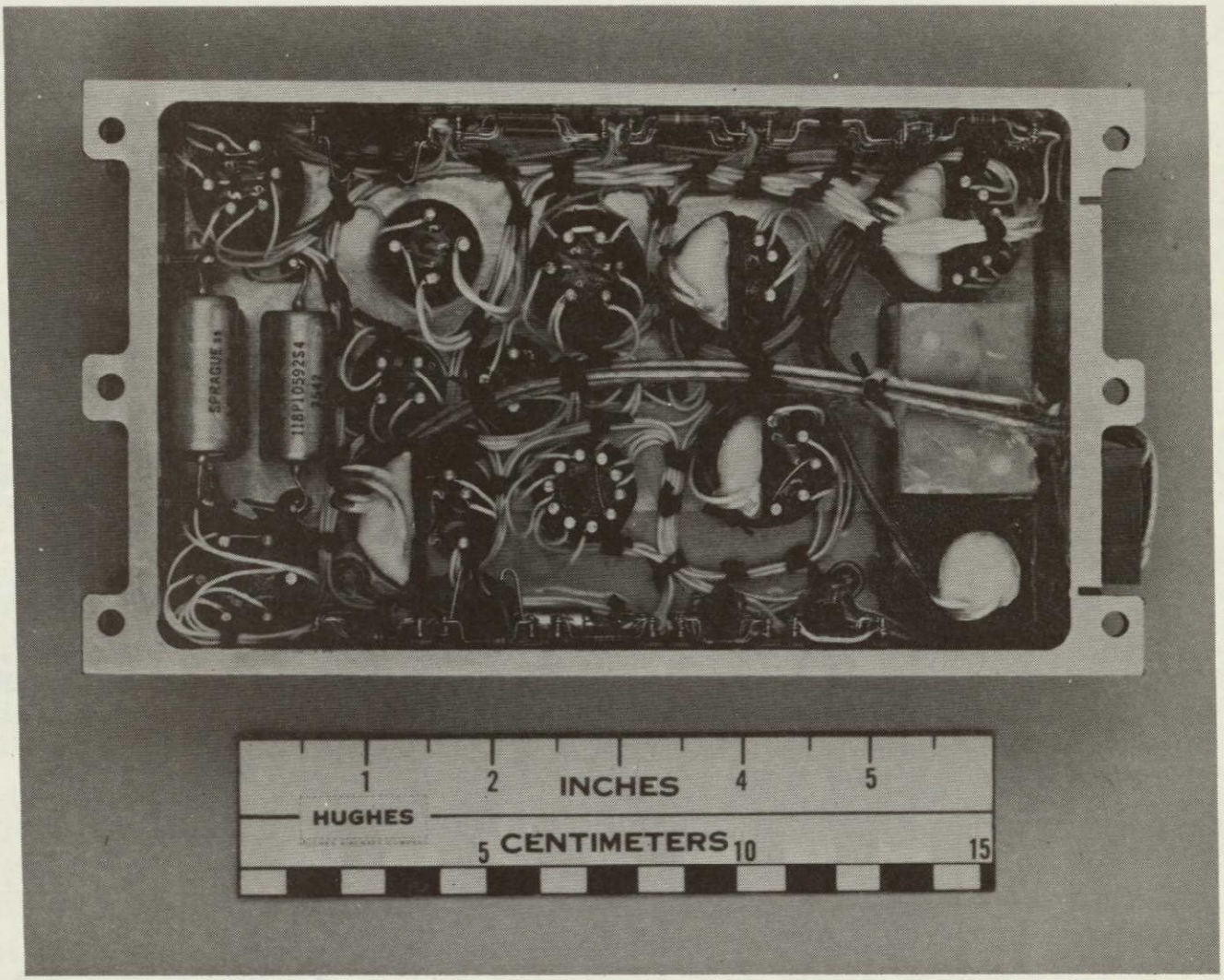

Figure 12. Power electronics module.

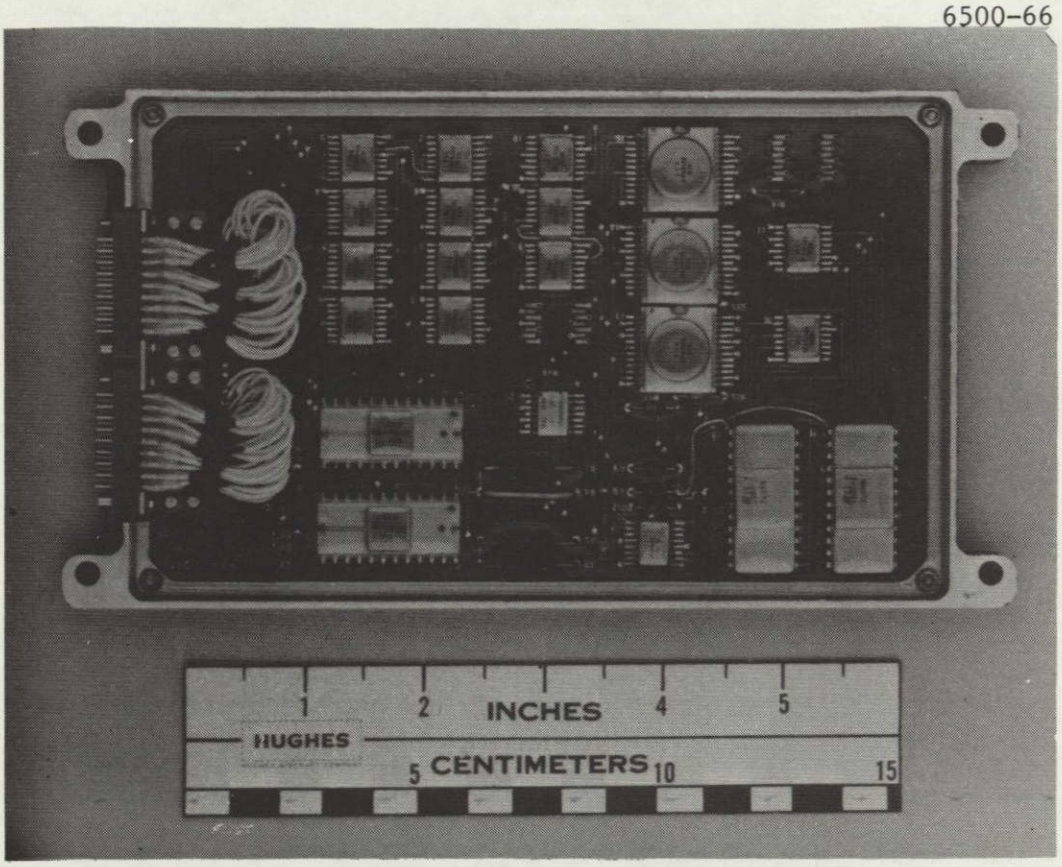

(a) Component side

Figure 13. Digital-interface module.

77-54933

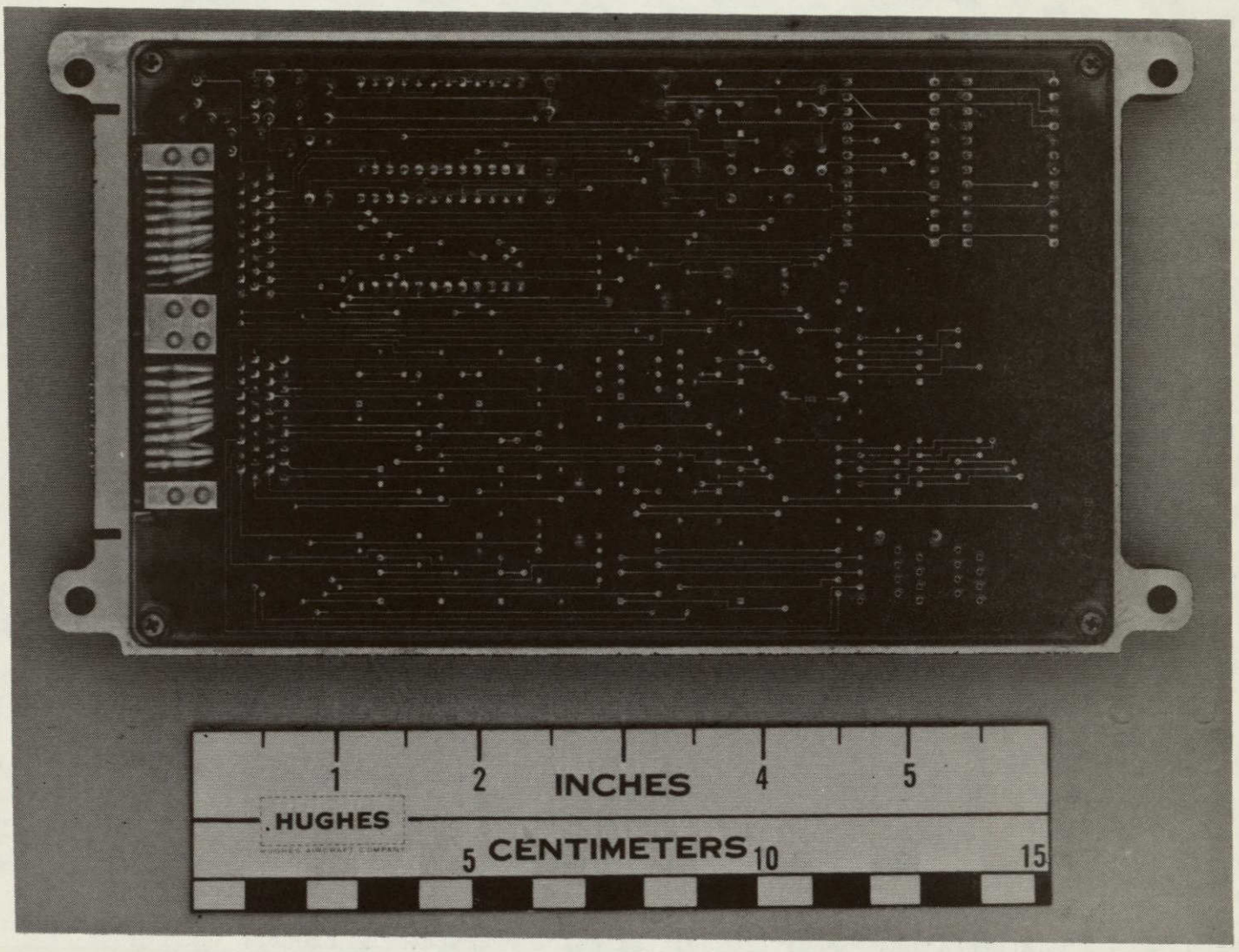

(b) Printed wiring side

Figure 13. Digital-interface module.

the module frame. The printed circuit cards used here are four-layer cards. The top and bottom layers are the circuit wiring, and the middle layers are the logic power positive and return. This was done to provide a ground-plane shield for each card and thereby reduce the noise environment seen by the circuitry.

The use of a 96 Vac power distribution system allows all moderate-power and light-power supplies to tap power from the main ac power system and provide high-voltage isolation at the same time through the use of transformers. The two high-power supplies, discharge and screen, are designed to operate directly off of the main bus supply. This allows higher efficiencies overall by eliminating any preregulation stages. This design approach allows for multiple spacecraft usage, with minimum design change to compensate for different main bus characteristics of the satellites.

The output electrical requirements for the PEU are listed in Table 6. The power processor must operate with a main input bus of 70 ± 20 Vdc and an auxiliary input bus of 28 Vdc.

When operating into a static load, 150.6 W of power was consumed from the 70 ± 20 Vdc bus; this corresponds to a power-conversion efficiency of 76.9%. An additional 4.86 W is drawn by the DIU from the 28 Vdc bus.

The grounding scheme used within the PEU is designed to isolate the control electronics, solar-panel power return (spacecraft), and the thruster. This minimizes noise interaction within the EM thruster system. It also reduces susceptibility to external noise and helps to maintain a low amount of radiated noise from the EM thruster system. A grounding block diagram is shown in Figure 14.

3. Supply Characteristics

The power supplies of the PEU can be broken into four categories: Magnetic-Amplifier-controlled (MA-controlled) ac heaters, MA-controlled dc supplies, transistor switching regulators, and a linear regulator. The use of magnetic amplifiers allows pulse-width control of the output current with a high degree of accuracy, inherent high efficiency of

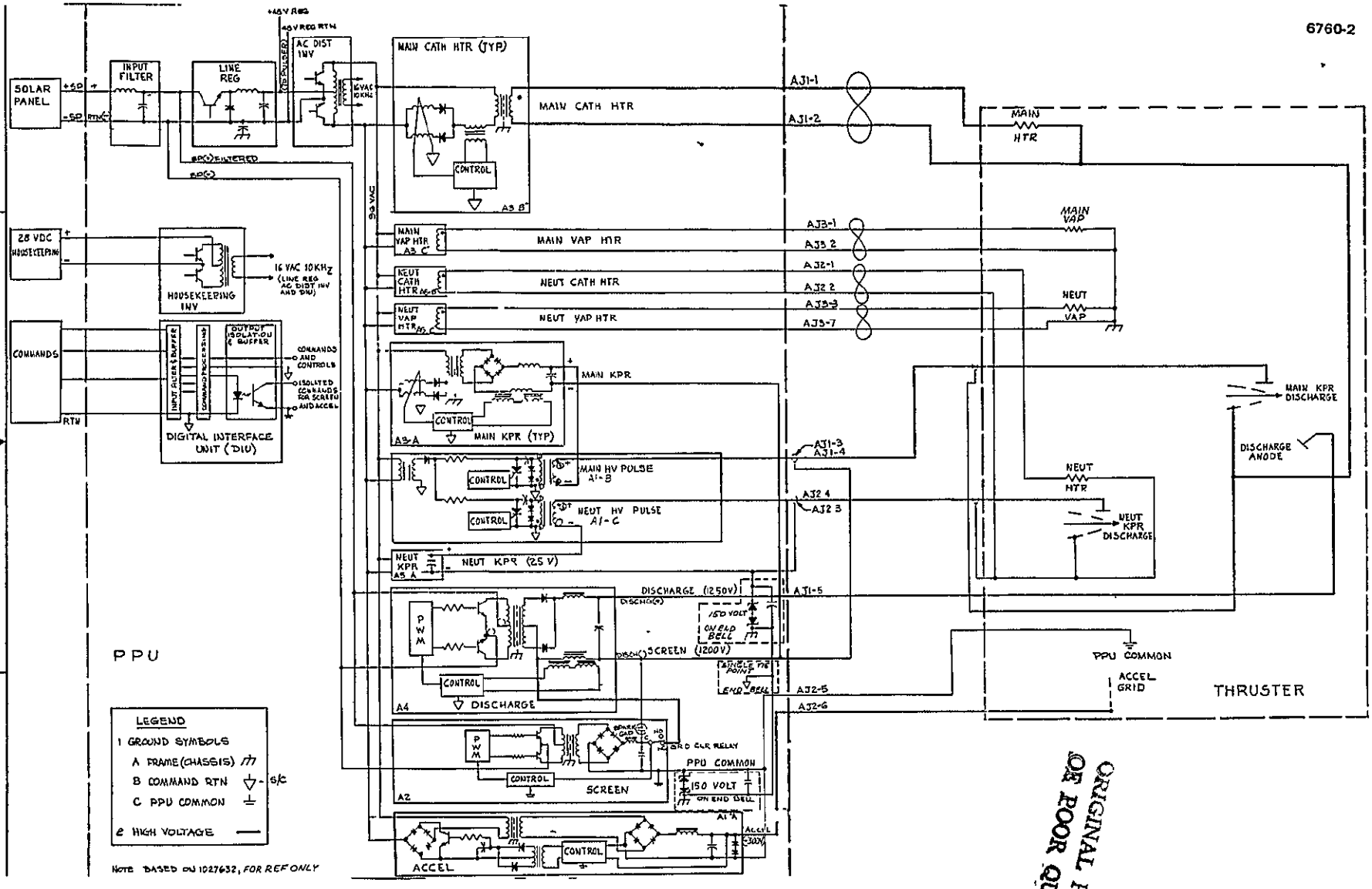

Figure 14. Grounding block diagram.

pulse-width modulation, and isolation between three separate grounds (power return, spacecraft, and PPU ground). (See Figure 14 for the grounding scheme.) Figure 15 is the control circuitry used for the ac and dc MA supplies. The difference between the control circuitry used in the ac and dc supplies is shown in Figure 16. The ac heaters employ a current transformer in the primary leg of the output transformer and develop an output feedback control of the magnetic amplifier. The dc heaters (main and neutralizer keeper supplies) also use current feedback, but it is derived from a current transductor in the dc return leg of the output of the supply. Figure 17 shows the output (V_o versus I_o) characteristics of an MA-controlled ac heater supply. The output characteristics (V_o versus I_o) of the dc MA-controlled supplies are shown in Figure 18. A 0 to 5 V signal from the DIU is used to control both the ac and dc MA supplies. The 5 V maximum input corresponds to the maximum current desired for each particular supply. Table 6 details the supply outputs. Figure 19 is the typical control characteristic (V_o versus I_o for several reference voltages) of the MA supplies.

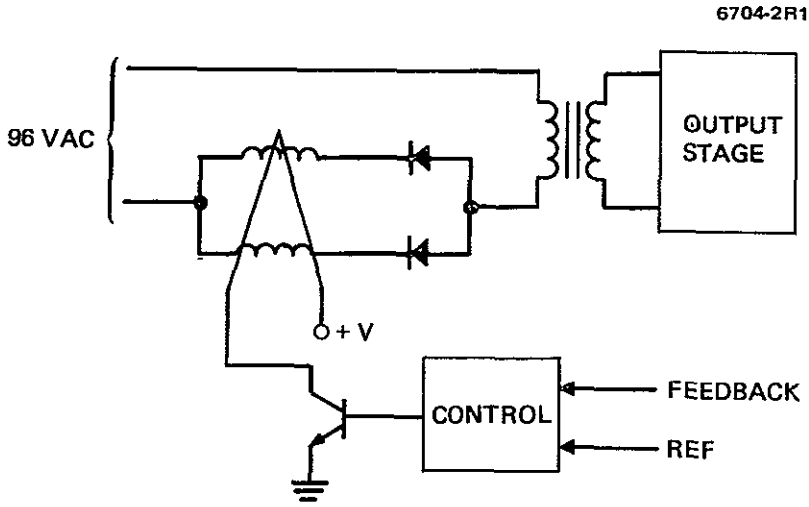

Figure 15. AC and dc control circuitry.

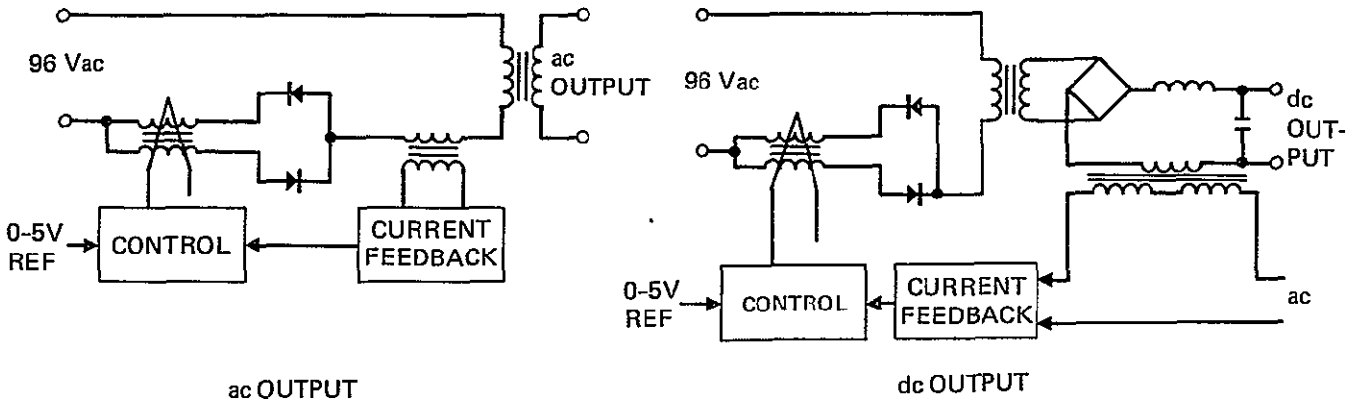

Figure 16. AC and dc I feedback control.

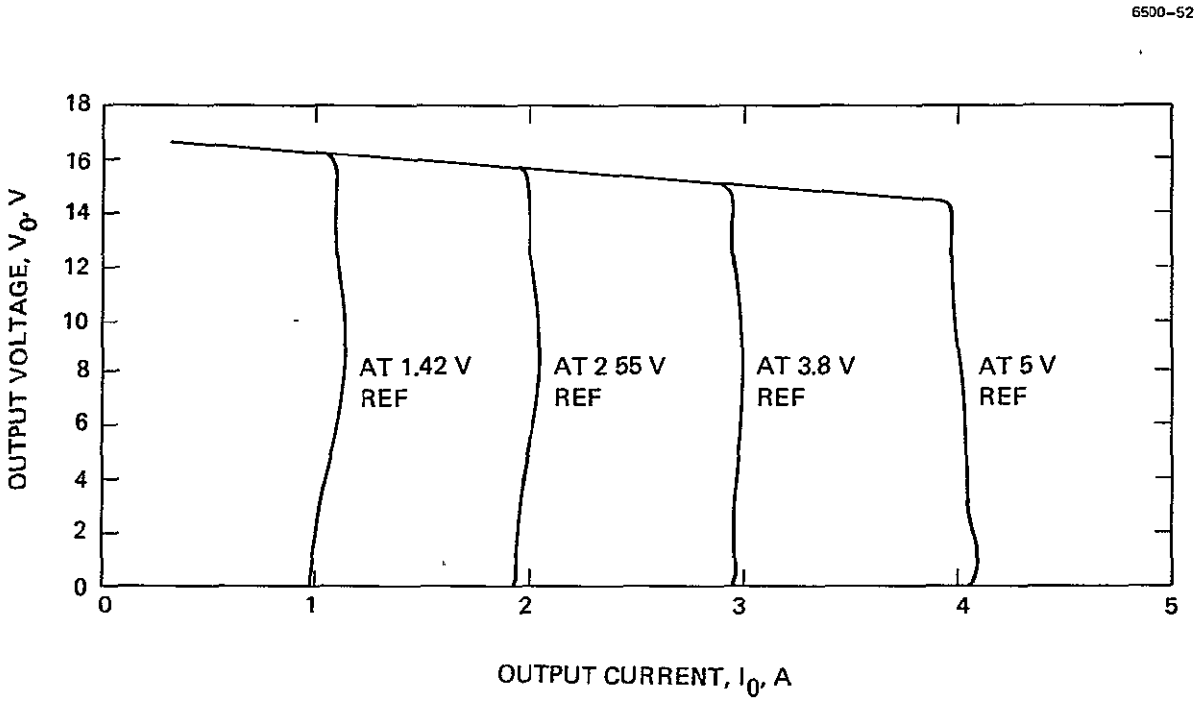

Figure 17. Main cathode heater.

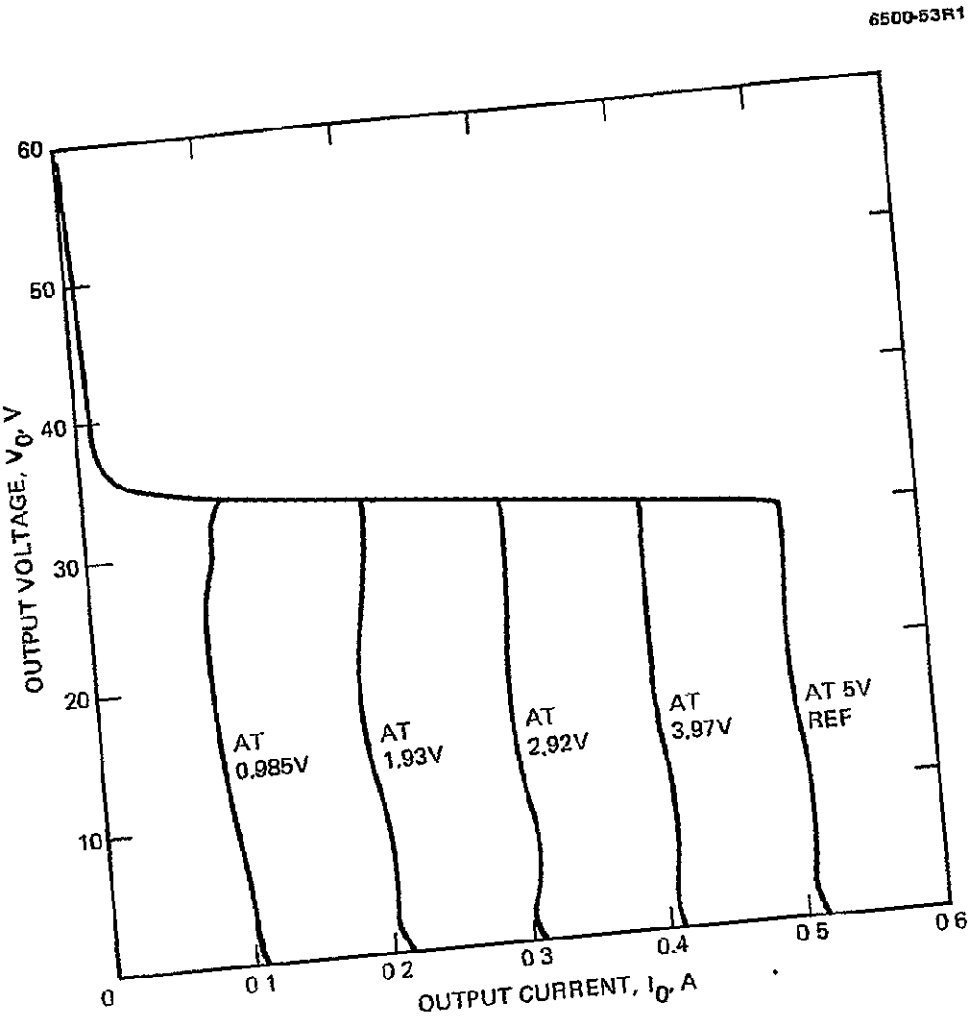

Figure 18. Main cathode keeper.

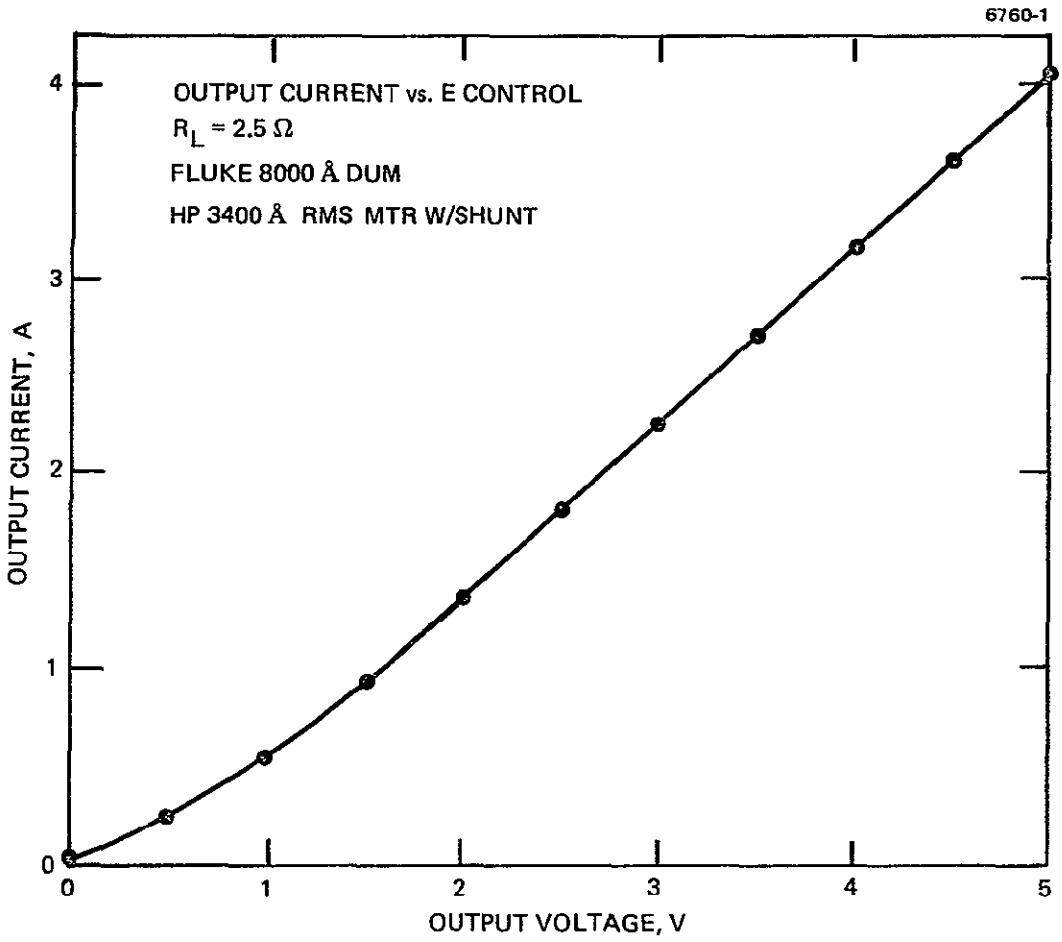

Figure 19. Main cathode heater.

The three-transistor switching regulators (screen, discharge, and ac distribution inverter) contain a common inverter module. Figure 20 is a schematic of the current feedback, crossover-protected inverter. Current feedback from the drive-transistor collectors boosts the base drive at elevated powers. This enhances the efficiency at moderate and low power levels by lowering the drive to the main transistors. Crossover protection within the inverter is also employed to maintain minimum transistor stress at or near 100% modulation.

The basic inverter design is employed at the three locations by modifying the output transformer to accommodate the requirements of each supply. Local feedback within the inverter circuit is also adjusted to compensate for: (1) high inductive loading on the ac distribution inverter, (2) relative resistive loading on the discharge supply, and (3) reflected capacitive loading (due to the high turns-ratio) on the screen supply.

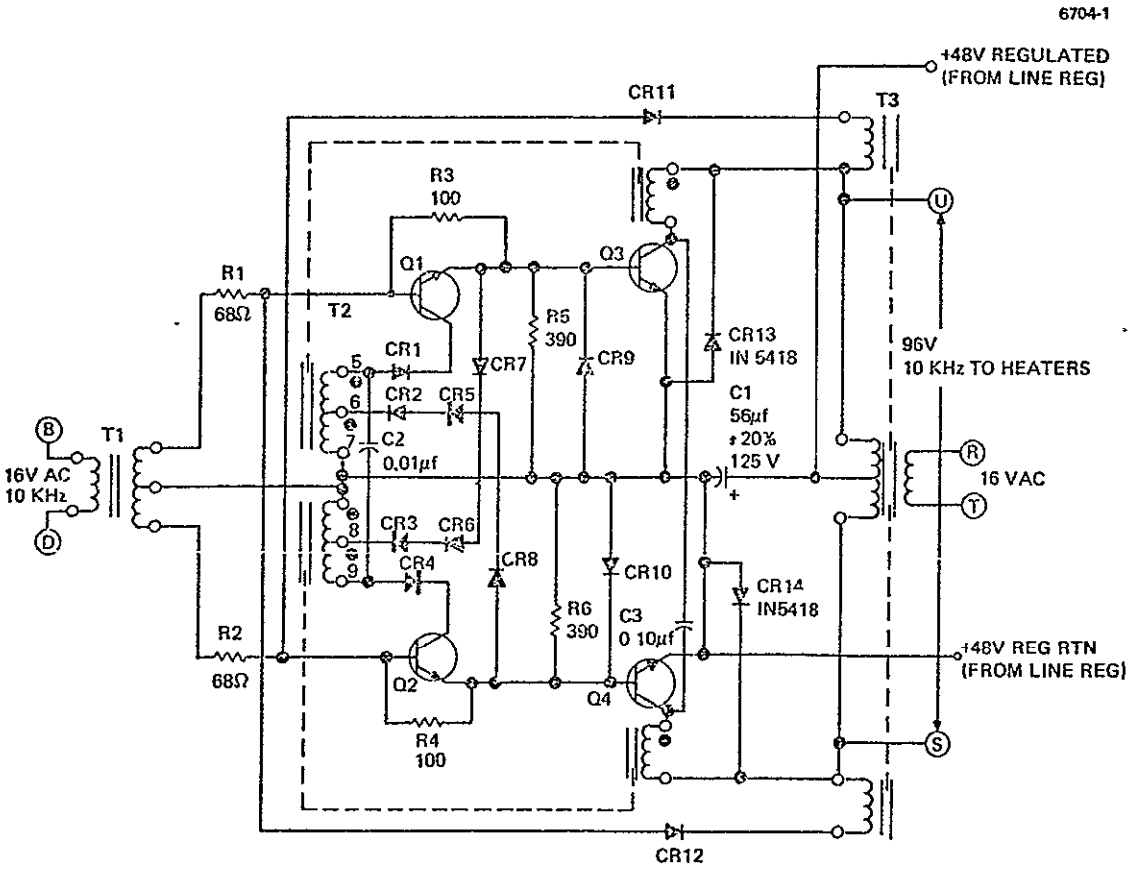

Figure 20. Basic inverter.

Figure 21 shows the basic pulse-width modulated (PWM) control used by two of the three supplies, the screen and discharge supplies. The basic carrier frequency of 10 kHz drives through the two transformers to the basic inverter circuit. The low-level transistor switch is driven by the PWM control logic, which allows either full 100% modulation (with the transistor commanded on) or various control pulse widths at an intermediate control level. By examining the waveforms in Figure 22, it is seen that the modulator is capable of 0 to 100% modulation about the fundamental carrier frequency.

Variations in feedback technique allow this inverter design to extend from voltage control to current control and any percentage combination of both. The ac-distribution inverter employs no pulsewidth modulator control. It is driven from a pre-regulated 48 V supply and its output is protected from damage by the control employed within the current-limited MAs and other loads attached.

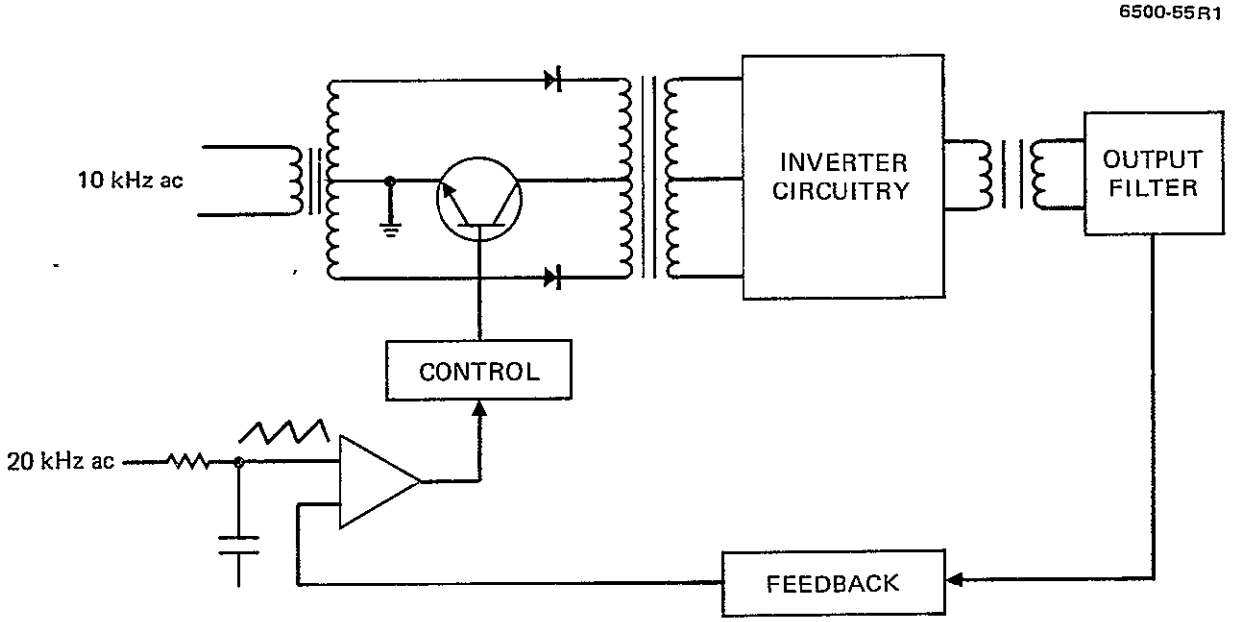

Figure 21. Pulse width modulated drive to inverter circuitry.

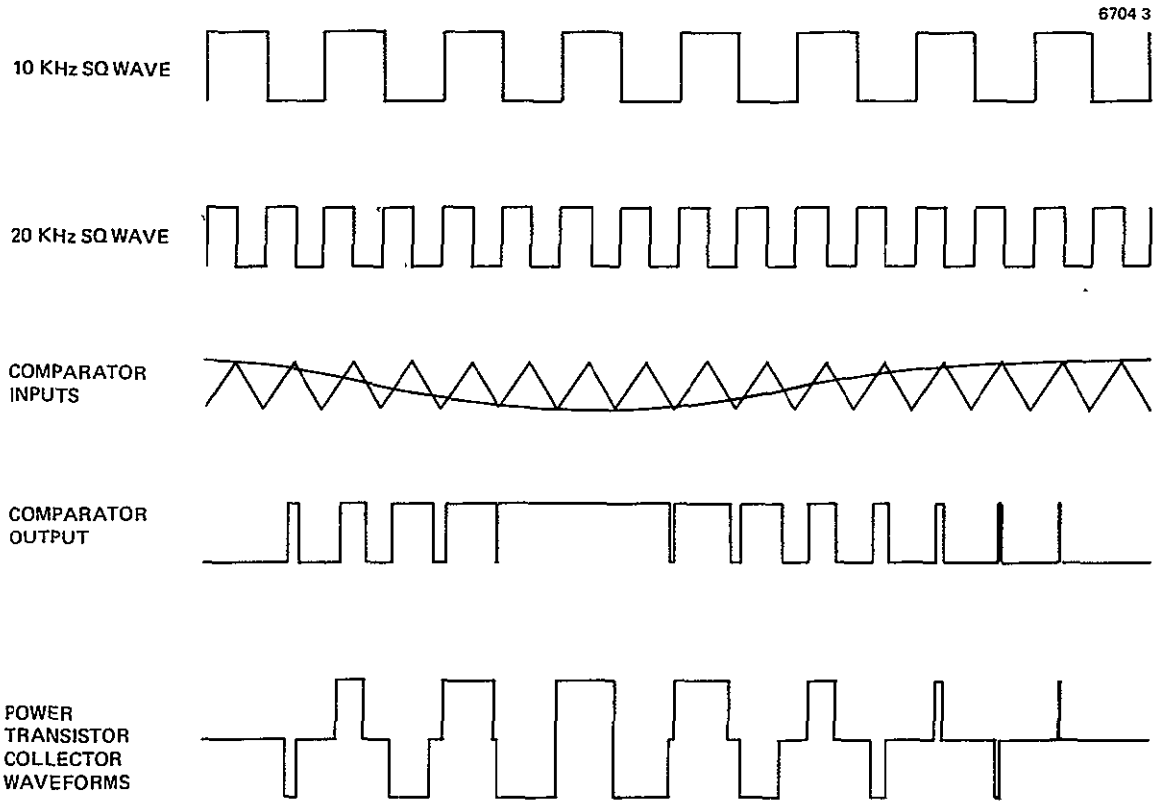

Figure 22. Pulse width modulator waveforms.

The discharge supply uses a current transductor in its output return to supply feedback for control of the PWM electronics. This provides inherent short-circuit-proof supply characteristics.

The load and output current of the discharge supply may vary. The input voltage can also vary independently with load and time, depending on the spacecraft used. The PWM control compensates for all of these variations and maintains high-efficiency operation.

The screen supply uses voltage feedbacks from the supply output which is "or" ed with the output of a fast-attach, slow-decay, ripple regulator that senses the supply output current to obtain current limiting. Since the output voltage and load of the screen supply remain essentially constant during operation, the PWM control is used primarily for line compensation and high-efficiency operation.

The screen and discharge supplies are controlled from the DIU. The discharge-supply output current is proportional to the 0 to 5 V reference. The screen supply is turned on and off by a 0 to 5 V command.

The linear-regulated accelerator supply is a voltage regulated (-300 Vdc), short-circuit-proof, series-pass-transistor design. The regulation is accomplished within a bridge network on the primary (96 Vac) side of the output transformer (see Figure 23). Magnetic isolation is used to maintain the integrity of the various grounds used in the system. Because of the low power involved (0.09 W), this normally inefficient design allows a low-voltage transistor to be used for the regulation; this greatly improves the reliability over any regulation techniques used in the higher voltage secondary.

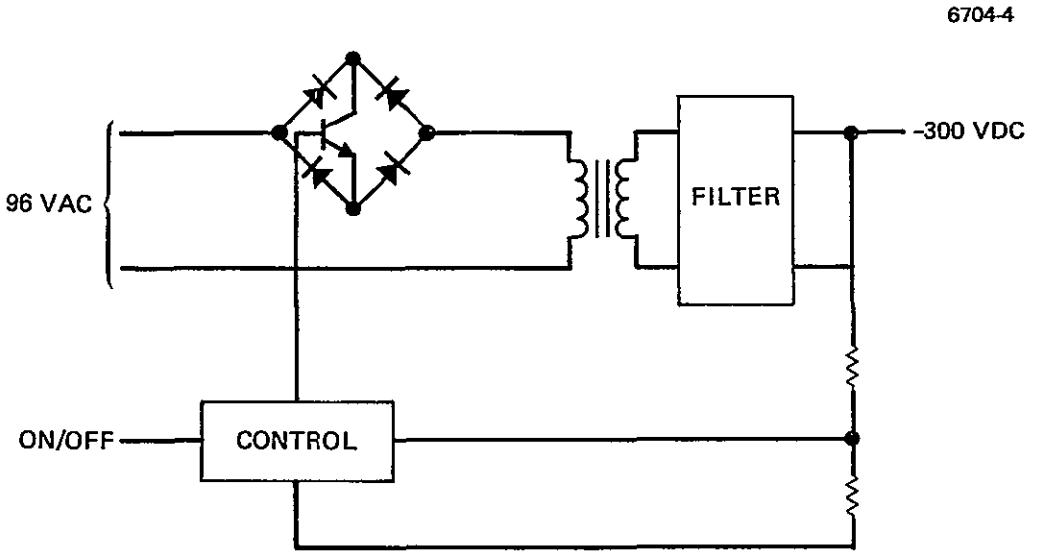

Figure 23. Accelerator supply.

The only supply not yet discussed is not directly associated with the output of the PEU. The 48-V line regulator is an extremely high-efficiency, constant-frequency (10 kHz) switching regulator used to preregulate the 70 ± 20 Vdc line for use by the ac distribution inverter. This preregulator is a voltage-feedback design. The control loop is compensated to allow for the negative impedance loading reflected through the ac distribution inverter from the magnetic amplifier supplies. The 70 ± 20 Vdc line is protected from any switching noise by an L-C line filter.

The high-voltage pulser circuits are included in the overall design to aid in the ignition of the neutralizer and main-keeper supplies. The output-transformer secondary is wired in series with each pulser's respective keeper supply. When activated by command, a 3 to 5 μsec internal pulse is directed to the keeper gap within the ion thruster to assist in the keeper-plasma ignition. The isolated circuitry runs directly from the 96-Vac line. The magnetics and terminals associated with the 5-kV pulse are all potted with a special uralane encapsulant material.

4. DIU Description

The DIU design philosophy complements the multiple-spacecraft-usage approach of the PEU. The entire PEU is controlled by 0 to 5 V commands issued by the DIU. The separately constructed units provide for logic-design changes in the DIU to properly interface with the on-board spacecraft telemetry and command systems employed in any spacecraft. The present design (with serial-data input lines) was chosen to minimize interwiring complexity of the spacecraft interface.

The present design is intended to be used with a sophisticated computer with the capability of maintaining proper thruster operation. The main automatic function included in the DIU design is the ability to recycle the thruster to normal operation after the occurrence of an arc in the thruster. The basic functions of the DIU are to:

- Provide storage for the computer serial commands
- Convert some of the commands to setpoint-control signals
- Provide D/A conversion of certain commands
- Turn off the PEU if the input power exceeds 200 W or if the solar cell bus falls below 50 Vdc
- Provide closed-loop control to the two vaporizer supplies
- Provide A/D conversion of the telemetry signals for use by the computer
- Recycle the thruster should an arc occur
- Generate a computer interrupt should an out-of-tolerance thruster-operating condition occur
- Provide drive to the thrust-vectoring gimbal motors.

The EM DIU uses CMOS-type logic elements wherever possible. This was done to reduce the standby power consumption and raise the system efficiency. The DIU receives its power from a housekeeping inverter that is in the DIU and operates from a +28 Vdc input-power bus. Power is sent from the housekeeping inverter to the line regulator and distribution inverter for power switching synchronization.

The DIU input circuitry includes all of the circuitry necessary to allow loading of the commands into the storage registers. A block diagram of the DIU input is shown in Figure 24. (The Command Code Dictionary is given in Appendix A.) The serial-input data is converted to parallel data by a serial-input shift register. The destination storage registers receive load commands from address-decode circuitry. The address decode also uses the outputs from the bit counter and parity checker to generate the load command.

The data bits held in the storage registers are used for a variety of functions. Certain bits are used to determine the states of the interrupt overrides. Other bits are used to control the on-off status of the individual supplies. The outputs of three of the registers are

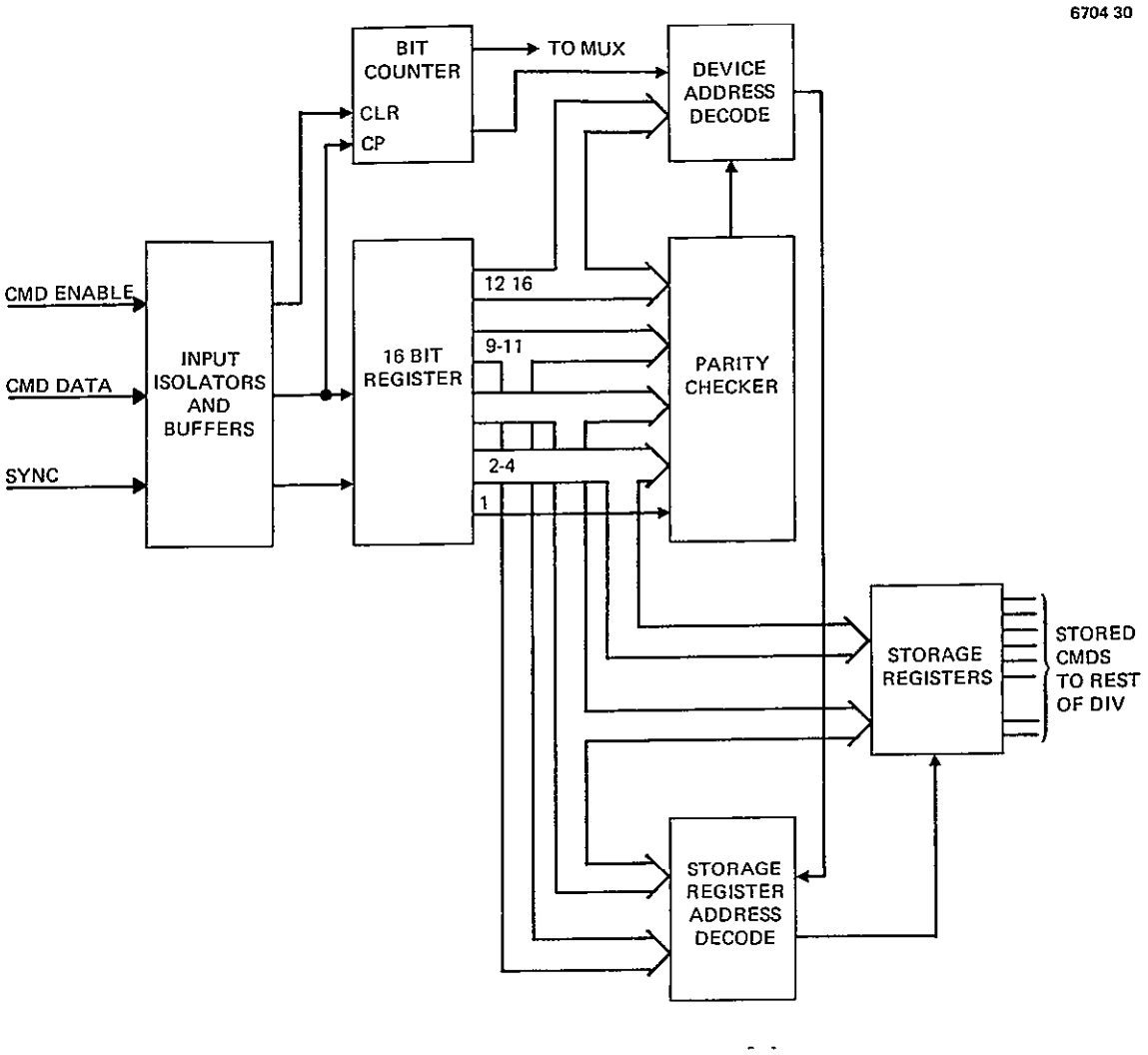

Figure 24. Block diagram of DIU input.

buffered and used as inputs to D/A converters. The outputs of the converters are used as the 0 to 5 V references for the cathode-vaporizer loop, the neutralizer-vaporizer loop, and the discharge-supply current. The operating set points for the other supplies are determined by multiplex (MUX) switches which are controlled by bits stored in the registers.

The DIU also contains the error amplifiers that provide closed-loop control of the cathode and neutralizer vaporizers. These amplifiers compare the telemetry from certain supplies to references from the D/A converters and appropriately adjust the control signals to the vaporizer supplies. For example, the amplifier that is in the neutralizer-vaporizer loop compares the telemetry of the neutralizer-keeper voltage (V_{NK}) to a D/A reference and adjusts the control signal to the neutralizer-vaporizer supply to maintain the keeper voltage at the desired value. The amplifier in the cathode-vaporizer loop operates in a similar fashion except that it is controlled by the difference between the telemetries of the discharge supply voltage and the discharge-keeper voltage ($V_D - V_{DK}$).

The thruster is recycled, whenever an arc occurs, by circuitry that primarily consists of three mono-stable multivibrators that are triggered by an overload of the screen supply. The multivibrators control the length of time that the screen and accel supplies are turned off and the discharge supply is cut back. The length of time for these events can be adjusted by changing an R-C time constant associated with each multivibrator.

An interrupt can be generated by the DIU depending on certain thruster operating conditions and the status of interrupt-override bits. The DIU monitors the values of the telemetry channels of the beam current, accel current, and neutralizer-keeper current. If any of these values goes beyond a predetermined limit (providing the appropriate override is not set), the interrupt will be generated and the thruster system will be shut down. Also, an interrupt will be generated (and thruster system shut-down will occur) if the system is left on for 12 hr without updating the screen-on command or if excessive recycling occurs. The thruster system will also be shut down if the solar-panel

bus voltage falls below 50 V or the input power from this bus exceeds 200 W.

When a measurement request is received by the DIU, the requested analog-telemetry channel is switched to an A/D converter through a MUX switch. The output of the A/D converter is then loaded into a parallel-to-serial shift register. At the appropriate time in the DIU command response, the contents of the register are shifted onto the response line to obtain the desired serial data.

The two gimbal motors in the thruster gimbal receive their drive from the DIU. The commands to actuate the gimbal motors define which motor is to be driven, in which direction, and for how many steps. The format of these commands is given in the Command Code Dictionary (Appendix A).

5. Cables (High Voltage)

The various supplies within the PEU are interconnected in a standard manner by cables and connectors located on one end of the housing. The connectors are locked into place by the use of double-screw mating. These connectors are of the type commonly used aboard various spacecraft.

The high-voltage interconnections (refer to Figure 14, the grounding schematic) within the PEU are secured by direct soldering of high-voltage wire to special terminals. These connections are then potted with a uralane encapsulant to maintain high-voltage integrity, and the entire interconnection area (both low and high voltages) is covered with a sheet metal protector.

The output connectors to the thruster are of flight quality, and the high voltages are handled with specially prepared high-voltage cables and Reynolds Series 1807 connectors. The high-voltage-cable assemblies are prepared at the Hughes Components and Materials Laboratories and extensively tested prior to installation and use. A carefully planned shielding scheme is used to isolate and protect all adjacent cabling from the +1200 V screen potential and the +5 kV ignition pulses carried within the cables.

SECTION 3

TESTING

Testing performed under this program began with a series of optimization tests of a Government Furnished Equipment (GFE) 8-cm SIT-8 thruster (SIT-8). This was followed by acceptance testing of the optimized EM 8-cm Thruster and concluded with an EM 8-cm Thruster System Cycling Test. These tests are described in this section; the parameter nomenclature, test circuitry, and calculation procedures are described in Appendix B.

A. THRUSTER OPTIMIZATION

Optimization of a SIT-8 was undertaken at the beginning of this program. The basic configuration of the 8-cm EM Thruster (as specified by the critical dimensions indicated in Figure 25) were determined by these tests which were directed towards optimizing discharge specific energy ε_I, discharge propellant utilization η'_{Hg}, and neutralizer coupling characteristics, while maintaining stability of thruster operation. The discharge specific energy is given in watts per beam ampere instead of the usual energy per beam ion. The small number of multiply charged ions that exist make the use of the usual eV/ion imprecise. The numerical sequence of the optimization tests began with Test No. 25.

1. Tests Nos. 25, 26, and 28

Test No. 25 was performed with the unmodified SIT-8 discharge chamber without the separate igniter electrodes for the keepers that had existed during an earlier program. Operation of this configuration was marred by regions of noisy and unstable operation when it has operated far from the nominal set point. These instabilities were felt to be unacceptable because extinction of the discharge would result from passing through an unstable operating region. In Test No. 26, the thruster endplate was moved upstream by 1.27 cm while leaving the cathode-to-screen and cathode cup polepiece (CCP)-to-screen (dimension L)

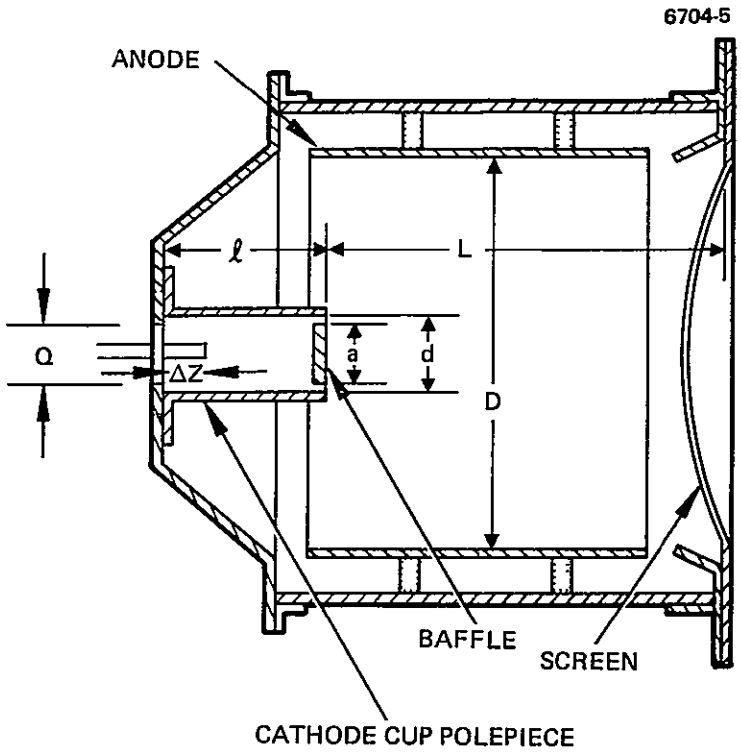

L = DISCHARGE CHAMBER LENGTH

D = DISCHARGE CHAMBER (ANODE) DIAMETER

ℓ = CATHODE-CUP POLEPIECE (CCP) LENGTH

d = CCP DIAMETER

a = BAFFLE DIAMETER

ΔZ = DISTANCE FROM CATHODE TIP TO POSITION (NEAR THRUSTER ENDPLATE) WHERE AXIAL MAGNETIC FIELD VANISHES

Q = DIAMETER OF OPENING ON THRUSTER ENDPLATE

Figure 25. Schematic of the thruster discharge chamber configuration.

distances unchanged. This was accomplished with the aid of a thruster-shortener configuration similar to what is formed by mounting the end-plate of Figure 25 in a reverse orientation. Although this configuration exhibited a somewhat reduced level of performance, thruster operation was marked by the total absence of unacceptable instabilities. This enhanced thruster stability and permitted continuous variation of the discharge current from near zero to I_D = 1.5 A without encountering the high-amplitude, low-frequency oscillations typical of earlier configurations when they were operated far from the nominal setpoint. Stability of operation was largely insensitive to a wide range of variations in both discharge and main-keeper current, although performance, of course, varied with the choice of operating point. The significant reduction of the thruster performance that resulted from the change to the shortened discharge chamber indicated the need for reoptimization about the new configuration. The extent of thruster performance reduction is seen in tabular form in Table 7 by comparing the discharge-chamber propellant utilization, $\hat{\eta}_{Hg}$, and the discharge specific energy, ε_I, for Tests Nos. 25 and 26.

The cathodes used in Tests Nos. 25 and 26 had porous-tungsten inserts and required 10 W of power to maintain a low keeper voltage and avoid discharge extinction. The next test was performed in an effort to eliminate this cathode power, which had to be supplied to the discharge and neutralizer cathodes. In Test No. 28, the configuration was unchanged from that of Test No. 26, except that rolled tantalum-foil cathode inserts (coated with R-500 mix) replaced the impregnated porous-tungsten inserts. Once ignited, both the discharge and neutralizer cathodes ran at low keeper voltages without the need of tip power. The discharge could be varied smoothly from 50 mA < I_D < 1.5 A (even with no discharge-keeper current) without unacceptable instability, and operated well over a wide range of discharge voltages. The rolled tantalum-foil inserts were used in all subsequent tests.

Table 7. Optimization Summary for Tests Nos. 25, 26, and 28

Test No.	Configuration Description	Discharge-Chamber Propellant Utilization, $\tilde{\eta}_{Hg}$%	Discharge Specific Energy (Including Keeper Losses) ε_I, W/A	Required Discharge-Cathode-Tip Heater Power, W
25	• No igniters	81.4	413	10.0
	• Full-Length Discharge Chamber	74.1	381	10.0
	• Porous Inserts			
26	• No Igniters	79.0	481	10.5
	• Shortened Discharge Chamber	78.1	467	10.5
	• Porous Inserts			
28	• No Igniters	70.6	458	0
	• Shortened Discharge Chamber	68.5	369	0
	• Ta foil Inserts			

5911

2. Tests Nos. 29, 30, 31, 32, and 33

For Tests Nos. 29-33, several variations in the baffle diameter and a cathode-tip position, ΔZ, were investigated, and a new discharge chamber was tested in which the overall length was reduced. Results of these tests are shown in Table 8. The length of this new, shorter discharge chamber was selected to make it equivalent to the original chamber with a shortener in place. This was done to verify the results gained with the shortener and because the two chambers would not be expected to operate exactly the same (i.e., the equivalence is not exact).

In Tests Nos. 29 and 30, two different baffle sizes were evaluated in the shortened-chamber configuration. Both tests produced highly stable, quiet operation, but the thruster could not reach high beam currents, even with the larger (a = 2.06 cm) baffle.

Test No. 31 was performed to determine if the stability and limited-beam-current characteristics of previous tests were due to the fact that the chamber was shorter, or that the cathode location was now at the zero-magnetic-field point (near the plane of the endplate): the thruster was returned to its normal full-length configuration, but the cathode was pulled back to the plane of the endplate. Resulting performance was very poor, with violent instabilities prevalent throughout the operating range. Higher beam currents were inaccessible, as in the shortened-chamber tests.

These results led to the tentative conclusion that (a) the cathode-to-CCP distance must be close to the normal SIT-8 value for the stability of operation, and (b) the difficulty in achieving higher beam currents results from the placement of the cathode in the plane of the endplate.

Based on the interpretation above, Test No. 32 was conducted with the chamber shortener in place, but with the cathode pushed downstream to $\Delta Z = 0.26$ cm. This change restored the available beam current to the design value $I_B = 72$ mA, while retaining some of the stability properties of Test No. 29. However, operation with a discharge-keeper current $I_{DK} < 100$ mA would cause the thruster to go out, and the discharge current contained transient spikes up to $\tilde{I}_D = 2$ A in amplitude.

Table 8. Optimization Summary for Tests Nos. 29, 30, 31, 32, and 33

Test No.	Test Configuration	Δz,[a] cm	Baffle Diameter, a, cm	Cathode to CCP lip Spacing, cm	Discharge Chamber Mass Utilization, $\tilde{\eta}'_{Hg}$, %	Discharge Energy ε_I, W/A	Beam Current I_B, mA	Stability	Noise
29	Full-length chamber with 1.27 cm shortner	0.00	1.91	1.77	70.6	458	59	Completely stable over full operating range	Extremely quiet; $\tilde{I}_D$ = 600 mA p-p at 1 MHz
30	Full-length chamber with 1.27 cm shortner	0.00	2.06	1.77	65.4	510	52	Completely stable over full operating range	Extremely quiet; $\tilde{I}_D$ = 600 mA p-p at 1 MHz
31	Full length chamber; no shortner; cathode pulled back	0.00	1.91	1.77	62.2	663	54	Highly unstable at all operating points	Strong oscillation at 17 kHz, $\tilde{I}_D \approx 1$ A p-p
32	Full-length chamber with 1.27 cm shorter	0.26	1.91	1.06	70.6	508	72	Stable, except goes out for $I_{DK} < 100$ mA	Transient spike noise; $\tilde{I}_D \approx 2$ A p-p
33	New short chamber with dished end plate	0.03	1.91	1.67	70.7	540	71	Completely stable over full operating range	Transient spike noise; $\tilde{I}_D \approx 2$ A p-p

Operating Parameters: V_B = 1200V; V_A = -300V; V_D = 40V (except Test No. 33, where V_D = 36.5V)

[a]Δz = Distance downstream to the cathode tip from the point (near thruster endplate) at which the axial magnetic field vanishes.

5911

For Test No. 33, a new, shorter shell was fabricated, employing shorter magnets and a dished endplate. The dished endplate afforded greater structural rigidity than the flat endplate previously employed. For this test, axial cathode placement was between the values employed in Tests Nos. 30 and 32, but closer to the plane-of-the-endplate location employed in Tests Nos. 29 to 30. Thruster performance in this configuration was highly stable, but retained the transient spikes in the discharge current that characterized the configuration of Test No. 32. Also, high beam currents were reached only at high discharge current and low discharge voltage.

To summarize the results of this group of tests, two variables were altered to investigate the effects on thruster performance: cathode-to-CCP lip distance and cathode-to-endplate distance. Increasing the cathode-to-CCP lip spacing from the standard SIT-8 value was found to produce instability and high noise levels. When the cathode-CCP lip spacing was at its normal value and the endplate plane was made to coincide with the cathode tip (by changing the thruster length), thruster operation was characterized by great stability but reduced beam-current capability.

3. Tests Nos. 34, 35, 36, and 37

This group of tests was conducted to evaluate the performance of the GFE thruster with the ion machined SHAG beam-extraction system.[5] The thruster was tested in three different configurations with a short discharge chamber and once with the normal, full-length chamber. The results are summarized in Table 9.

Initial operation of the thruster with the short discharge chamber and SHAG optics was performed in Test No. 34. In this configuration, the axial cathode location was left unchanged from the plane-of-the-endplate position employed previously in Test No. 33. Thruster performance was poor in this configuration, achieving a discharge-chamber propellant utilization $\tilde{\eta}_{Hg}$ = 70% at ε_I = 487 W/A. In addition, the thruster stability was poor, with a high level of discharge-current noise.

Table 9. Optimization Summary of Tests Nos. 34, 35, 36, and 37

Test No.	Configuration Description	Stability Trends	Discharge-Chamber Propellant Utilization $\tilde{\eta}'_{Hg}$, %	Discharge Specific Energy ε_I, W/A	Discharge Voltage, V_D, V
34	Short Chamber	Poor, Noisy	70	487	40
35	Short Chamber, 16 magnets	Very Poor	Unable to obtain data		
36	Full Length Chamber 10 Magnets	Poor	92	302	40
37	Short Chamber 8 Magnets	Very Good	92 83	420 295	34 30

5911

In Test No. 35, additional magnets were fitted to the thruster. A peak axial magnetic field of B_{zmax} = 93 G was produced with 16 magnets. In this configuration, the thruster was violently unstable, with a visibly flashing discharge. Application of beam voltage failed to extract a beam, producing only large accel currents, and, finally, discharge extinction.

The standard full-length chamber was employed with the SHAG extraction system in Test No. 36 to establish a baseline performance level for comparison with the short-chamber tests. This configuration proved to be highly efficient, but suffered from poor stability and limited operating range. In particular, any sudden change in operating parameters, or even a gradual change beyond narrow limits, would produce a violent discharge-mode transition; the resultant mode was characterized by high discharge voltage, producing vaporizer runaway. In addition, no beam was extracted in this mode, although a large beam current was incident on the accelerator grid. Although the full-length SIT-8 configuration with SHAG extraction produced a dramatically high performance, it was not acceptable.

In Test No. 37, the short discharge chamber was employed; this time with the cathode tip placed upstream from the thruster endplate. This unusual geometry was chosen after surveying previous test results in which a discharge-chamber shortener had been used in the full-length thruster shell. Of these tests, best stability was achieved when the cathode tip was upstream of the point at which the axial magnetic field vanishes. The use of a dished endplate with the short thruster shell caused this zero-field point to move upstream and required relocation of the cathode.

The thruster in this configuration displayed great stability, high performance, and remarkable immunity to variations of operating parameters (see Table 10 for representative operation in Test No. 37). Abrupt changes in discharge or keeper currents did not produce instability or mode-switching; the discharge current could be varied smoothly from zero to $I_D \geq 1$ A without instability and with a smooth continuous response of

Table 10. 8-EM Thruster Operating Conditions at 1 mlb Nominal Thrust

Test Point No.	37-1		37-6	
Thrust[a] (ideal), T, N, (mlb)	5.30 (1.19)		5.21 (1.17)	
Specific impulse,[a] Isp, sec	2974		2700	
Total input power, P_T, W	136.7		125.9	
Total efficiency,[a] η, %	56.3		54.7	
Power efficiency, η_E, %	65.7		70.4	
Total utilization,[a] $\tilde{\eta}_{Hg}$, %	85.6		77.7	
Discharge utilization,[a] $\tilde{\eta}'_{Hg}$, %	91.9		83.2	
Total neutral flow, I_{HG}, mA	86.4		94.0	
Power/thrust,[a] W/N, (W/mlb)	25.8 (114.8)		24.1 (107.4)	
W/A excluding keeper, V	423		288	
W/A including keeper, ε_I, V	433		300	
Beam current, I_B, mA	74		73	
Anode to neutralizer-tip potential, V_B, V	1234		1230	
Neutralizer floating potential, V_N, V	-20		-15	
Output beam power, P_B, W		89.84		88.70
Accelerator voltage, V_A, V	-300		-300	
Accelerator drain current, I_A, mA	0.70		0.44	
Accelerator drain power, P_A, W		0.21		0.13
Discharge voltage, V_D, V	34		30	
Emission current, I_N, A	0.92		0.70	
Discharge power, P_D, W		31.3		21.0
Discharge				
Keeper voltage, V_{DK}, V	8.0		9.5	
Keeper current, I_{DK}, A	0.100		0.100	
Keeper power, P_{DK}, W		0.8		0.95
Heater voltage, V_{DH}, V	0		0	
Heater current, I_{DH}, A	0		0	
Heater power, P_{DH}, W		0		0
Vaporizer voltage, V_{DV}, V	3.9		4.1	
Vaporizer current, I_{DV}, A	1.4		1.5	
Vaporizer power, P_{DV}, W		5.5		6.2
Flow rate, I_{DHg}	80.5		87.7	
Neutralizer:				
Keeper voltage, V_{NK}, V	14.0		14.0	
Keeper current, I_{NK}, A	0.400		0.400	
Keeper power, P_{NK}, W		5.60		5.60
Heater voltage, V_{NH}, V	0		0	
Heater current, I_{NH}, A	0		0	
Heater power, P_{NH}, W		0		0
Vaporizer voltage, V_{NV}, V	2.3		2.5	
Vaporizer current, I_{NV}, A	0.85		0.90	
Vaporizer power, P_{NV}, W		1.96		2.20
Flowrate, I_{NHg}, mA	5.9		6.3	
Neutralizer coupling power, P_N, W		1.44		1.10

[a]Accounting for neutralizer floating potential V_N, but neglecting beam divergence and double ionization.

5911

the beam current. Also, a wide range of discharge voltages could be employed, with good performance available even at a discharge voltage V = 30 V. The performance obtained in this configuration is compared with previous test results in Figure 26. The two curves at left represent data taken with the SIT-8 fitted with conventional extraction electrodes. The leftmost curve corresponds to configurations using a discharge-chamber shortener, while the second curve represents operation with an unshortened chamber and no auxiliary electrodes. The remaining two curves display the results of Tests Nos. 36 and 37.

The curve to the extreme right represents the performance in the full-length-shell configuration employed in Test No. 36; the curve immediately to the left corresponds to Test No. 37, in which the short chamber was used. Inspection of these curves invited two immediate conclusions. First, use of the SHAG optics afforded a dramatically high performance in either configuration; second, the mild reduction of thruster performance in the short-chamber configuration was not fully eliminated. However, operation of the short-chamber thruster has only been performed at reduced discharge voltages. These results indicated that steps had to be taken to increase the discharge voltage.

4. Tests Nos. 38, 39, 40, 41,42, 44, and 45

Those tests leading to Test No. 37 provided the understanding that axial placement of the main-cathode tip relative to the thruster endplate was critical for achieving stable operation; this is because the magnetic field lines near the opening in the endplate diverge strongly, so that a slight axial repositioning of the cathode tip alters the primary-electron trajectories in a dramatic fashion.

In Tests Nos. 38-45 (see Table 11), higher performance was sought from the short-chamber configuration by modifications introduced to induce operation at higher discharge voltages. It was found that increasing the magnetic field strength to achieve this end produced violent instabilities, but that performance was enhanced by the higher operating voltage ($V_D \gtrsim 40V$). In the configuration of Test No. 45, higher voltage was achieved by increasing the baffle diameter from

Table 11. Optimization Summary of Tests Nos. 38, 39, 40, 41, 42, 44, and 45[a]

Test No.	Configuration Description	Stability Trends From Previous Test	Discharge-Chamber Propellant Utilization $\tilde{\eta}'_{Hg}$, %	Discharge Specific Energy ε_I, W/A	Discharge Voltage, V_D, V
38	Add 4 magnets for total of 12	Highly unstable	95	461	40
39	10 magnets	Still unstable, but improved	91	316	36
40	8 magnets; cathode moved 0.127 cm downstream	Worsened stability	91	423	40
41	Return cathode to test 37 location; open propellant diversion ports	Marginally unstable, but marked improvement	95 86	428 310	36.5 31.5
42	Shorten screen collar 0.635 cm	Essentially no change	92 85	396 336	34.4 31.8
44	Replace full-length screen collar, ports still open	Essentially no change	94	410	40
45	Larger baffle: a = 2.064 cm	Essentially no change	98 95	356 276	37 36

[a]Test No. 43, with the photoetched SHAG optics, was the configuration of test No. 37 and is described in the text.

5911

a = 1.905 to a = 2.064 cm and opening propellant-diversion ports in the cathode-cup polepiece. This operation at higher discharge voltage produced the expected performance gain.

5. Tests Nos. 46, 47, and 48

The remaining optimization tests were undertaken to obtain the desired discharge-current stability and increased value of discharge voltage. As an initial step toward achieving discharge-current stability, the diameter of the thruster-endplate opening was increased to a value Q = 3.56 cm so as to reduce the magnitude of the magnetic-field near the opening in the endplate to the minimum value determined by the cathode-cup polepiece itself. The purpose of the subsequent test sequence was to concentrate attention in two areas: first, the axial cathode location was varied to achieve improved stability of operation; second, baffle diameter, a, and the transparency of propellant-diversion ports were varied to achieve the desired discharge voltage ($V_D \approx 37$ V) at the design beam current $I_B = 72$ mA. The test results are tabulated in Table 12.

In the first of the tests (Test No. 46), the cathode was placed 2.22 cm upstream of the endplate, at the location where the axial magnetic field gradient was zero ($\nabla B \cdot z = 0$). The stability of this test was only average, and performance was markedly below that of previous configurations. Accordingly, in Test No. 47, the cathode was returned to its former (Test No. 37) location, in which the tip was 0.343 cm upstream of the downstream surface of the endplate. This configuration proved to be more stable than other configurations and marked a return of high performance. In the configuration of Test No. 47, the thruster operated over a wide range of discharge voltages and currents, but required very low discharge-keeper current ($I_{DK} \leq 50$ mA) to avoid mode-changing-type instabilities. The cathode arrangement employed in this test (cathode tip 0.343 cm upstream of the endplate) represented the best compromise between stability and performance achieved and was retained in the next test. The remaining time was employed to optimize the baffle diameter and propellant-diversion-port transparency.

Table 12. Optimization Summary of Tests Nos. 46, 47, and 48

Test No.	Cathode Tip Placement,[a] cm	Baffle Diameter	Propellant Diversion Ports	Discharge Chamber Propellant Utilization $\tilde{\eta}'_{Hg}$, %	Discharge Specific Energy ε_I, W/A	Discharge Voltage, V_D, V
46	2.22	2.06	Open	87.2	405	34
47	0.34	2.06	Open	96.6	284	38
				93.0	272	37
				91.8	248	35
48	0.34	2.06	Closed	98.1	377	35
				85.0	310	32
				78.2	266	30

[a]Values are distance upstream of the downstream surface of the endplate.

5911

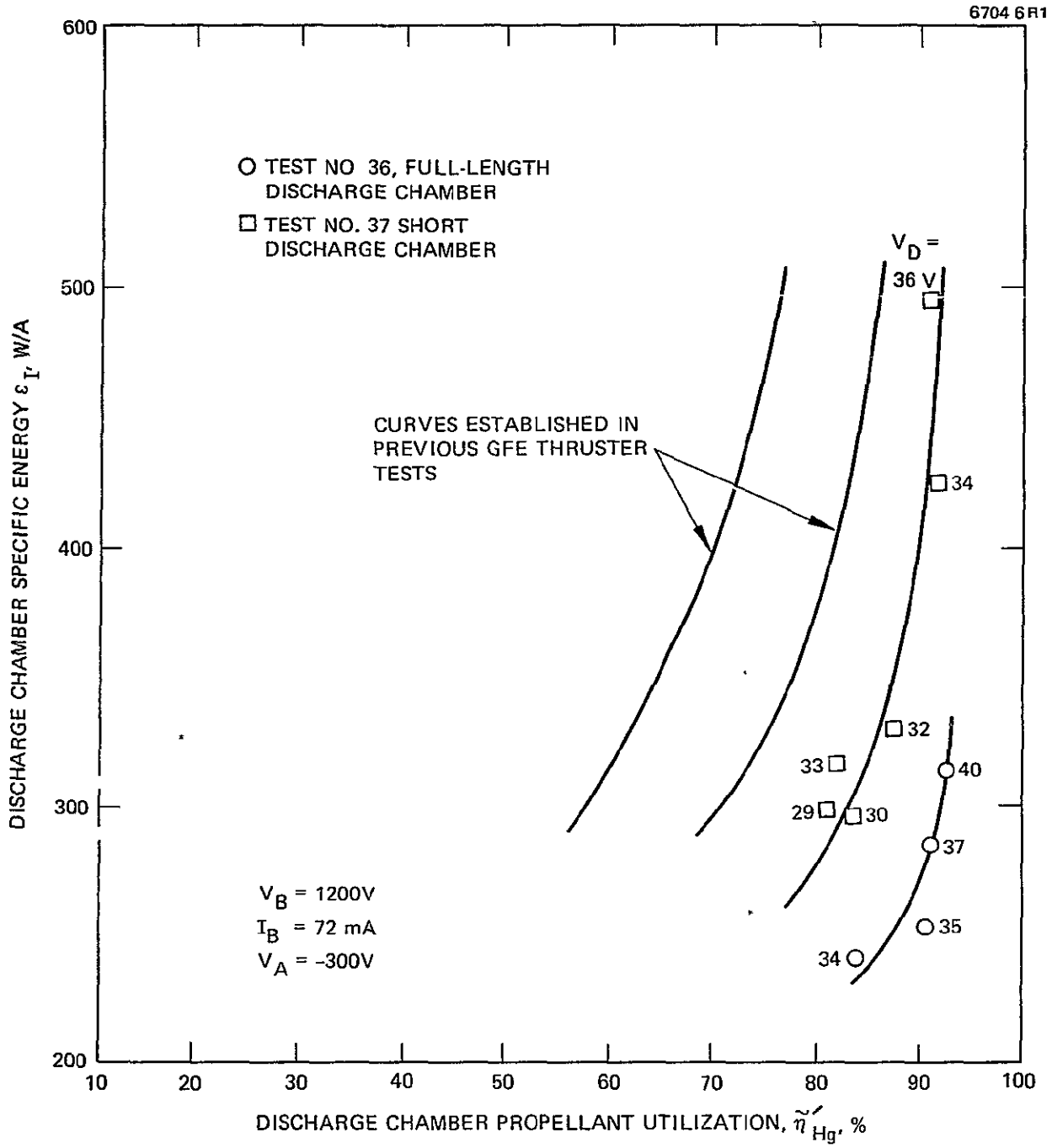

Figure 26. SIT-8 thruster performance with SHAG extraction electrodes. (Discharge current I_D and mercury flowrate $I_{D,Hg}$ are adjusted to maintain constant screen current I_S).

Operation of the thruster in all tests previous to Test No. 45 had employed a baffle diameter a = 1.905 cm; these tests were characterized by operation at relatively low discharge voltage. Accordingly, an increased baffle diameter of a = 2.064 cm was employed in Test No. 45 to increase the discharge voltage. This change produced an improved performance. In Test No. 48, the ported cathode-cup polepiece was replaced with a nonported element to evaluate the efficacy of the propellant diversion ports. The effect of this change can be seen clearly in Figure 27. The configurations of Tests Nos. 47 and 48 are identical except that the propellant-diversion ports were open in Test 47 and closed in Test No. 48. The data plotted in Figure 27 show that closing the ports produced operation at lower discharge voltage, with a corresponding performance degradation. A final variation in baffling was evaluated in which open ports were employed with a large (a = 2.22 cm) baffle. Since the results of this test (Test No. 49) proved not to be repeatable, they are not presented.

6. Final Configuration

The final configuration that was chosen for the 8-cm EM thruster is characterized by high performance, good stability, and operation at a moderate discharge voltage (36 V < V_D < 38 V). The dimensions are listed in Table 13.

7. Cathode Startup

Neutralizer and discharge-cathode startup characteristics were investigated during Tests Nos. 32 and 33. Before these tests began, the thruster was exposed to the laboratory ambient environment during thruster modifications. The initial startup conditions were recorded, as well as the second startup, after being in the off condition overnight in the vacuum environment. The initial startup conditions for the neutralizer cathode are shown in Table 14. The only cathode

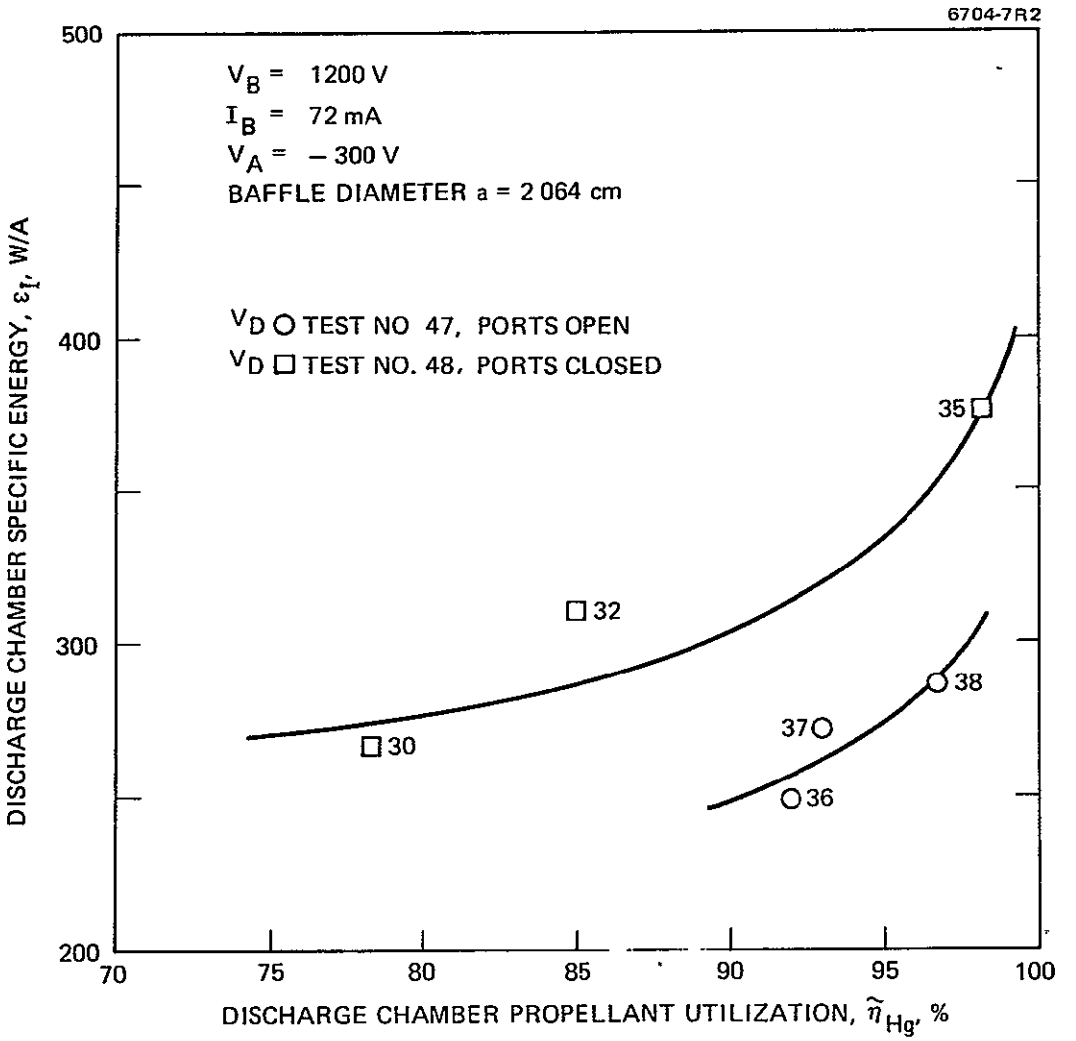

Figure 27. SIT-8 thruster performance with propellant diffusion ports open and closed. Ion machined grid set.

Table 13. EM 8-cm Thruster Dimensions

Outer shell O.D.	9.398 cm
Anode I.D., D	8.563 cm
Anode length	6.805 cm
Outer shell length	7.849 cm
Endplate dish depth	0.635 cm
Optics dish depth	0.330 cm
Discharge chamber length, L	6.747 cm
CCP length, ℓ	1.742 cm
Screen polepiece length	0.635 cm
Upstream magnetic flange length	0.475 cm
Screen polepiece inner diameter	8.407 cm
Number of magnets	8
Magnet length	7.823 cm
Downstream magnetic collar length	1.168 cm
Baffle diameter, a	2.065 cm
CCP diameter, d	3.810 cm
CCP wall thickness	0.127 cm
Number of CCP ports	16 holes
Port diameter	0.783 cm
Diameter of opening in thruster endplate, Q	3.560 cm
Downstream distance from cathode tip to position (near thruster endplate) where magnetic field vanishes, ΔZ	-0.343 cm
Tantalum coating thickness (endplate and CCP)	0.0127/0.0203 cm
Anode to screen polepiece spacing	0.152/0.191 cm
Anode to endplate spacing	0.254 cm

5911

conditioning provided was Ohmic heating of P_{NH} = 20 W* to the cathode tip before going through the startup sequence. The keeper voltage was about V_{NK} = 600 V and was manually turned on for each of the settings listed in the table.

It can be seen from Table 14 that P_H = 30 W was required for initial neutralizer cathode startup. Initial startup characteristics of the discharge cathode were similar, except that a mercury flowrate I_{NHg} > 100 mA was required for starting at P_{DH} = 30 W. Both cathodes could be restarted after cooldown with P_H = 25 W of tip heater power and flowrates comparable with initial startup. It may be concluded that the startup sequence used demands that 30 W be furnished to the cathode heaters for the first start. This power requirement could probably be lowered by using a longer preheat period.

8. Neutralizer Coupling

The SIT-8 thruster was also used to investigate neutralizer coupling to the ion beam. The axes of the neutralizer and thruster were pointed in the same direction. The neutralizer axis was located radially outward from the thruster axis to clear the thruster body with sufficient distance to avoid mechanical or electrical interference. The axial location of the neutralizer cathode was determined by the requirement

Table 14. Initial Neutralizer Startup Characteristics

Test No. 32			Test No. 33		
P_{NH}, W	I_{NHg}, mA	Start at V_{NK} = 600 V	P_{NH}, W	I_{NHg}, mA	Start at V_{NK} = 600 V
20	14.7, 40.5	No	20	16.2	No
20	67, 108	No	25	15.2, 41, 64	No
25	26, 112	No	30	29	No
30	31.5	Yes	30	64	Yes

5911

*Powers reported here are those measured at the power supply; about 10% of this power is dropped in the cables to the thruster.

that the leading edge of the neutralizer-keeper electrode lie on a line which intersects the thruster axis at a 45° angle and which passes through the outermost aperture (closest to the neutralizer) of the accel electrode. This position was kept constant for the two tests performed.

For neutralizer keeper currents of 500 mA and 750 mA, there existed a neutralizer flowrate I_{NK} which gave a minimum coupling voltage. Increasing or decreasing I_{NHg} away from this value caused the coupling voltage V_N to increase. This behavior is shown in Figure 28 (for a 0.127-cm-diameter keeper aperture) where curves of coupling voltage, V_N, versus neutralizer flowrate, I_{NHg}, are plotted for three values of I_{NK}. This configuration required an unacceptable mercury equivalent flowrate of I_{NKHg} = 10 mA. A second coupling test was performed after enlarging the keeper aperture to 0.18-cm diameter. The results were quite good and are shown in Figure 29. For equivalent flowrate above I_{NHg} = 5 mA, the general shape of the curves changes very little with flowrate. This configuration produced repeatable coupling at the design flowrate and keeper current.

B. THRUSTER ACCEPTANCE

The testing of the 8-cm EM thruster follows a detailed Thruster Performance Acceptance Plan.[18] The results of these characterization tests are presented in the subtopics which follow.

1. Iron Filing Map

An iron filing map of the 8-cm EM thruster (S/N 901) discharge chamber is shown in Figure 30. This was made with all magentic circuit elements in place (screen, polepiece, magnets, endplate, cathode-cup polepiece), but without the nonmagnetic ion-extraction grids. It can be seen that the magnetic field diverges at the end of the discharge chamber.

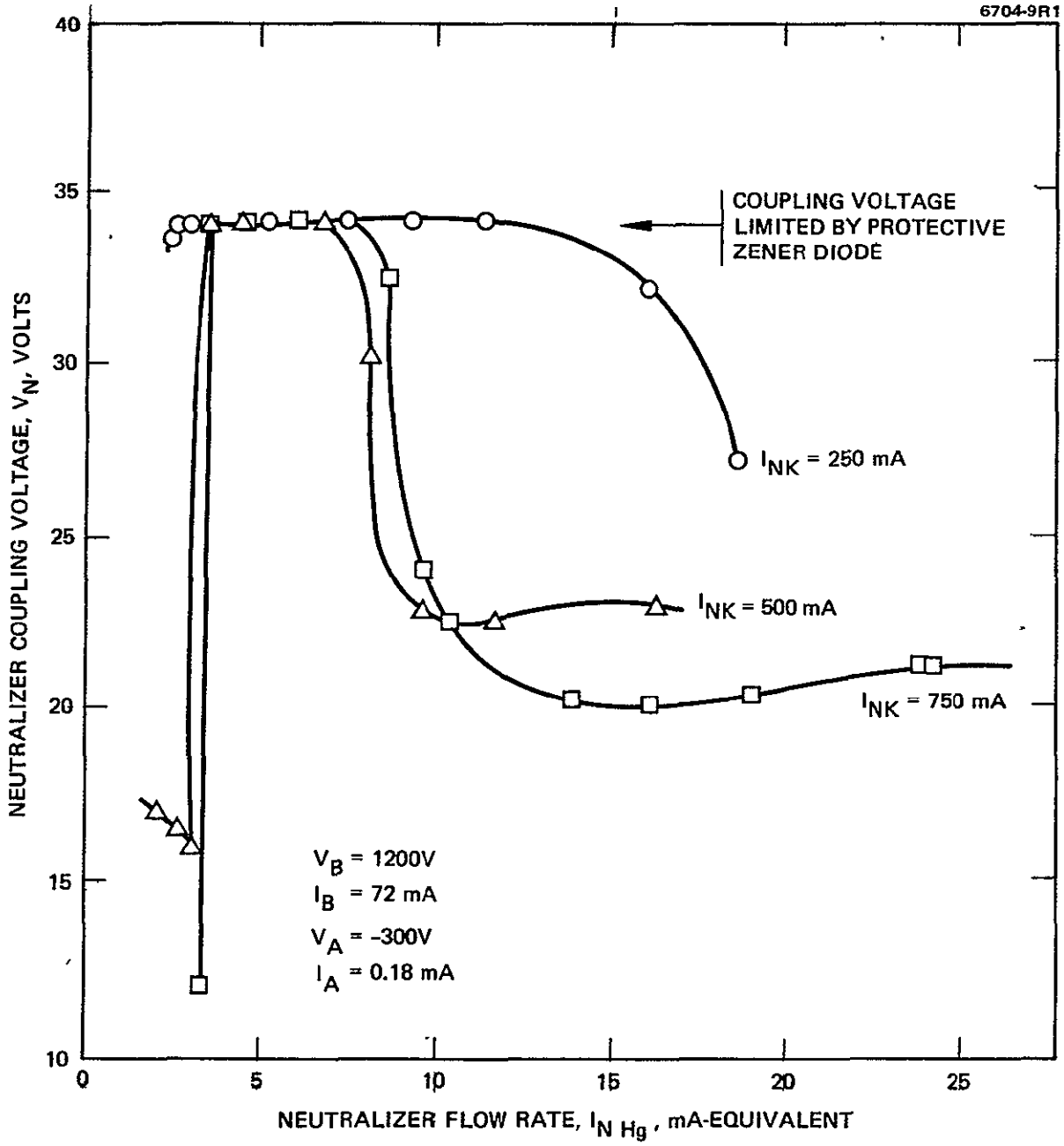

Figure 28. Neutralizer coupling characteristics with keeper aperture diameter of 0.127 cm.

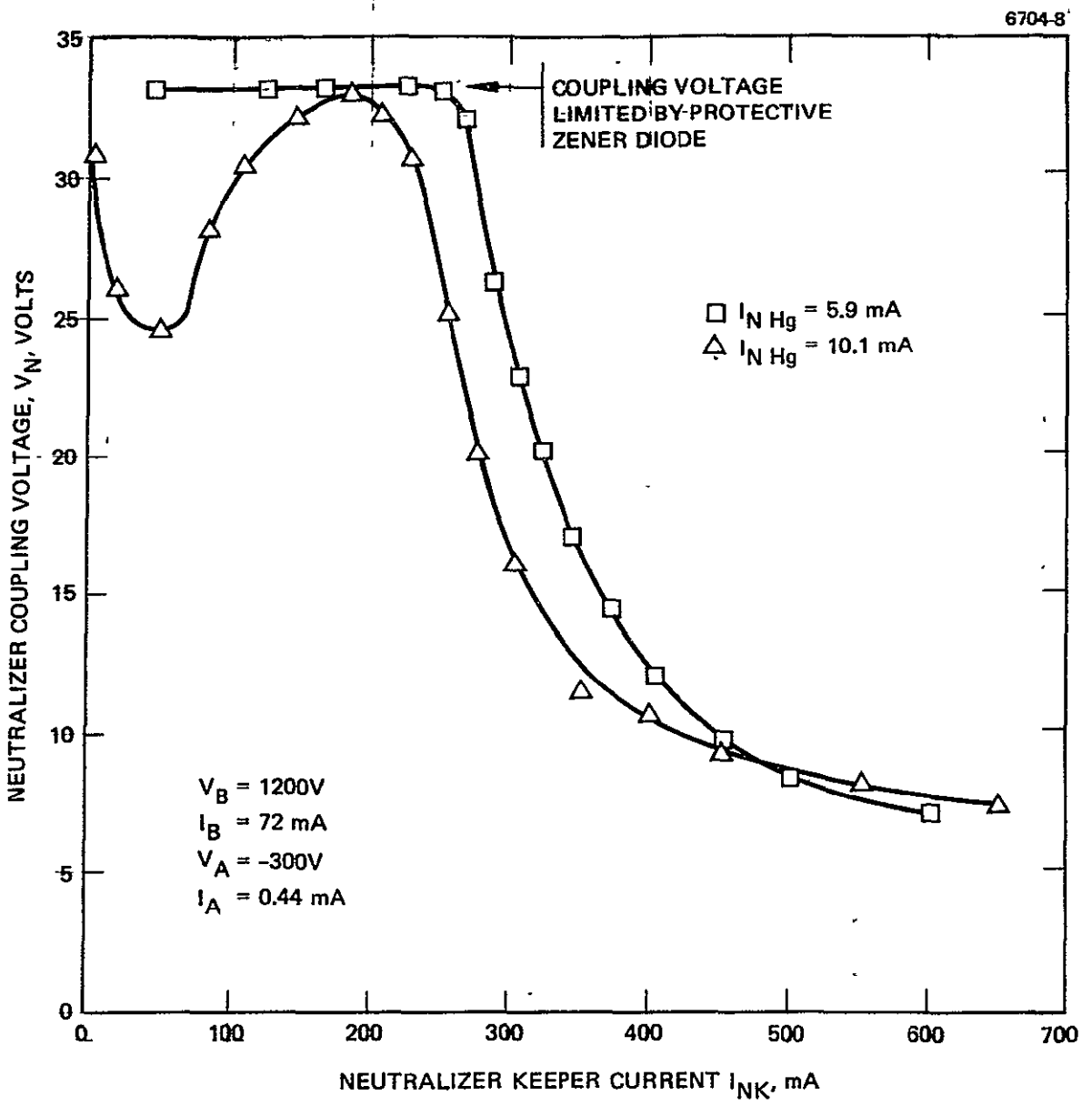

Figure 29. Neutralizer coupling characteristics with keeper aperture diameter of 0.18 cm.

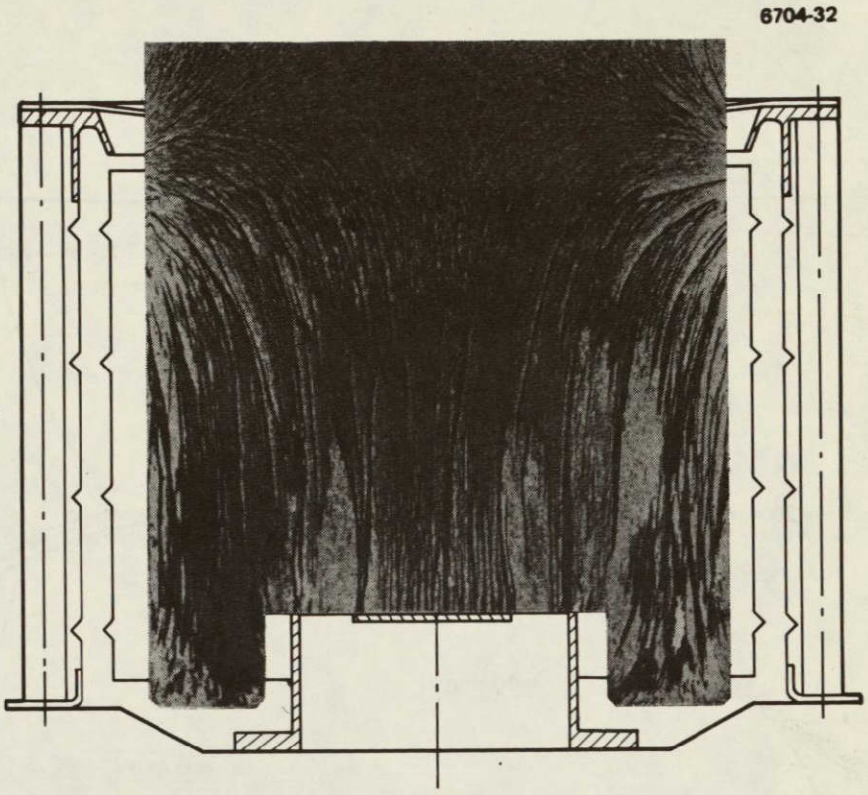

Figure 30. Iron filing map of 8-cm EM thruster (S/N 901).

2. Thruster Magnetic-Field-Strength Measurements

Magnetic-field-strength measurements were made within the discharge chamber with the extraction-grids removed. Plots of the measurements for various radial and axial locations are shown in Figure 31. Curves are labeled for the radial distances r = 0 through r = 30 mm. The screen is located at z = 0, and the lip of the cathode-cup polepiece is located at z = 53.2 mm. On axis, the magnetic field maximum is $B_{z(max)}$(r = 0 cm) = 5.30 mT at z_m = 53.4 mm, and the on-axis minimum magnetic field is B_z = 0 at z = -0 5.5 mm. The maximum external magnetic field was measured and found to be B_{ext} = 6.8 mT at the coordinates z = - 6.4 mm and r = 45.7 mm.

Active element magnetic fields in the EM 8-cm thruster are small

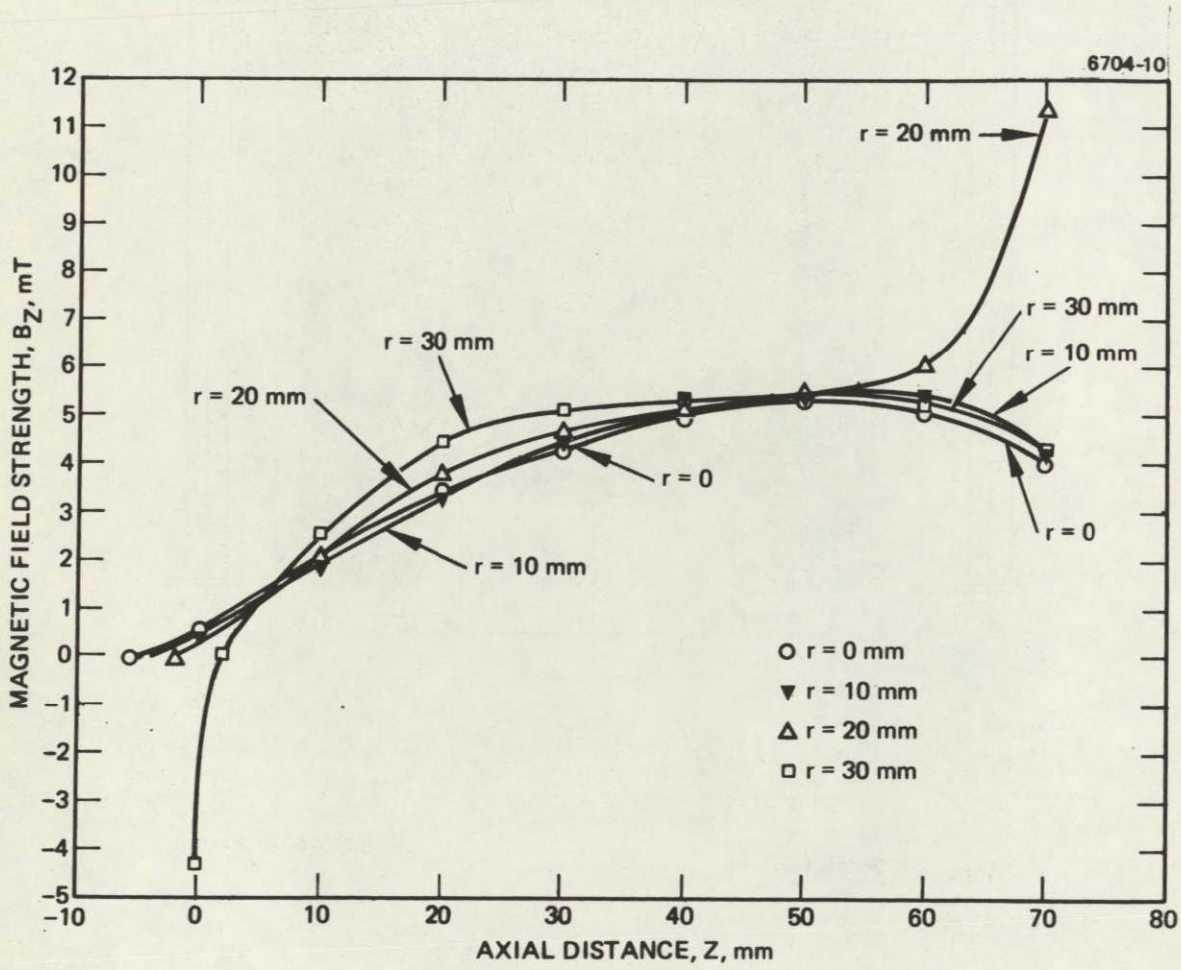

Figure 31. EMT axial magnetic field (S/N 901).

compared to the permanent moments due to the magnets. At distances from the thruster comparable to or larger than thruster dimensions, this field is essentially a magnetic dipole, falling off as the cube of the separation distance, r, from the field to the thruster. The radial and orthogonal components of the field, B_r and B_θ, respectively, for the dipole have the following measured characteristics for the 8-cm thruster:[19]

$$B_r = \frac{1932 \cos \theta}{r^3}$$

$$B_\theta = \frac{966 \sin \theta}{r^3} \quad ,$$

where the magnetic fields are stated in gamma (1 gamma = 10^{-5} G), and r is in meters. The measured fields are not considered to have significant impact on most geosynchronous spacecraft components.

3. Test for Gas Content of Mercury Feedlines

A test for the gas content (or voids) in the neutralizer and discharge cathode feed lines (between the burettes and vaporizers) was made by applying 1 atm of pressure to the mercury in the burettes and recording the change in column height. The glass burettes inner diameters were approximately 1 mm. The measured volume drops were 0.0365 ml for the neutralizer burette and 0.0258 ml for the main burette. These values were consistent with an acceptably low gas and void content to permit accurate measurement.

4. Vaporizer Flow Calibration

Flowrates for both vaporizers were obtained as a function of the vaporizer temperature as indicated by the resistance of a platinum sensor mounted near the vaporizers. These flowrates were obtained with ignited keepers and 5 W supplied to the cathode tip heaters. The flowrates for the discharge vaporizer and neutralizer vaporizer are shown in Figures 32 and 33, respectively. The resistance values have been

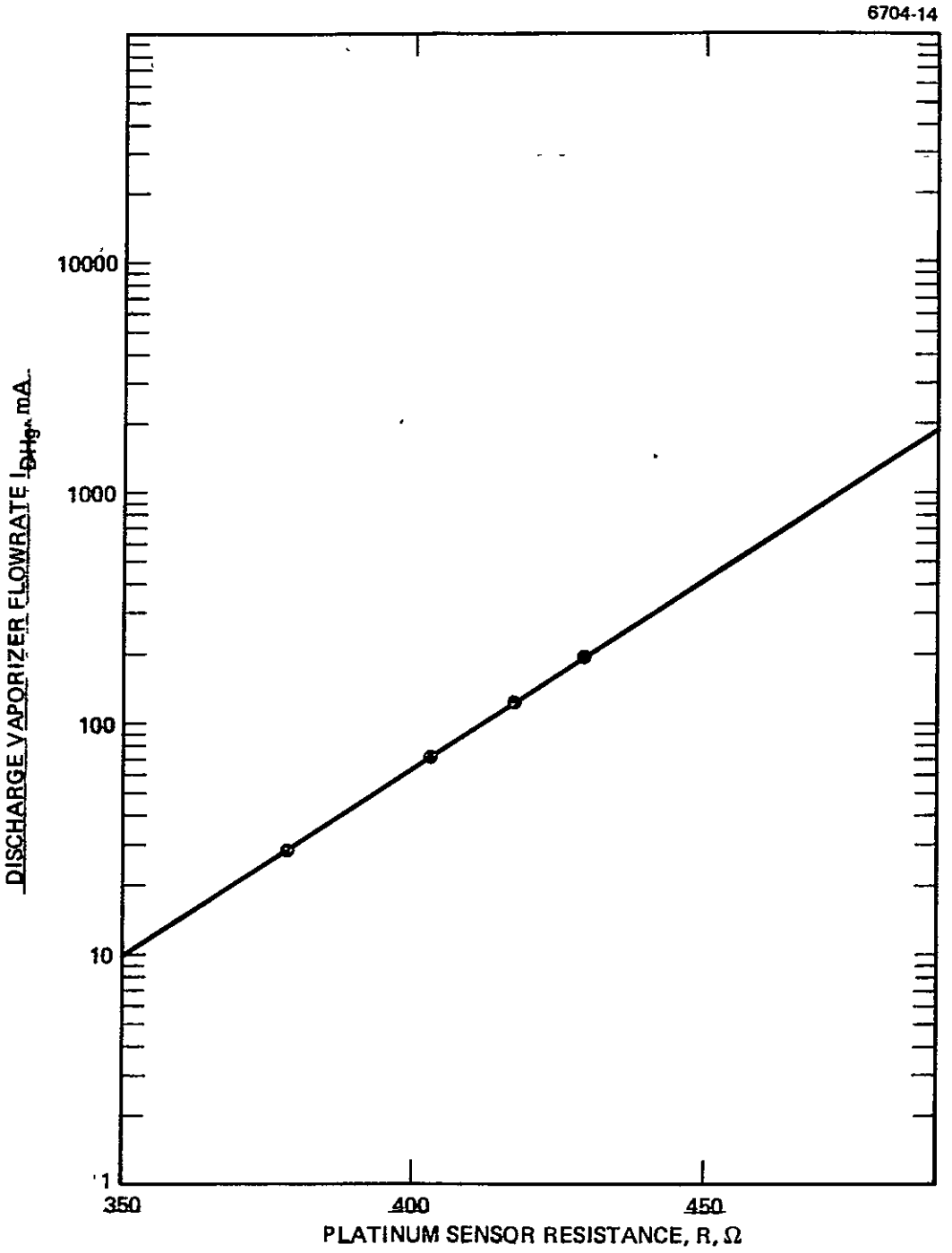

Figure 32. Discharge vaporizer flowrate as a function of sensor resistance (S/N 901).

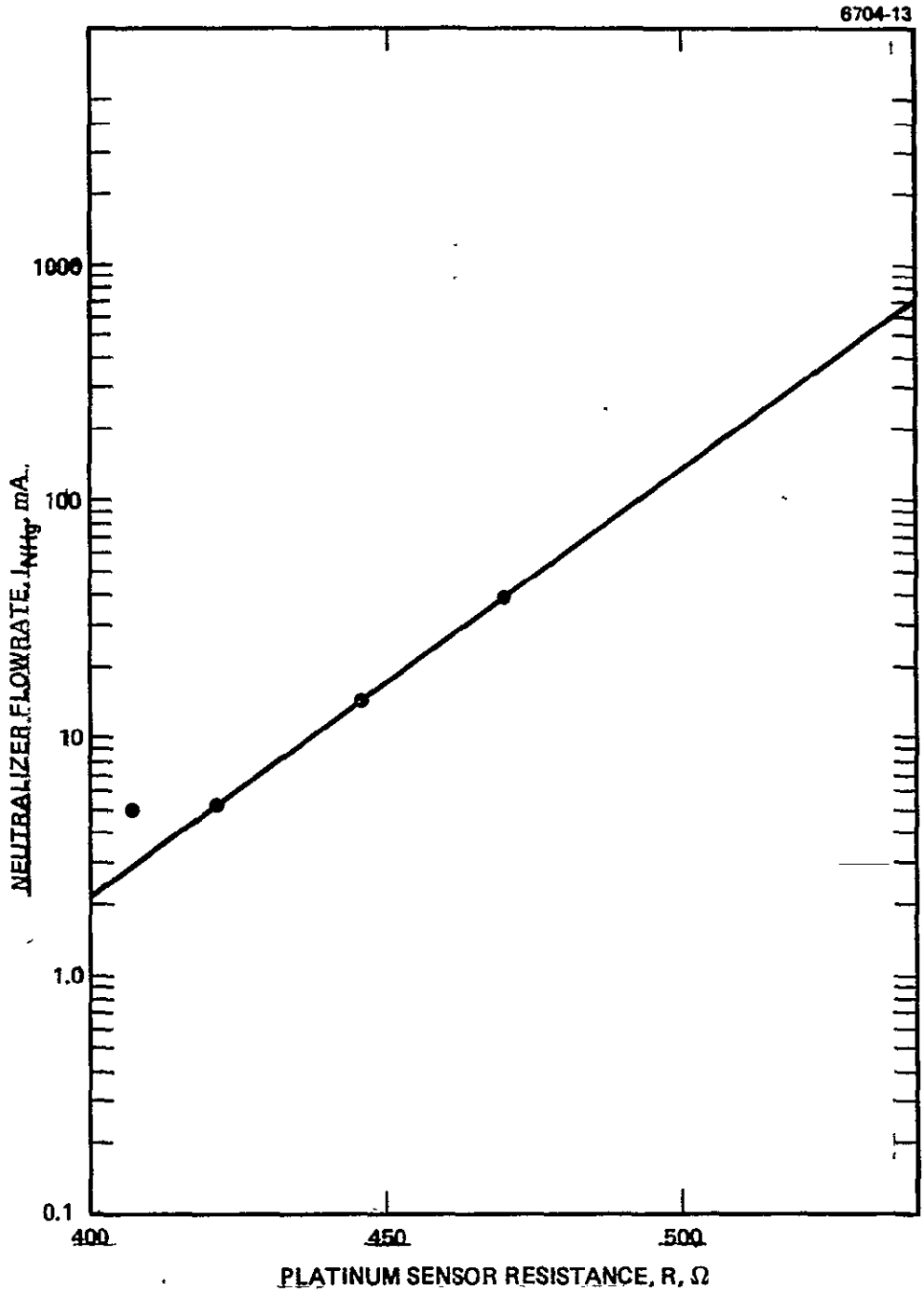

Figure 33. Neutralizer vaporizer flowrate as a function of sensor resistance (S/N 901).

converted to temperatures, and flowrates have been plotted as a function of 1/T in Figures 34 and 35.

5. Performance Test

The 8-cm EM thruster was tested for performance at two points. The first was made at $(V_D - V_{DK}) = 29$ V and the second at $V_D = 40$ V. These results are presented in Table 15. These results neglect the effects of beam spreading and doubly charged ions (these corrections were obtained, however, and are presented in the next section on beam profiles).

During the performance test, the backstreaming limit for electrons was obtained by varying the accelerator voltage V_A while maintaining $|V_A| + |V_S| = 1500$ V. These results are shown in Figure 36. Backstreaming set in at $V_A > -100$ V.

The neutralizer-keeper-voltage variation as a function of vaporizer flowrate is presented in Figure 37. The nominal mercury flowrate operating point of $I_{NHg} = 6$ mA produces a keeper voltage $V_{NK} = 12.5$ V. The neutralizer-keeper voltage V_{NK} was found to be relatively constant for various values of neutralizer current I_{NK}; however, the coupling voltage V_N did change for the same current variations, as can be seen in Figure 38. At the nominal operating point of $I_{NK} = 500$ mA, the coupling voltage was $V_N = 8$ V.

6. Beam Profiles

The beams at the two set points described above (i.e., $V_D - V_{DK} = 29$ V and $V_D = 40$ V) were analyzed with an ExB-type ion velocity analyzer. The beam profiles for the two set points are shown in Figures 39 and 40. The curves in Figures 39 and 40 are the intensities of the singly charged ions (solid lines) and the doubly charged ions (dashed lines) for four ExB analyzer radial positions as functions of the angle between the axis of the ExB analyzer and the axis of the vacuum chamber. The current maximums occurring at -3° indicates that the thruster axis was displaced 3° from the center line of the vacuum chamber. The displacement is taken

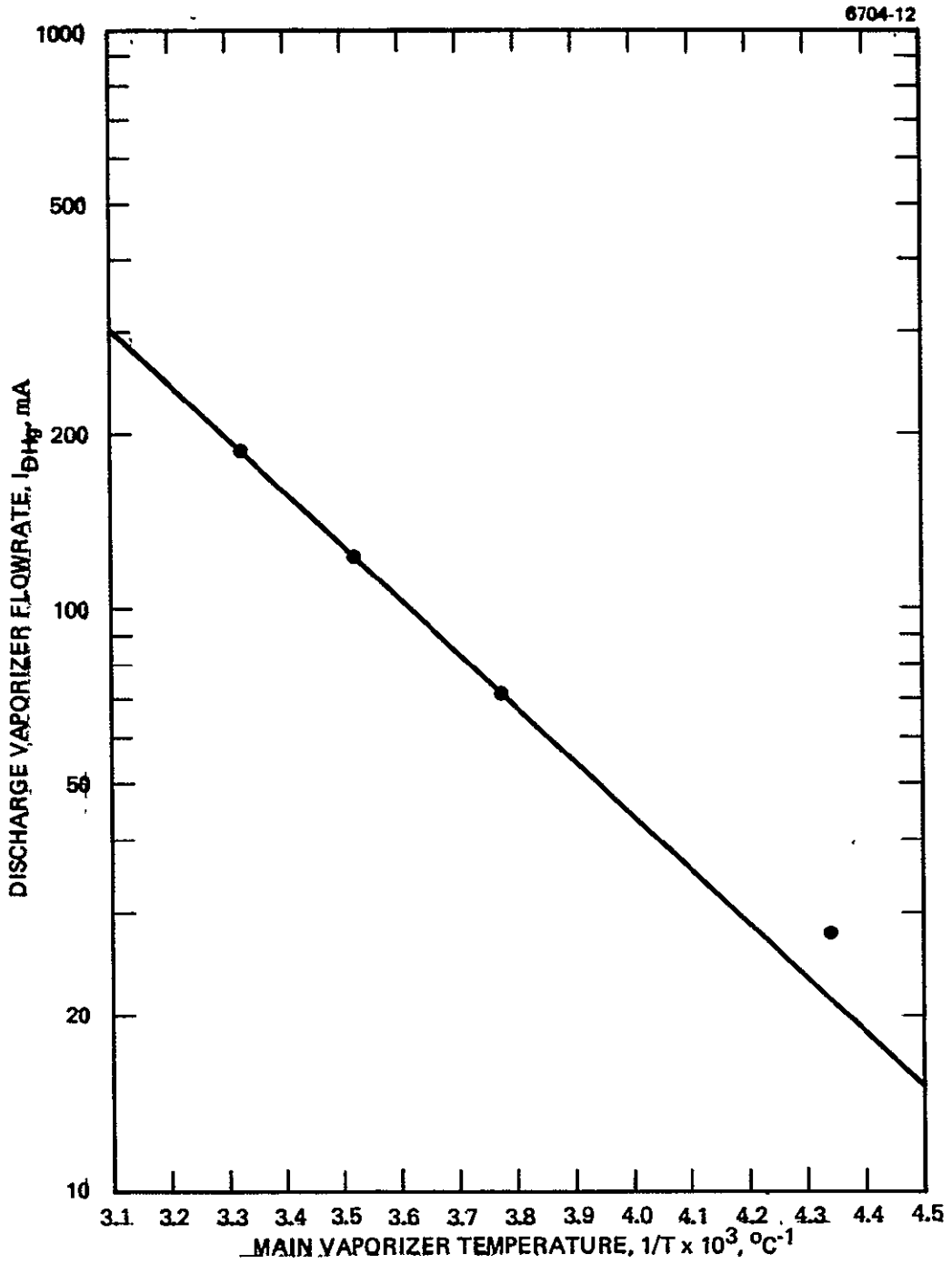

Figure 34. Discharge vaporizer flowrate as a function of 1/T (S/N 901).

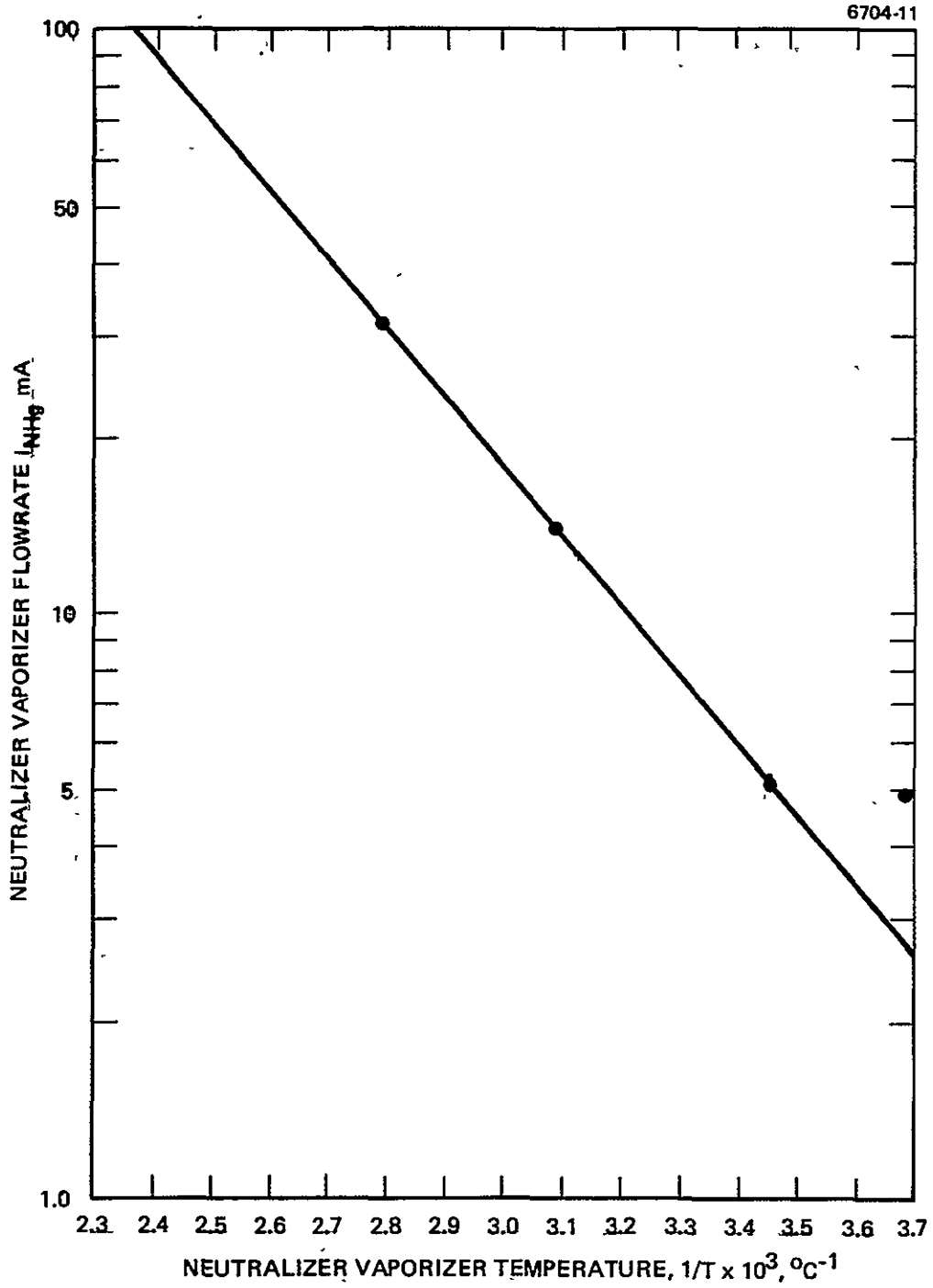

Figure 35. Neutralizer vaporizer flowrate as a function of 1/T (S/N 901)

Table 15. EM 8-CM Performance (S/N 901) (Uncorrected)

	(V_D-V_{DK}) = 29 V		V_D = 40 V	
Thrust[a] (ideal) T, N, (mlb)	4.98 (1 12)		4.89 (1 10)	
Specific impulse,[a] I_{SP}, sec	2716		2909	
Total input power, P_T, W	119.5		125.0	
Total efficiency,[a] $\tilde{\eta}$, percent	56.8		58.2	
Total efficiency, η_E, percent	72.1		69.0	
Total utilization,[a] $\tilde{\eta}_{HG}$, percent	78.8		84 4	
Discharge utilization,[a] η_{HG} percent	84.4		90.3	
Total neutral flow, I_{HG} mA	91.4		85.3	
Power/thrust,[a] W/N, (W/mlb)	23.4 (104.2)		24.5 (109.0)	
W/A excluding keeper, V	221		311	
W/A including keeper, ϵ_I, V	230		318	
Beam current, I_B, mA	72		72	
Anode-to-neutralizer tip potential, V_B, V	1205		1205	
Neutralizer coupling potential, V_N, V	-7.9		-7 8	
Output beam power, P_B W		86.2		86.2
Accelerator voltage, V_A, V	-300		-300	
Accelerator drain current, I_A, mA	0 17		0.24	
Accelerator drain power, P_A W		0.3		0 4
Discharge voltage, V_D, V	35		40	
Discharge current, I_D, A	0.455		0.565	
Discharge power, P_D, W		15.9		22.6
Discharge.				
Keeper voltage, V_{DK}, V	6		5.1	
Keeper current, I_{DK}, A	0 100		0.100	
Keeper power, P_{DK} W		0.6		0.5
Heater voltage, V_{DH}, V	0		0	
Heater current, I_{DH}, A	0		0	
Heater power, P_{DH}, W		0		0
Vaporizer voltage, V_{DV}, V	4.9		4.55	
Vaporizer current, I_{DV}, A	1.68		1.58	
Vaporizer power, P_{DV}, W		8.2		7.2
Flowrate, I_{DHG},mA	84.8		79 7	
Neutralizer				
Keeper voltage, V_{NK}, V	13		13.2	
Keeper current, I_{NK}, A	0.500		0.500	
Keeper power, P_{NK}, W		6.5		6.6
Heater voltage, V_{NH}, V	0		0	
Heater current, I_{NH}, A	0		0	
Heater power, P_{NH}, W		0		0
Vaporizer voltage, V_{NV}, V	2.0		1.8	
Vaporizer current, I_{NV}, A	0.6		0.5	
Vaporizer power, P_{NV}, W		1.2		0.4
Flowrate, I_{NHG}, mA	6.6		5 6	
Neutralizer coupling power, P_N, W		0 6		0.6

*Accounting for neutralizer floating potential, V_N, but neglecting effects due to beam divergence and the presence of double-charged ions.

5911

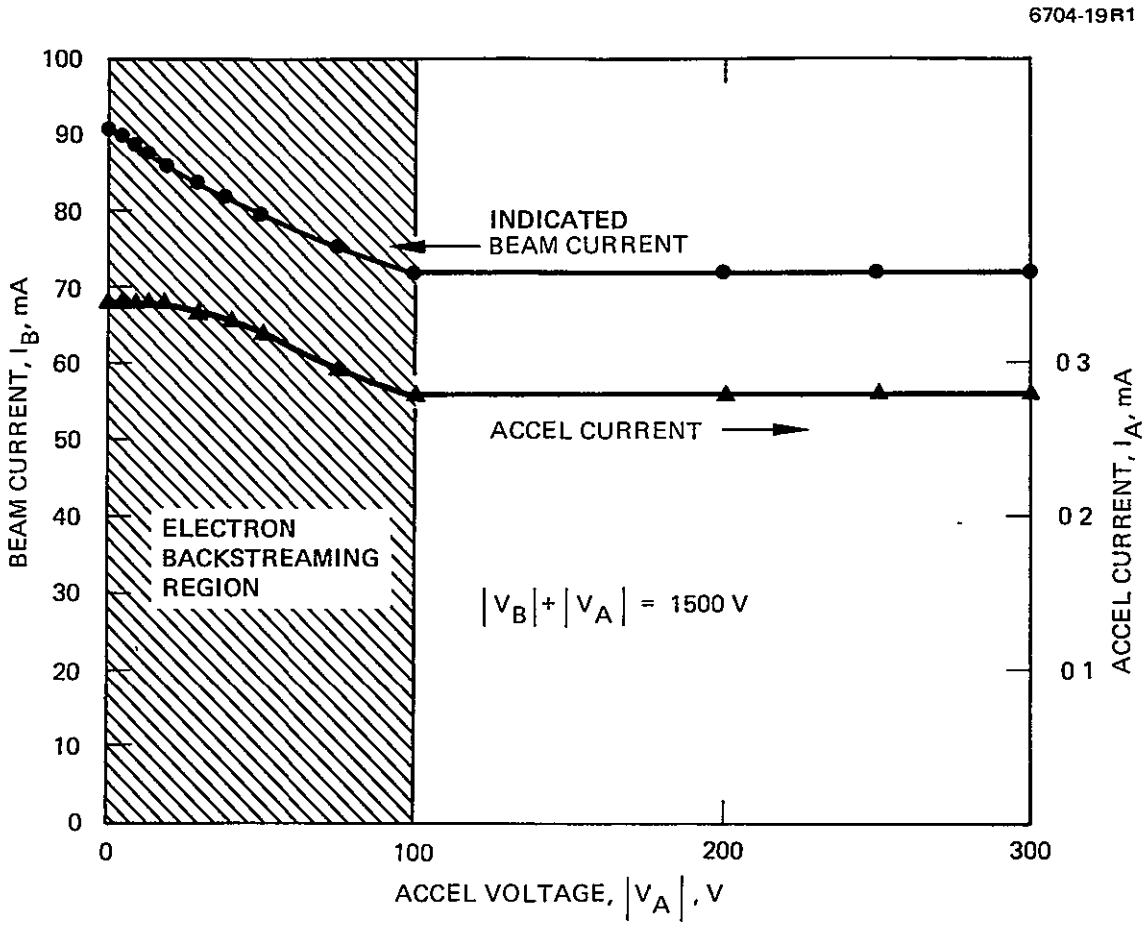

Figure 36. Beam current, I_B, and accel current, I_A as a function of accel voltage. $|V_B| + |V_A| = 1500$ V (S/N 901).

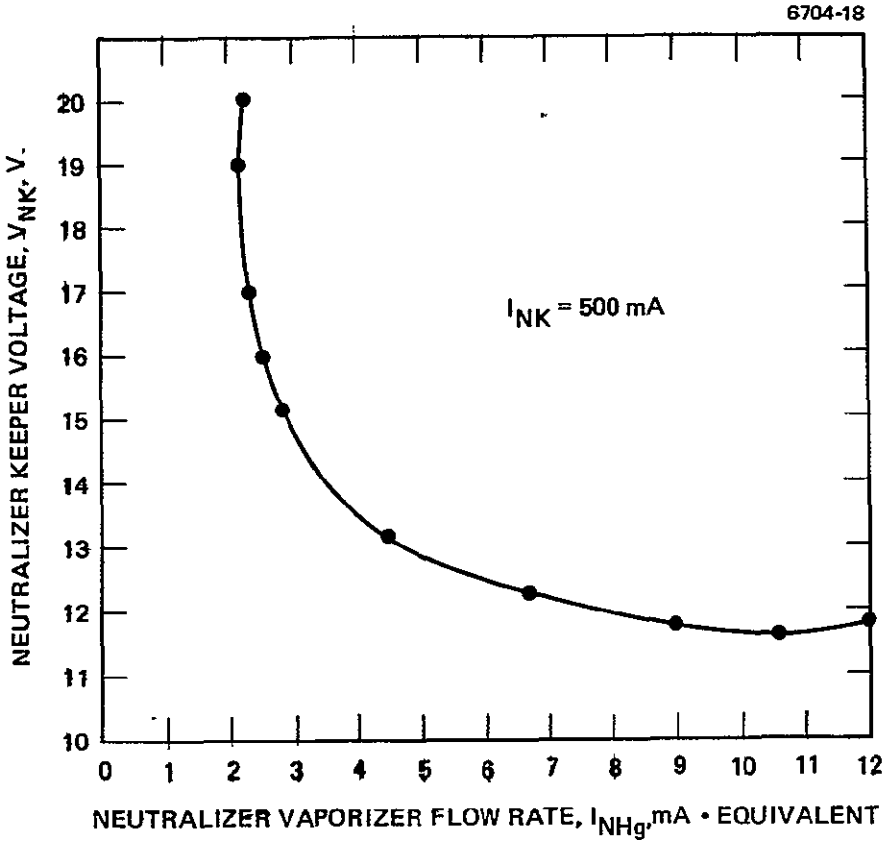

Figure 37. Neutralizer keeper voltage as a function of mercury flowrate (S/N 901).

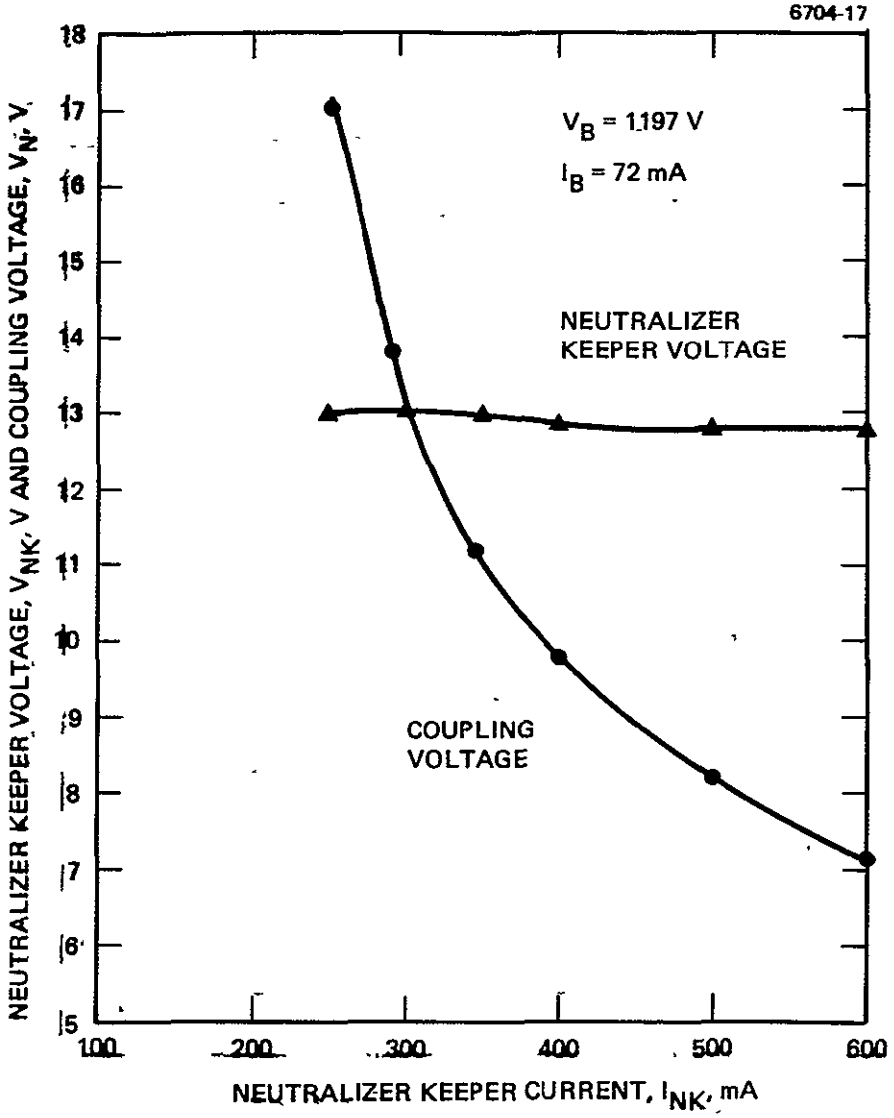

Figure 38. Neutralizer keeper and coupling voltage as a function of neutralizer keeper current (S/N 901).

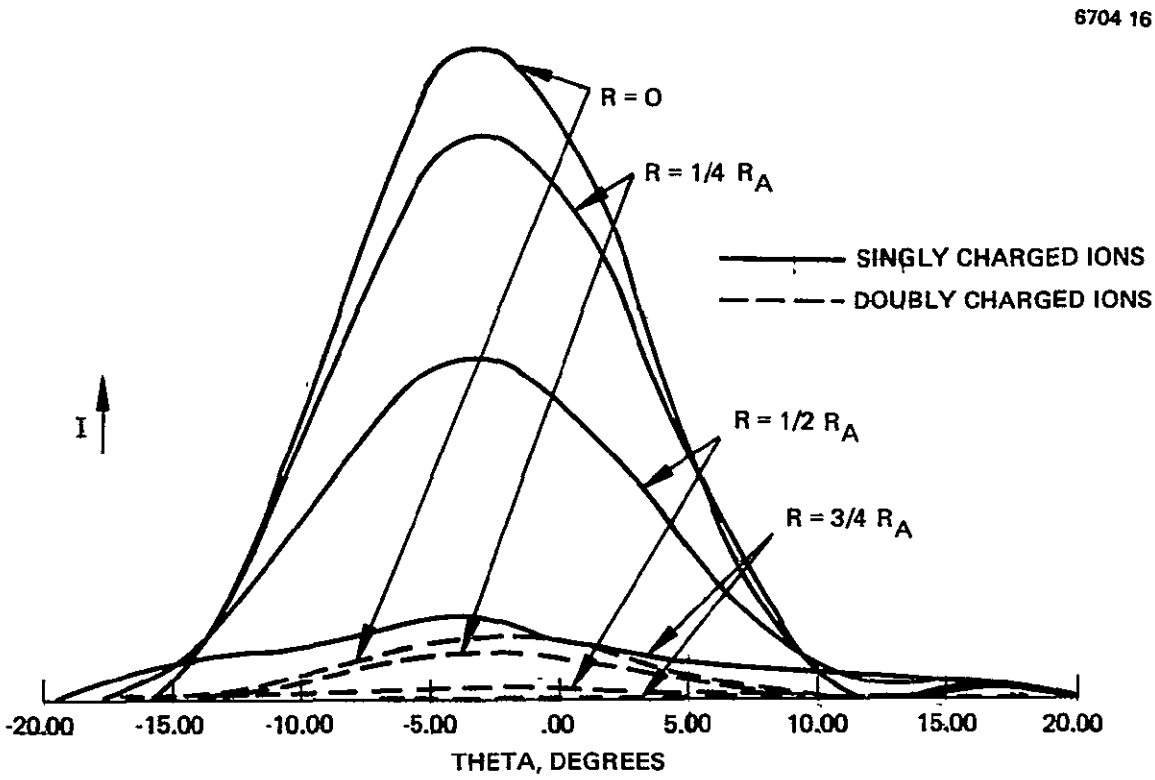

Figure 39. Beam profile for S/N 901 8-cm EM thruster with $[(V_D - V_{DK}) = 29\ V]$.

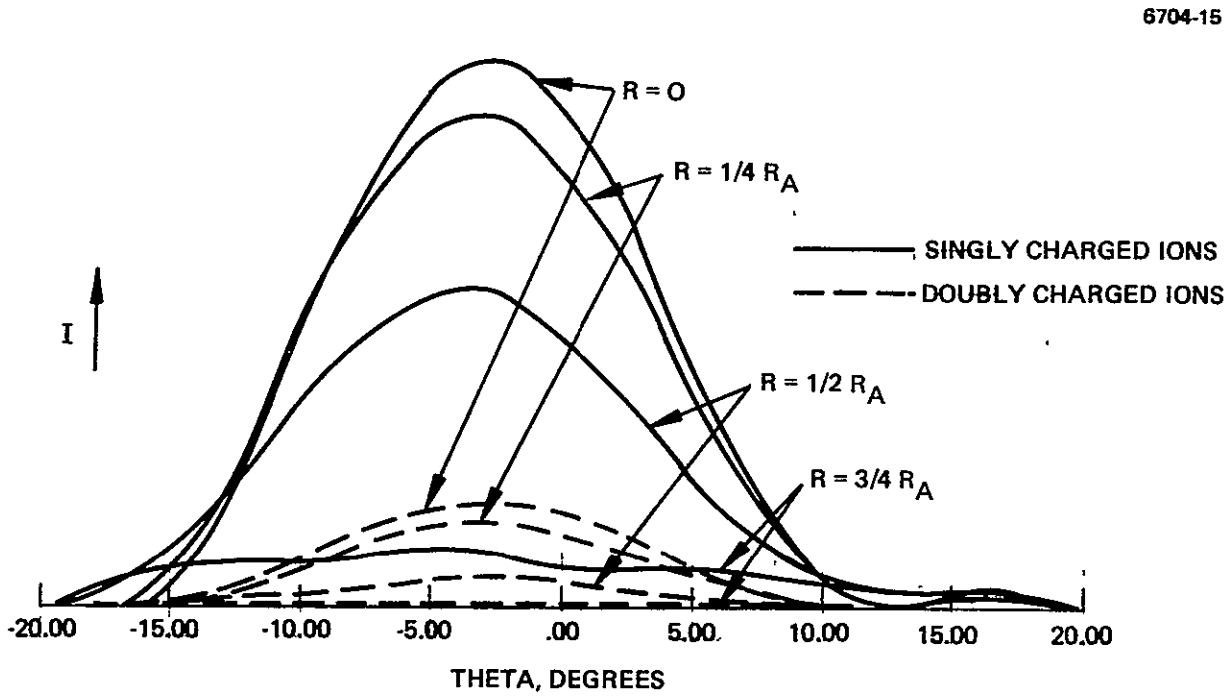

Figure 40. Beam profile for S/N 901 8-cm EM with [V_D = 40 V].

into consideration when the correction factors are calculated and are listed in Table 16. Applying these corrections to the two set points listed in Table 15 yields the information listed in Table 17.

7. Stability Characterization

The thruster was evaluated for operating stability. An unstable condition was defined as: (1) sudden change in discharge impedance, (2) large amplitude excursion of discharge current, (3) high accel currents, or (4) keeper or discharge extinction. The following sequence of variations was carried out after the thruster was brought to its nominal operating point.

- Discharge-cathode keeper current was varied from 100 mA $\leq I_{DK} \leq$ 500 mA while maintaining $(V_D - V_{DK})$ = 29 V and I_B = 72 mA.
- Discharge-chamber current was varied from 200 mA $I_D \leq$ 800 mA while maintaining $(V_D - V_{DK})$ = 29 V.
- Voltage difference between discharge chamber and discharge keeper was varied from 25 V $\leq (V_D - V_{DK}) \leq$ 33 V while maintaining beam current I_B = 72 mA.

Table 16. Correction Factors[a] for 8-cm EMT

Setpoint	$\frac{I_B^{++}}{I_{B,\,Total}}$	γ	α	F_T	$\eta_{Hg}/\tilde{\eta}_{Hg}$
$(V_D - V_{DK})$ = 29 V	0.0498	0.9781	0.9854	0.9926	0.9751
V_D = 40 V	0.0988	0.9629	0.9710	0.9917	0.9506

[a]The following definitions apply (see Appendix B)

$\frac{I_B^{++}}{I_{B,Total}} = \frac{2\beta}{1+2\beta}$ = Total fractional beam content of doubly charged ions.

$\gamma = \alpha \times F_T$ = Thrust correction factor.

α = Thrust correction for doubly charged ions.

F_T = Thrust correction for beam spreading.

$\frac{\eta_{Hg}}{\tilde{\eta}_{Hg}} = \frac{1+\beta}{1+2\beta}$ = Discharge chamber propellant utilization correction for doubly charged ions.

5911

Table 17. 8-cm EMT Performance (Corrected)

	V_D-V_{DK} = 29 V		V_D = 40 V	
Thrust[a], T, N, (mlb)	1.12		1.10	
Specific impulse,[a] I_{sp}, sec	2657		2801	
Total input power, P_T, W	119.5		125.0	
Total efficiency,[a] η, percent	55.3		55.3	
Power efficiency, η_E, percent	72.1		69.0	
Total utilization,[a] η_{HG}, percent	76.8		80 2	
Discharge utilization,[a] η'_{HG} percent	82.8		85 8	
Total neutral flow, mA	91.4		85.3	
Power/thrust, W/N, η_{Hg} (W/mlb)	105.8		112.6	
W/A excluding keeper, V	227		327	
W/A including keeper, ϵ_I, V	235		335	
Beam current, I_B, A	72		72	
Anode-to-neutralizer tip potential, V_B, V	1205		1205	
Neutralizer coupling potential, V_N, V	7.9		7.8	
Output beam power, P_B, W		86.2		86.2
Accelerator voltage, V_A, V	-300		-300	
Accelerator drain current, I_A, mA	0 17		0.24	
Accelerator drain power, P_A, W		0.3		0.4
Discharge voltage, V_D, V	35		40	
Discharge current, I_D, A	0.455		0.565	
Discharge power, P_D, W		15.9		22 6
Cathode				
Keeper voltage, V_{DK}, V	6		5.1	
Keeper current, I_{DK}, A	0.1		0 1	
Keeper power, P_{DK}, W		0.6		0.5
Heater voltage, V_{DH}, V	0		0	
Heater current, I_{DH}, A	0		0	
Heater power, P_{DH}, W		0		0
Vaporizer Voltage, V_{DV}, V	4.9		4.55	
Vaporizer current, I_{DV}, A	1 68		1.58	
Vaporizer power, P_{DV}, W		8.2		7 2
Flowrate, I_{DHg}, mA	84.8		79.7	
Neutralizer				
Keeper voltage, V_{NK}, V	13		13.2	
Keeper current, I_{NK}, A	0.500		0.500	
Keeper power, P_{NK}, W		6.5		6.6
Heater voltage, V_{NH}, V	0		0	
Heater current, I_{NH}, A	0		0	
Heater power, P_{NH}, W		0		0
Vaporizer voltage, V_{NV}, V	2.0		1.8	
Vaporizer power, P_{NV}, W		1.2		0.9
Flowrate, mA	6 6		5 6	
Neutralizer coupling power, P_N, W		0.6		0.6

[a]Accounting for nuetralizer floating potential V_N and including effects due to beam divergence and the presence of doubly charged ions.

5911

- The previous two items were carried out for I_{DK} = 100 mA, 200 mA, and 360 mA.

The thruster showed remarkable stability for all of the above variations except for the combination of low keeper current $I_{DK} \approx 100$ mA and low discharge current $I_D \approx 200$ mA. The stable region comprised peak to peak currents of 80 mA < I_D < 140 mA and frequencies of 0.4 to 1 MHz. A typical trace for the stable condition is shown in Figure 41. The upper trace is dc plus noise (200 mA/cm) and the lower trace is noise only (50 mA/cm). The frequency is about 0.6 mHz. The unstable region could be reached in two ways: the first, by keeping I_{DK} = 100 mA and lowering I_D = 200 mA; and the second, by keeping I_D = 200 mA and lowering I_{DK} = 155 mA. A typical trace of this condition is shown in Figure 42. The large peak-to-peak values indicate that the discharge was essentially cycling on and off at about 40 Hz. A flicker could be observed in the light from the discharge chamber during this unstable operation. Lowering either I_{DK} or I_D while this flickering was occurring would extinguish the discharge and keeper currents. Since the beam current value was only I_B = 46 mA for the unstable condition, this unstable point is not close to the nominal operating point of I_B = 72 mA.

8. Discharge Chamber Propellant Utilization

As a matter of interest, the discharge chamber propellant utilization $\tilde{\eta}_{Hg}$ (uncorrected for Hg^{++}) was measured as a function of $(V_D - V_{DK})$. This is shown in Figure 43. At $(V_D - V_{DK})$ = 29 V there is a variation of about ± 4%. It is believed that the utilization measurements are more reproducible than shown. For this reason, the same data was replotted as a function of discharge voltage V_D only in Figure 44. The spread from a smooth curve is less than ± 1/2%. It appears that the discharge-chamber voltage V_D is a more representative measure of thruster utilization than is $(V_D - V_{DK})$; however, this should be investigated further.

6704-27

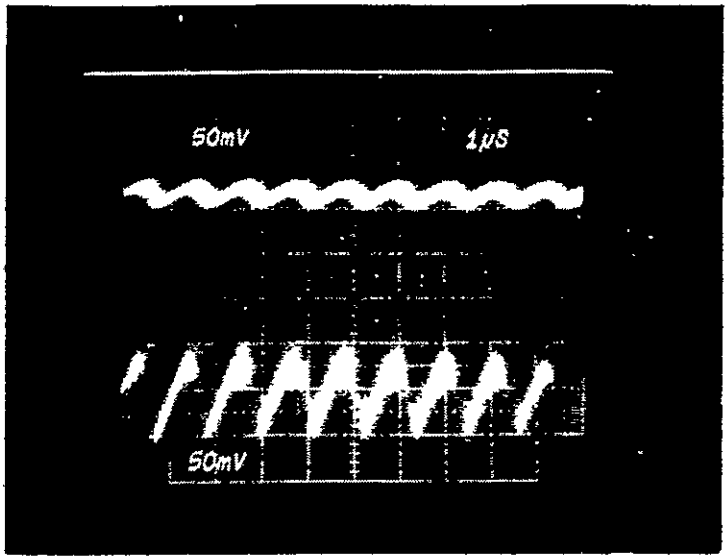

Figure 41. Typical discharge chamber current. Spectrum (stable). Top curve is dc plus noise (200 mA/cm). Lower curve is noise only (50 mA/cm). f ≈ 0.6 MHz.

6704-28

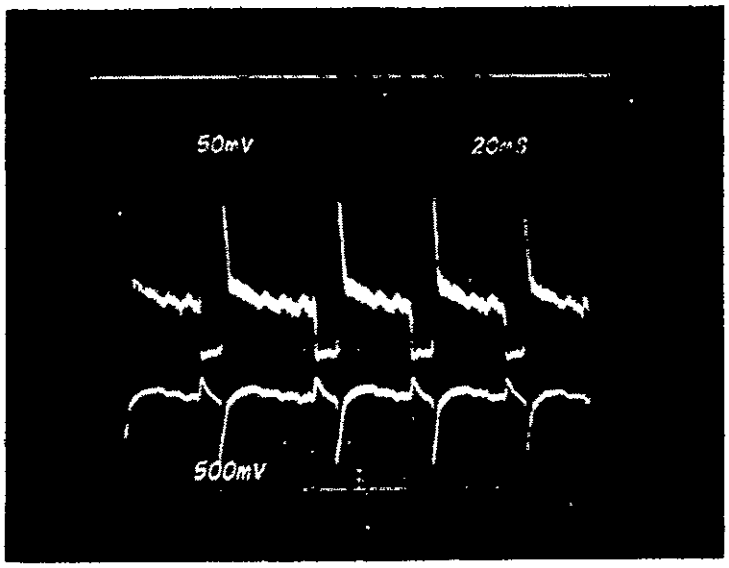

Figure 42. Typical discharge chamber current spectrum (unstable). Top curve is dc plus noise (200 mA/cm). Lower curve is noise only (500 mA/cm). f ≈ 40 Hz.

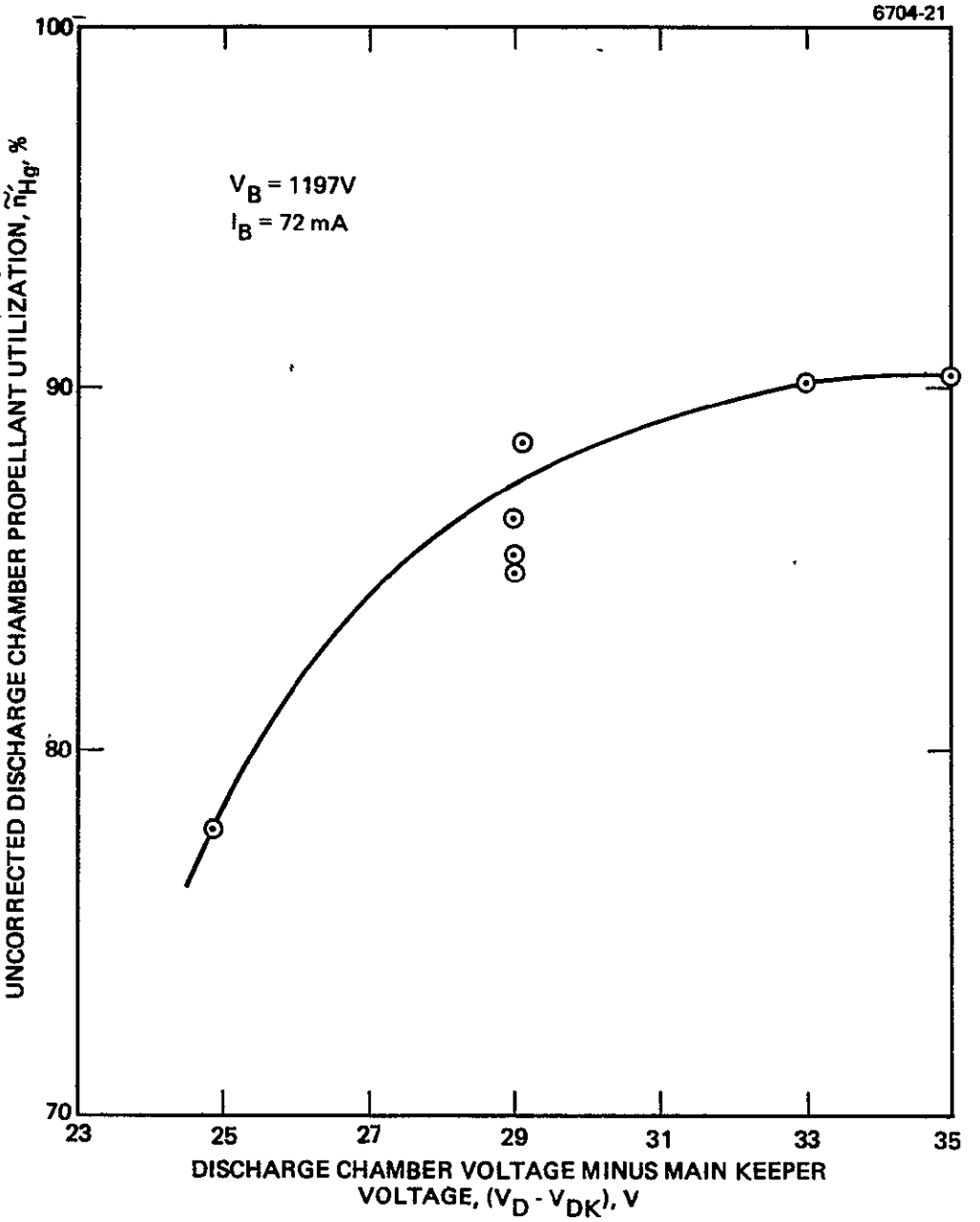

Figure 43. Uncorrected discharge chamber propellant utilization as a function of (V_D - V_{DK}) for thruster S/N 901.

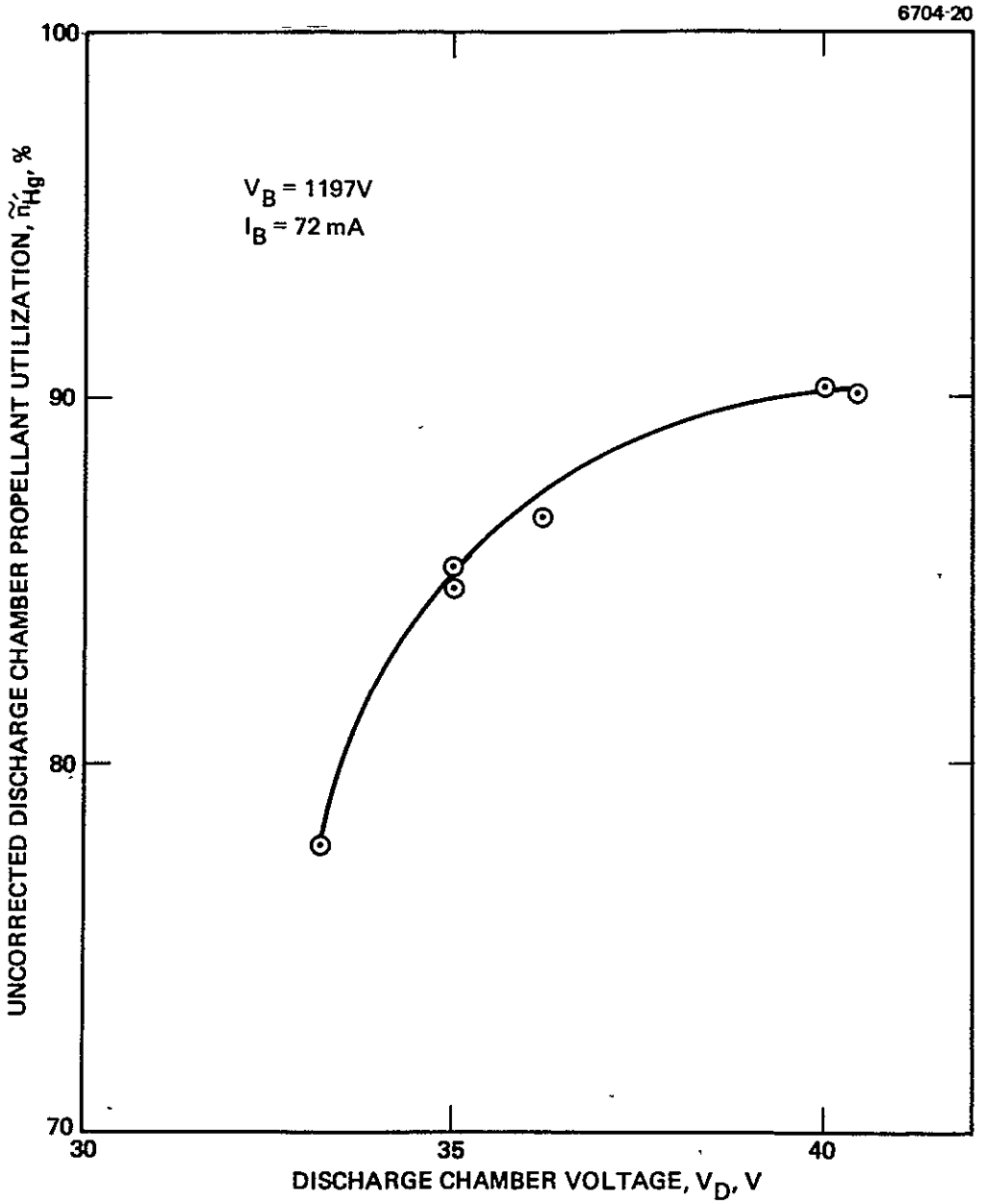

Figure 44. Uncorrected discharge chamber propellant utilization as a function of V_D for thruster S/N 901.

C. SYSTEM INTEGRATION AND CYCLIC TEST

The concluding technical requirement of this program was to conduct a 10-cycle thermal-vacuum test of the 8-cm Thruster Subsystem. Between the conclusion of the thruster acceptance test (described in the previous section) and the beginning of the cyclic test, it was necessary to mate the thruster to the propellant reservoir, fill and pressurize the reservoir, and conduct integration testing of the PEU and DIU with the thruster/reservoir combination.

1. Reservoir Filling

The filling procedure for the propellant reservoir required evacuating the reservoir and expellant chamber, filling the reservoir with vacuum-distilled mercury, and filling the pressurant chamber with nitrogen gas plus krypton as a tracer element. To meet these filling requirements, the filling system shown schematically in Figure 45 was built. The procedure used to fill the reservoir consisted of the following steps:

- Evacuation of the pressurant-chamber half of the reservoir assembly.
- Evacuation of the filling system and propellant reservoir.
- Vacuum-distillation of mercury into the external reservoir.
- Transfer of mercury under vacuum from the external reservoir via the piston to the EM propellant reservoir.
- Filling of pressurant chamber with nitrogen to 193 kPa (28 psia).
- Filling of pressurant chamber with krypton to 241 kPa (35 psia).*
- Withdrawing 1% of the mercury from the propellant reservoir.

*After the system cyclic test had been completed, it was discovered that, due to a mechanical mismatch between the present chamber valve and the filling system valve V8 (see Figure 45), the pressurant pressure had decreased from 35 psia to atmospheric pressure while the filling system was being disconnected. This mechanical mismatch has since been corrected.

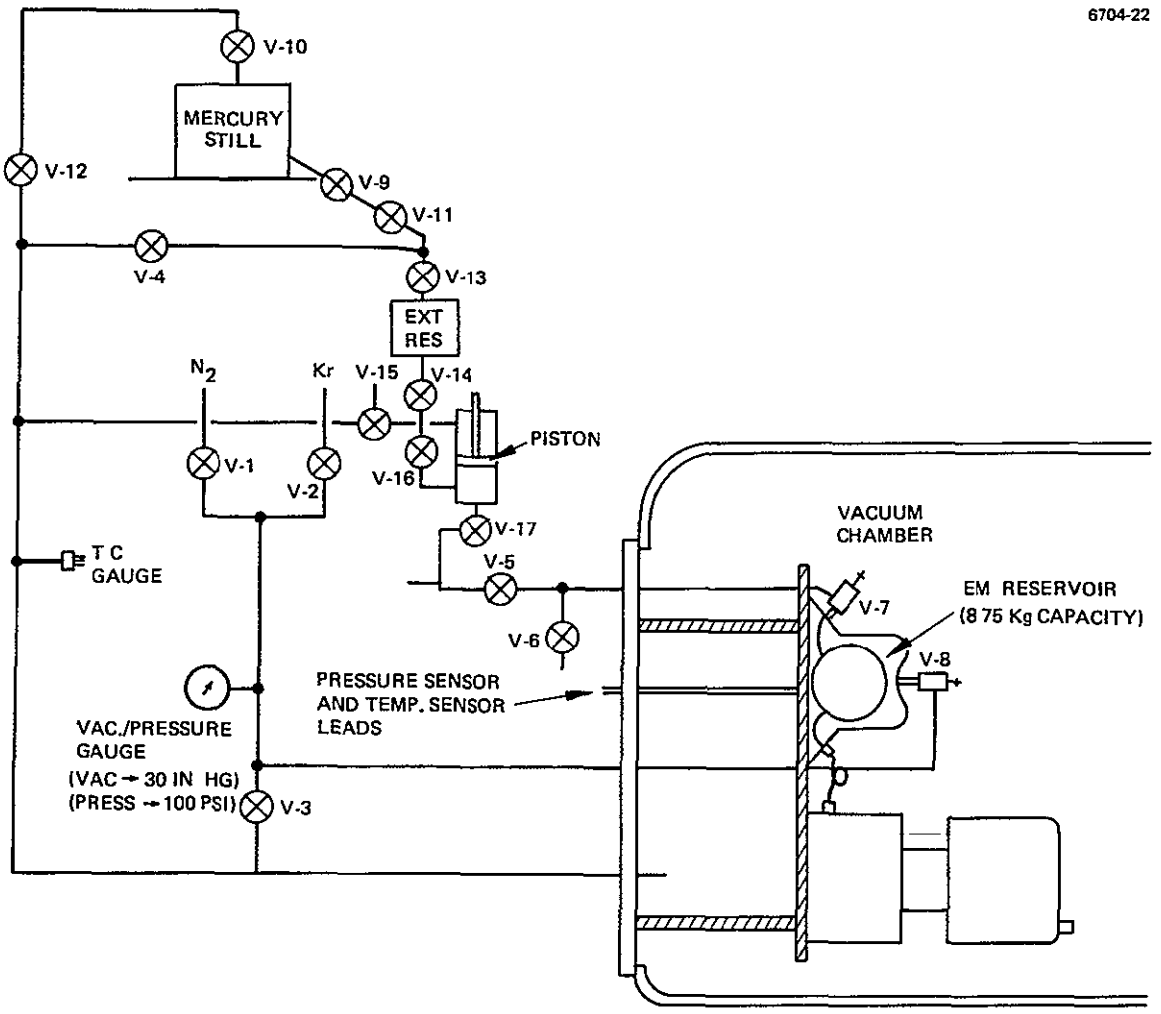

Figure 45. 8-cm EM reservoir filling system.

2. Thruster/EM Power Processor Integration

Upon completion of reservoir filling, the thruster (mounted on the gimbal assembly) and the reservoir were installed in the HRL 5-ft-diameter vacuum chamber for system integration testing with the EM power processor. The first test was a confirmation with 60 Hz lab supplies of the thruster electrical performance measured during the earlier thruster-performance acceptance test. As shown in Table 18, the results obtained were very similar to the acceptance test data. The higher discharge keeper voltage V_{DK} that was observed is an expected result of not conditioning the cathode for 24 hr as had been done prior to taking the performance test data.

Following the confirmation test with 60 Hz supplies, the thruster was connected to the EM power processor unit. The initial thruster startup with the EM power processor was very smooth. The ion beam was at full power 71 min after the power was first applied to both cathode heaters, with 38 of the 71 min being used to condition the cathodes. No evidence of any system problems was observed in operating at the point recorded in Table 18 for January 1977, which was taken 129 min after cathode heater power was first applied to the EM 8-cm thruster with the EM power processor.

Subsequent testing did reveal one system control-loop problem and a design oversight that affected accuracy of three telemetry channels. The control-loop problem was observed while attempting to operate at a discharge voltage V_D = 40 V, the second operating point evaluated during the thruster acceptance test (see Table 18). At V_D = 40 V discharge voltage, the (V_D-V_{DK}) loop (which controls the discharge-vaporizer power) was unstable and would limit-cycle. This problem was eliminated by modifying the loop gain and frequency-transfer characteristics. After the change, the transition proceeded very smoothly in either direction in response to step changes in the setpoint in the range 33 V < V_D < 42 V.

The telemetry readouts for discharge voltage V_D, discharge-keeper voltage V_{DK}, and neutralizer-keeper voltage V_{NK} were found to be in

Table 18. EM 8-CM Integration Test Results

Lab	Date	Power Supplies	V_S (V)	I_B (mA)	V_A (V)	I_A (mA)	V_D (V)	I_D (mA)	V_{DK} (V)	I_{DK} (mA)	V_{NK} (V)	I_{NK} (mA)	V_N (V)	T_{DV} (°C)	T_{NV} (°C)	Comments
Pipette Feed-sys-tem	9/76	60 Hz	1165	72	-300	0.17	35	455	6	100	13	500	-7.9	273	292	
	9/76	60 Hz	1165	72	-300	0.24	40	565	5.1	100	13.2	500	-7.8	271	290	
EM Pres-sur-ized Re-ser-voir	1/27/77	60 Hz	1180	73	-300	0.16	35.2	465	8.2	100	12.8	500	-8.1	274	298	
	1/28/77	EM PPU	1180	72	-300	0.27	33[a]	440[a]	7.9[a]	108	13[a]	495	-9	275	287	
	2/2/77	EM PPU	1180	72	-3-0	0.27	34[a]	440[a]	8.6[a]	108	14.2[a]	495	-9	272	272	
	2/3/77	EM PPU	1170	72	-300	0.27	34.7 33.7	440[a]	11.7 8.3	108	12.1 12.7	495	-9	257 257	277 271	Telemetry External DVM
	2/5/77	EM PPU	1180 1171	72	-300 -299	0.31	35.9 34.7	440[a]	8.6 8.75	108	13.2 14.0	495	-9 -7.8	252 253	284 284	Telemetry External DVM
	2/8/77	EM PPU	1180	72	-298	0.23	35.1	456	7.8	108	13.2	495	-9	257	293	
	2/8/77	EM PPU	1180	70	-298	0.31	40.2	564	7.4	108	13.2	495	-9	257	293	

[a]Corrected for telemetry errors discovered after data was taken.

error when compared to the actual voltages measured at the outputs of the power supplies. In addition to providing an output signal for display on the test console, each of these three telemetry signals are used as input signals to the vaporizer-control loops in the DIU. The source of the telemetry error was identified as loading of the telemetry outputs by the control-loop summing circuits. The problem was eliminated by inserting a unity-gain buffer amplifier between the telemetry circuit and the control-loop summing circuit.

Thruster restart after a brief cold-soak was also demonstrated. Liquid nitrogen was left in the vacuum-chamber cryoliner overnight and in the morning the cathode-vaporizer temperature was -40°C, the neutralizer-vaporizer temperature was -50°C. (All temperatures were obtained from the EM-system telemetry readouts.) The same startup procedure that had been used throughout this test phase was used for the cold-soak restart. Thus, cathode-heater power was applied for approximately 15 min at each of the first three setpoints followed by discharge-vaporizer and neutralizer-vaporizer power-on, neutralizer-keeper ignition, discharge-keeper ignition, discharge, and beam-on. Thruster startup was normal and the beam was at full power 82 min after the application of the cathode-heater power. The only change in operating parameters noted after the cold restart was a reduction in the vaporizer temperature.* As shown in Table 18, the neutralizer-vaporizer temperature subsequently increased to the previous operating range.

This test phase was concluded with the operating conditions shown in Table 18 for 8 February 1977. Thruster operation was stable and repeatable over a discharge voltage range 33 V < V_D < 42 V. System convergence to within this commanded range from outside operating points was also investigated and found to occur smoothly.

*This behavior may have indicated a partial intrusion of liquid mercury into the porous-tungsten vaporizer plug as a result of vaporizer heating after mercury freezing.

3. Cycling Test

Subsystem readiness for the thermal-vacuum cyclic test was confirmed during the integration testing with the power processor external to the vacuum chamber, as described in the previous section. Upon completion of the system integration testing, the PPU was mounted on the system test fixture, as shown in Figure 46, and installed in the HRL 5-ft-diameter vacuum chamber. Before applying any power to the PPU while in vacuum, the system was evacuated for 19 hr. During the last 4 hr, power was applied to the baseplate heater, which brought the PPU to approximately 40°C.

The initial startup with the subsystem in vacuum followed the procedure presented in Table 19. Both neutralizer-keeper and discharge-keeper ignition occurred upon the initial application of keeper voltage without the use of the high-voltage pulsers which are built into the PPU. Before proceeding with discharge ignition, the cathodes were conditioned for 19.5 hr by operating with the keeper ignited and low level, cathode-heater power applied.

At the end of the cathode conditioning period, the discharge was ignited immediately upon application of discharge voltage. A few minutes were allowed for the discharge chamber to warm up and evaporate mercury that might have condensed during the cathode conditioning period. The screen and accelerator voltages were then applied, and the beam came on without any recycles. The thruster was operated for 1 hr without incident, and then it was shut down to let it cool off for the beginning of the first of the 10 thermal-vacuum cycles.

The startup procedure followed during the cyclic test was:

- At t = 0 discharge-cathode-heater and neutralizer-cathode-heater power on at setpoint 6 and discharge-vaporizer and neutralizer-vaporizer power on at setpoint 3
- At t = 10 min, ignite keepers and discharge.*

*The discharge keeper and discharge itself were ignited in less than 10 min on several cycles when the telemetry indicated they were trying to ignite from the voltage supplied by the telemetry isolation transformers.

- At t = 15 min apply high voltages to bring on beam.

A complete test cycle consisted of the 15-min startup segment 1-3/4 hr of beam-on time and 1 hr of cool-down time before the start of the next cycle.

The performance of the EM 8-cm subsystem during the thermal-vacuum cyclic test was very good. In fact, the only deviations from "text book" performance were the two problems with the discharge-current telemetry transconductor described below. Thruster system performance for the 10 cycles is summarized in Table 20.

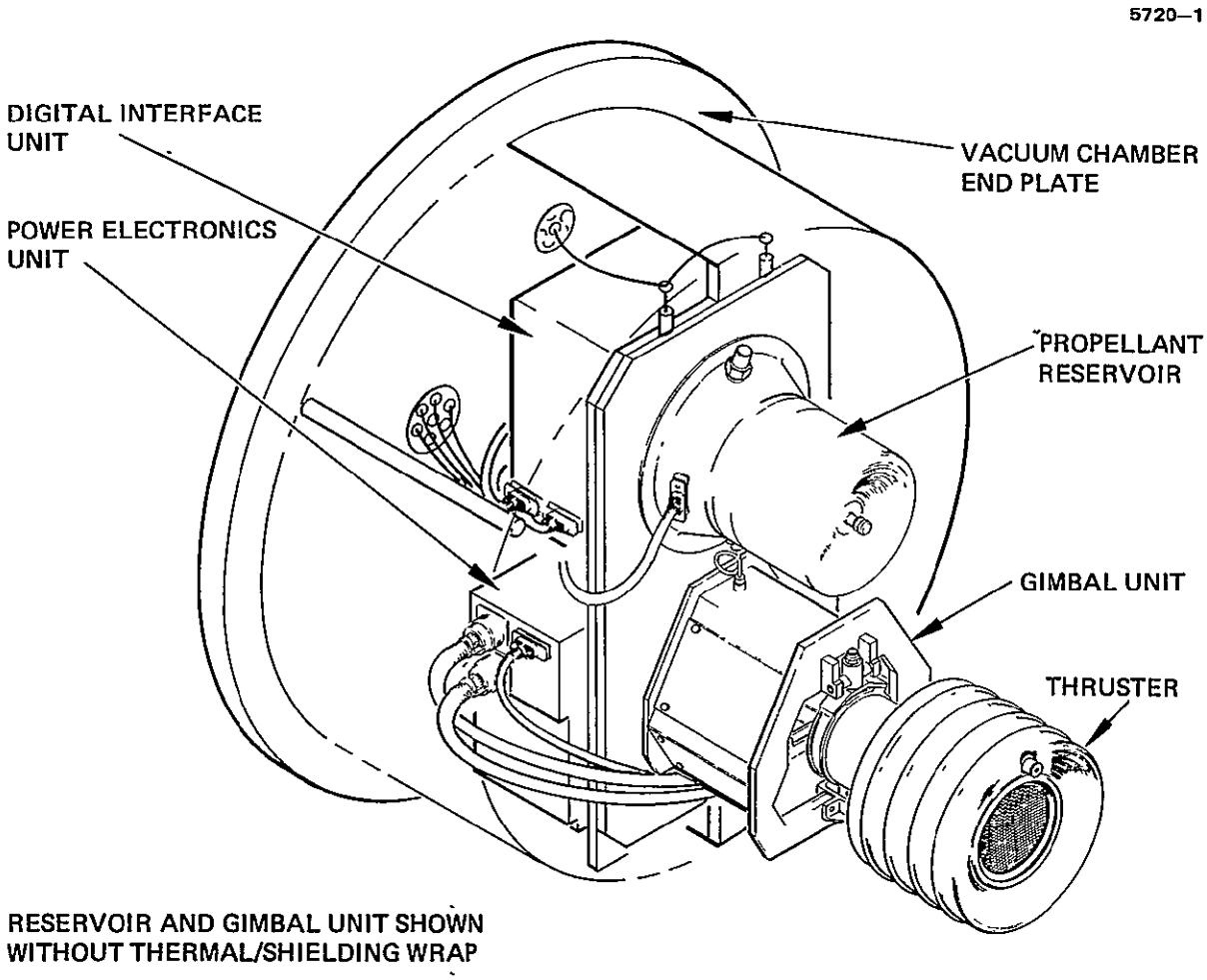

Figure 46. Subsystem configuration for thermal-vacuum cyclic test.

The first two cycles were completed without any deviations from normal operation or procedures. At I_B = 72 mA, total system input power was P_{IN} = 165 W. As shown in Table 20, most operating parameters for the two cycles were very similar. The lower discharge voltage during the second cycle is the normal consequence of an improvement in discharge-keeper voltage, since the discharge vaporizer is controlled to maintain the quantity (V_D - V_{DK})=constant.

One minute before the completion of what would have been the third cycle, the system began a series of high-voltage recycles. After approximately 30 recycles, the discharge-current-telemetry meter jumped to a full scale reading and the discharge-voltage telemetry went to zero. Visual observation of the thruster revealed that the discharge was out. The discharge-current telemetry continued to read full scale even with the discharge supply commanded off.

Table 19. 8-cm EM Thruster Startup First Start
(After Exposure to P>5 x 10^{-6} Torr)

Criterion	Action
t = 0	Discharge-cathode heater and neutralizer-cathode heater on at setpoint 2 (approx. 4 W)
t = 15 min	Discharge heater and neutralizer heater to setpoint 3 (approx. 8 W)
t = 30 min	Discharge heater and neutralizer heater to setpoint 4 (approx. 19 W)
t = 45 min	Discharge heater and neutralizer heater to setpoint 6 (approx. 25 W)
t = 75 min	Discharge vaporizer and neutralizer vaporizer on at setpoint 3
T_{NV} = 342°C	Adjust P_{NV} as necessary to maintain T_{NV} - 342°C (approx. 24 mA)
T_{DV} = 277°C	Adjust P_{DV} as necessary to maintain T_{DV} = 277°C (approx. 100 mA)
t = 120 min	Neutralizer-keeper voltage on; discharge-keeper voltage on

5911

Table 20. 8-cm EM System Cycle Test Performance Summary Averages of Telemetry Readouts*

Cycle No.	Beam		Accel		Discharge		Disch Kpr.		Neut. Kpr.		Coupling	Vap. Temp.		Remarks
	V_s (V)	I_s (mA)	V_A (V)	I_A (mA)	V_D (V)	I_D (mA)	V_{DK} (mA)	I_{DK} (mA)	V_{NK} (V)	I_{NK} (mA)	V_N (V)	Disch. (°C)	Neut. (°C)	
1	1180	72	300	0.23	34.7	456	7.3	108	13.1	495	10	256	286	
2	1180	72	300	0 27	34.1	456	6.6	108	13.2	495	10	256	285	
3	1180	72	300	0.27	34.1	456	7.4	108	12.5	495	10	256	297	New I_D Telemetry Transductor
4	1180	72	300	0.30	33.6	456	6.9	108	12.5	495	10	256	296	
5	1180[a]	69[a]	300[a]	0.22[a]	32.7[a]	N/A	8.6[a]	108[a]	12.9[a]	495[a]	10[a]	247[a]	295[a]	I_D T/M Inoperative
6	1180	69	300	0.23	32.5	N/A	8.4	108	12.9	495	10	246	297	
7	1180	65	300	0 27	32.7	N/A	8.9	108	12.9	495	10	253	292	
8	1180	69	300	0.25	32.7	N/A	8 9	108	13.6	495	10	246	286	Raised V_{NK} Setpoint
9	1180	69	300	0.23	32.5	N/A	8.5	108	13.7	495	10	245	286	
10	1180	69	300	0.24	32.5	N/A	8.4	108	13.7	495	10	245	288	

[a]For cycles 5 through 10 data is corrected for errors due to defective I_D transductor.

5911

After removal from the vacuum chamber and testing with resistive loads, a short-circuit was discovered inside the 411530-513 discharge-current transductor. The design was reviewed and modified, and a new transductor was built and installed. The previous design appeared completely adequate in static-voltage margin; however, this margin was further increased. The modified assembly was extensively exercised on resistive loads prior to reinstallation into the EMT subsystem. Initial checkout testing with the electronics outside and then inside the vacuum chamber revealed no operational problems. Cyclic testing of the thruster subsystem was then resumed.

Cycles 3 and 4 were completed without incident. Shortly after the beam was brought on for cycle 5, there were several high-voltage recycles. The discharge-current telemetry was then observed to be indicating full scale. However, the discharge did not go out as had been the case earlier when the first discharge-current transducer failed. After a period of experimentation with the discharge-supply commands (while observing the 70 V bus-current meter), it was determined that the subsystem was still functional though the discharge-current telemetry was inoperative. The fifth cycle was restarted, and the remainder of the thermal-vacuum test was completed without any other problems. It was noted that after the discharge-current-telemetry channel became inoperative the other telemetry channels were reading slightly high. The data presented in Table 20 has been corrected for this inaccuracy. Because of the uncertainty in (1) the amount of beam-current-telemetry offset and (2) the actual level of discharge current, the corrected beam was less than I_B = 72 mA for cycles 5 through 10.

During the thermal-vacuum cyclic test, temperatures were monitored at three locations on the PEU, two locations on the DIU, the propellant reservoir, and the baseplate for the reservoir and gimbal. Temperature monitoring of the PEU and DIU was accomplished by placing thermocouples between the unit mounting flanges and the heads of the screws that fastened the unit to the mounting plate. Locations monitored on the PEU were the input endbell, the discharge module, and the output endbell.

Locations monitored on the DIU were the input endbell and output endbell. The maximum and minimum temperatures measured for all seven locations are presented in Table 21. The temperatures measured at the start and end of each cycle are listed in Table 22.

Dummy-load testing of the discharge supply after completion of the cyclic test identified the cause of the discharge-current-telemetry problem as a defective transductor again. The replacement for the original transductor (which had failed) was now defective. Further investigation demonstrated that, because of the turns ratio, voltages in excess of the transductor rating could be induced across the gate windings when pulses below the screen-voltage potential were applied across the sense winding. Since it seems likely that most of the combined screen and accelerator potential would appear across the transductor sense winding during an interelectrode arc, the resulting induced voltage in the gate winding was probably the cause of both transductor failures. It was also demonstrated that a zener clamp across the gate windings would clamp the induced voltage to a level consistent with the transductor's rating. This modification was subsequently implemented in the EM PPU discharge-current-telemetry circuit and extensively tested under worst-case, transient overload conditions.

Table 21. 8-cm System Maximum and Minimum Temperatures Measured during Thermal-Vacuum Cyclic Test.

Location	Temperature (°C)	
	Maximum	Minimum
PEU Input Endbell Exterior	53	10
PEU Discharge Module Exterior	48.6	10.5
PEU Output Endbell Exterior	47	10.5
DIU Input Endbell Exterior	44	10.5
DIU Output Endbell Exterior	45	10
Propellant Reservoir	59	0.5
Reservoir & Gimbal Baseplate	61	8

5911

Table 22. EM 8-cm System Temperatures (°C) at Start and End of Operating Cycles during Thermal-Vacuum Cyclic Test

Cycle No.	Power Electronics Unit						Digital Interface Unit				Propellant Reservoir		Reservoir and Gimbal Baseplate	
	Input Endbell		Discharge Module		Output Endbell		Input Endbell		Output Endbell					
	Start	End	Start	End	Start	End	Start	End	Start	End	Start	End	Start	End
1	35	41.5	33	37.5	33	39.5	33	34	33	34	19	19	26.5	24.5
2	33.5	41	31.5	38	31.5	39.5	31.5	34	31.5	34	19	19	24.5	24.5
3	38.1	44.6	36.8	42.8	35	41.1	35	36.6	35.9	37.5	35	35	31.6	29.7
4	36.8	43.5	35	42	33.8	40	33.7	36	34.5	36.5	32	29	29.3	28.5
5	-	47.2	-	45.4	-	43.2	-	38.8	-	39.9	29	35	-	32.2
6	41.0	47.6	38.7	45.8	37	43.6	36.7	38.8	37.8	40	32	35	31.8	31.3
7	14.9	33.5	14.7	32.9	14.2	31.3	15.3	27.1	14	27.1	10	15	11.7	19.3
8	-	41.5	-	40.3	-	38.3	-	33.5	-	34.2	15	19	-	26.0
9	-	43.9	-	42.6	-	40.4	-	35.4	-	36.4	19	24	-	27.2
10	-	44.1	-	42.7	-	40.4	-	35.7	-	36.5	19	24	-	27.5

5911

4. Special Test Equipment

As previously mentioned, the DIU developed on this contract was intended to be used with a computer with the capability of maintaining proper thruster operation. It was, therefore, necessary to develop a piece of special test equipment that would allow an operator to easily exercise the PPU through its entire setpoint or control range when operating into either a dummy load or a thruster. The test equipment developed on this contract is called the "EM Power Processor Test Console," which is shown in Figure 47. The basic functions performed by the test console are as follows:

- Supplies the command data, sync, and enable signals to the DIU per the Command Code Dictionary (see Appendix A)
- Provides for automatic of manual modes of operation
- Allows supply setpoints and reference words to be selected by thumbwheel switches
- On and off control of the individual supplies
- Ability to set the interrupt overrides
- Detects transmit errors and invalid codes
- Displays telemetry on panel meters
- Three-digit display of scaled telemetry data
- Gimbal command capability
- Selection of even or odd parity of commands.

The test console can be operated in either the manual or the automatic mode. When operating in the manual mode, the bits of the command word are set using toggle switches mounted on the front panel. The command word is sent by depressing the MANUAL LOAD push-button switch. When operating in the automatic mode, the individual supply setpoints (and certain reference values) are selected by the front-panel thumbwheel switches. Supply on/off commands are set by toggle switches. The individual commands are sent by depressing the push button located just below the thumbwheel switch (or associated with the toggle switches).

Another method of loading commands is to depress the AUTOMATIC LOAD push button. When this is done, all commands of the dictionary are sent with values as determined by the front-panel switches. Additionally, the interrupt-overrides, keeper-pulsers, grid-clear, and gimbal commands are controlled by front-panel switches.

The telemetry data received from the power processor is displayed on panel meters on the test console. A listing of the various parameters monitored via telemetry is given in Table 23. The data received from the power processor is in seven-bit serial form. It is stored and converted to an analog signal by the test console so that it can be displayed on panel meters. In addition to the panel meters, the telemetry data can be displayed on a three-digit display. Unlike the meters which display the data as 0 to 5 V, the digital display presents the data in engineering units. For example, the screen voltage, which is 1180 V, is displayed as 118. The channel to be displayed digitally is selected by thumbwheel switches located directly beneath the display.

M11813

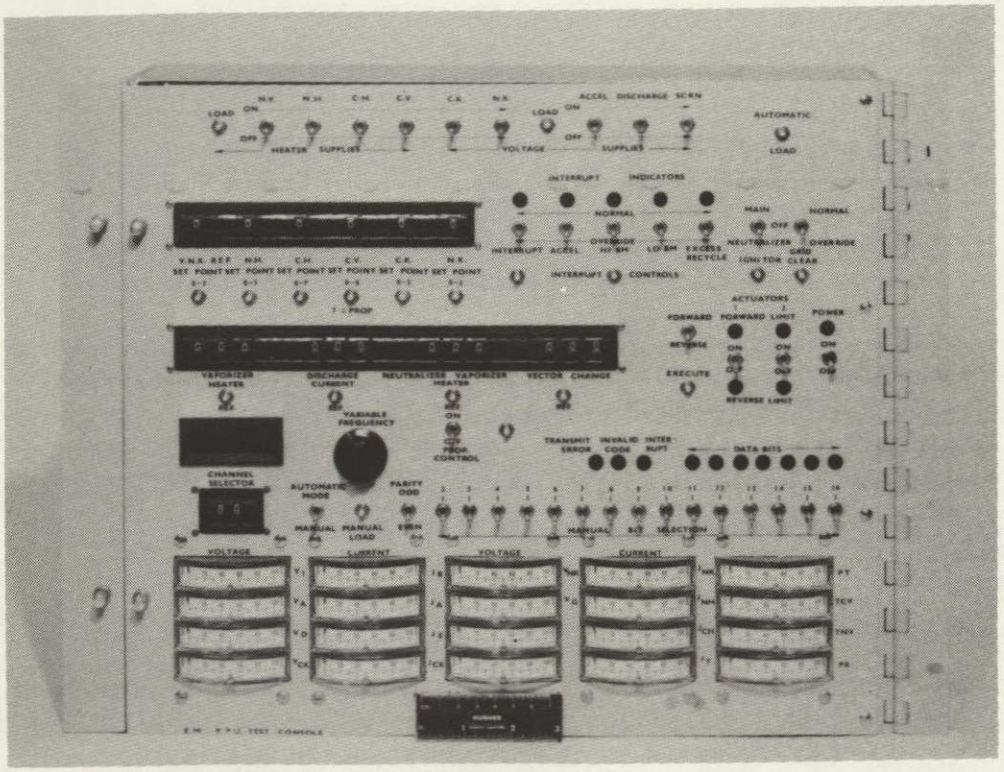

Figure 47. EM power processor test console.

Table 23. Power Processor Telemetry List

Display Channel	Parameter
20	Beam Current (I_B)
21	Net Accelerating Voltage (V_B)
22	Neutralizer emission current (I_N)
23	Discharge Voltage (V_D)
24	Neutralizer Floating Potential (V_N)
25	Accelerator Current (I_A)
26	Neutralizer Keeper Voltage (V_{NK})
27	Reservoir Pressure (P_r)
28	Accelerator Voltage (V_A)
29	Neutralizer Keeper Current (I_{NK})
30	Total Thruster System Current (I_{in})
31	Discharge Vaporizer Temperature (T_{DV})
32	Neutralizer Vaporizer Temperature (T_{NV})
33	Propellant Temperature (T_{Hg})
34	Discharge-Keeper Current (I_{DK})
35	Discharge-Keeper Voltage (V_{DK})
36	Neutralizer-Cathode-Tip Heater Current (I_{NH})
37	Discharge-Cathode-Tip Heater Current (I_{DH})

5911

There are several other functions in the test console that were included to either better simulate a computer interface or to allow more thorough testing of the Power Processor. For example, a toggle switch on the front panel allows the test console to send commands of either odd or even parity. This was done so that testing could be performed that ensured that only the power processor responded to commands of odd parity. An internal invalid-code detector circuit determines if any reference-word thumbwheel switches have been set to a value beyond the range of operation of the power processor. If this occurs, the INVALID CODE light will flash, and the test console will be prevented from issuing commands. The bit rate of the command data can be adjusted from approximately one to ten kilobits per second data rate by the VARIABLE FREQUENCY potentiometer. This allows testing of the power processor at the various bit rates that could be sent by the computer. The final function in the test console that will be discussed is the transmit error function. The circuitry that performs this function compares the power processor command response to the issued command. If the power processor response is correct, the command-enable line remains high allowing the power processor to execute the command. If, however, the response from power processor is incorrect, the TRANSMIT ERROR light will flash, and the enable line will go low. This will prevent the Power Processor from executing the command.

The test console was fabricated using a 14-in. swing-out panel for ease of servicing and for installation into existing equipment racks. The test console is presently installed in an enclosure that accepts the standard 14-in. panel.

REFERENCES

1. B.A. Banks, ed., "8-CM Mercury Ion Thruster System Technology," NASA TMX-71611, NASA Lewis Research Center, Cleveland, Ohio.

2. H.R. Kaufman, "An Ion Rocket with an Electron-Bombardment Ion Source," TN D-585, NASA Lewis Research Center, Cleveland, Ohio, January 1961.

3. J. Hyman, Jr., "8-CM Technology Thruster Development," Final Report NAS 3-17791, NASA CR-134-685, Hughes Research Laboratories, Malibu, CA 90265 July 1974.

4. M.A. Mantenieks and V.K. Rawlin, "Studies of Internal Sputtering on a 30-CM Ion Thruster," AIAA Paper 75-400, AIAA 11th Electric Propulsion Conference, March 19-21, 1975, New Orleans, Louisiana.

5. W.R. Hudson, "Auxiliary Propulsion Thruster Performance with Ion Machined Accelerator Grids," AIAA Paper 75-425, AIAA 11th Electric Propulsion Conference, March 19-21, 1975, New Orlean, Louisiana.

6. J. Hyman, Jr., "Development of a 5 CM-Flight-Qualified Mercury Ion Thruster, J. Spacecraft and Rockets, 10, 503-509, Aug. 1973.

7. S. Nakanishi and R.C. Finke, "A 9700-Hour Durability Test of a Five Centimeter Diameter Ion Thruster," AIAA Paper 73-1111, AIAA 10th Electric Propulsion Conference, Oct. 31 - Nov. 2, 1973, Stateline, Nevada.

8. J. Hyman, Jr. and R.L. Poeschel, "Satellite Control Mercury Ion Thruster," AIAA Paper 73-1132, (1973), Lake Tahoe, Nevada.

9. J. Hyman, Jr., et al., "One-Millipound Mercury Ion Thruster," J. Spacecraft and Rockets 13, 366-372 (1976).

10. S. Nakanishi, "A 15,000-Hour Cyclic Endurance Test of an 8-CM Diameter Mercury Ion Thruster," AIAA Paper 76-1022, AIAA International 12th Electric Propulsion Conference, Nov. 15-17, 1976, Key Biscayne, Florida.

11. R.C. Finke, B.G. Herron, and G.D. Gant, "Power Processing for Electric Propulsion," NASA TMX-71775, NASA Lewis Research Center, Cleveland, Ohio.

12. J. Hyman, Jr., "Design and Development of a Small Structurally Integrated Ion Thruster System," Final Report on Contract NAS 3-14129, NASA CR120821, Hughes Research Laboratories, October 1971.

13. J.L. Power, "Sputter Erosion and Deposition in the Discharge Chamber of a Small Mercury Ion Thruster," AIAA Paper 73-1109, AIAA 10th Electric Propulsion Conference, October 31 - November 2, 1973, Lake Tahoe, Nevada.

14. H.L. King, and R.L. Poeschel, "A 30 CM Ion Thruster Module," J. Spacecraft and Rockets 8, 420-423, April 1971.

15. W. Knauer, "Power Efficiency Limits of Kaufman Thruster Discharges," AIAA Paper 70-177, (1970) New York, New York.

16. J. Hyman, Jr., "Performance Optimized Small Structurally Integrated Ion Thruster System," Final Report on Contract NAS 3-15483, NASA CR-121183, Hughes Research Laboratories, May 1973.

17. E.G. Wintucky, "High Voltage Pulse Ignition of Mercury Discharge Hollow Cathodes," AIAA Paper 73-1140, AIAA 10th Electric Propulsion Conference, (1973), Lake Tahoe, Nevada.

18. Special Report — "Thruster Performance Acceptance Test Plan, "8-CM Engineering Model Thruster System, Contract NAS 3-18917, Hughes Research Laboratories, August 10, 1976.

19. "8 CM Mercury Ion Thruster Subsystem Users Manual," TRW Defense and Space Systems Group, July 1977.

APPENDIX A

EM 8-CM Thruster System Command Code Dictionary

Table A-1. Word Format

COMMAND WORD (TO PPU)																RESPONSE WORD (FROM PPU)							
PARITY BIT	MESSAGE DATA FIELD							COMMAND TYPE FIELD			COMMAND USER FIELD (DEVICE ADDRESS)					VERIFY BIT	DATA RESPONSE BITS						
																	COMMAND FLAG BIT						
1	2	3	4	5	6	7	8	9	10	11	12	13	14	15	16	17	18	19	20	21	22	23	24

BIT TIMES

Bit 1 Parity - Odd Parity for Bits 1 through 16

Bits 2 through 8 Message Data Field - Defines the Specific Command and Action Required within the Type Defined by the Command Type Field

Bits 9 through 11 Command Type Field - Defines the Type of Command that is to be performed, such as Set Reference Value, Power Supplies On/Off, Set Discrete Set Points, Initiate Measurement, etc.

Bits 12 through 16 Command User Field - Defines the Specific Power Processor of Other Spacecraft Device for which Command is Intended.

Bits 17, 18 Command Verify Bits - Bit 17 is Set = 1 by the PPU if the Transmission of the Command Word Requests a Measurement. For all Other Types of Command Words, this Bit is Set = 0 and Bit 18 is Set = 1. No response is made at bit times 17 and 18 if a parity error is detected or the received command is undefined.

Bits 18 through 24 Data Return Bits - 7 Bit Data from Analog Measurements or Discrete Status Word

5911

PAGE 124 INTENTIONALLY BLANK

Table A-2. Discrete Commands (Command Type #2)

x	-	-	-	-	-	-	-	0	1	0	x	x	x	x	x
1	2	3	4	5	6	7	8	9	10	11	12	13	14	15	16

BIT TIME

Function Word Number	VARIABLE	State	Bit Number 2	3	4	5	6	7	8	Function	Value
2-0	INTERRUPT OVERRIDE					0	0	0	0		
	HIGH BEAM	1	0	x	x					NORMAL	
	CURRENT	2	1	x	x					OVERRIDE	
	LOW BEAM	3	x	0	x					NORMAL	
	CURRENT	4	x	1	x					OVERRIDE	
	EXCESSIVE HIGH	5	x	x	0					NORMAL	
	VOLTAGE RECYCLING	6	x	x	1					OVERRIDE	
2-1	DISCHARGE VAPORIZER HEATER (I_{DV})	1	0	0	0	0	0	0	1	SET PT. #1	4 W (1.25A)
		2	1	0	0					SET PT. #2	7 W (1.64 A)
		3	0	1	0					SET PT. #3	8 W (1.75A)
		4	1	1	0					SET PT. #4	9 W (1.86A)
		5	0	0	1					SET PT. #5	12 W (2.13A)
		6	1	0	1					SET PT. #6	15 W (2.38A)
		7	0	1	1					SET PT. #7	18 W (2.60A)
		8	1	1	1					PROP. CONTROL	ON
2-2	NOT USED					0	0	1	0	NOT USED	--
2-3	NOT USED					0	0	1	1	NOT USED	--
2-4	NEUTRALIZER VAPORIZER HEATER (I_{NV})	1	0	0	0	0	1	0	0	SET PT. #1	0.8 W (0.49A)
		2	1	0	0					SET PT. #2	1.3 W (0.62A)
		3	0	1	0					SET PT. #3	1.5 W (0.67A)
		4	1	1	0					SET PT. #4	8 W (1.48A)
2-5	CATHODE HEATER	1	0	0	0	0	1	0	1	SET PT. #1	2 W (1.25A)
		2	1	0	0					SET PT. #2	4 W (1.66A)
		3	0	1	0					SET PT. #3	8 W(2.12A)
		4	1	1	0					SET PT. #4	20 W (2.92A)
		5	0	0	1					SET PT. #5	24 W (3.10A)
		6	1	0	1					SET PT. #6	28 W (3.28A)
		7	0	1	1					SET PT. #7	32 W (3.42A)
		8	1	1	1					SET PT. #8	36 W (3.57A)

*TBD's are engine dependent and shall be determined by the contractor and approved by the NASA program manager.

BIT = x means that the specified bit need not be determined for that function.

5911

Table A-2. Discrete Commands (Command Type #2) (Continued)

x	-	-	-	-	-	-	-	0	1	0	x	x	x	x	x
1	2	3	4	5	6	7	8	9	10	11	12	13	14	15	16

BIT TIME

Function Word Number	Variable	State	Bit Number 2	3	4	5	6	7	8	Function	Value
2-6	NEUTRALIZER HEATER I_{NH}	1	0	0	0	0	1	1	0	SET PT. #1	2 W (1.25A)
		2	1	0	0					SET PT. #2	4 W (1.66A)
		3	0	1	0					SET PT. #3	8 W (2.12A)
		4	1	1	0					SET PT. #4	16 W (2.71A)
		5	0	0	1					SET PT. #5	25 W (3.15A)
		6	1	0	1					SET PT. #6	28 V (3.27A)
		7	0	1	1					SET PT. #7	32 W (3.42A)
		8	1	1	1					SET PT. #8	36 W (3.57A)
2-7	DISCH. IGNITOR	1	1	0	x	0	1	1	1	PULSE	---
	NEUT. IGNITOR	2	0	1	x					PULSE	---
2-8	INTERRUPT OVERRIDE	1	x	x	0	1	0	0	0	NORMAL	---
	ACCEL CURRENT HIGH	2	x	x	1					OVERRIDE	---
2-9	DISCH. KEEPER (I_{DK})	1	0	0	x	1	0	0	1	SET PT. #1	60
		2	1	0	x					SET PT. #2	120
		3	0	1	x					SET PT. #3	360
		4	1	1	x					SET PT #4	500
2-10	NEUTRALIZER KEEPER (I_{NK})	1	0	0	x	1	0	1	0	SET PT. #1	360
		2	1	0	x					SET PT. #2	430
		3	0	1	x					SET PT. #3	500
		4	1	1	x					SET PT. #4	500
	INTERRUPT OVERRIDE	5	x	x	0					NORMAL	---
	NEUTRALIZER OFF	6	x	x	1					OVERRIDE	---
2-11	GRID CLEAR	1	x	x	0	1	0	1	1	NORMAL	---
		2	x	x	1					OVERRIDE	---

5911

Table A-2. Discrete Commands (Command Type #2) (Continued)

x	-	-	-	-	-	-	-	0	1	0	x	x	x	x	x
1	2	3	4	5	6	7	8	9	10	11	12	13	14	15	16

Function Word Number	Variable	State	Bit Number							Function	Value
			2	3	4	5	6	7	8		
2-12	NOT USED	1	0	0	0	1	1	0	0		
		2	1	0	0						
		3	0	1	0						
		4	1	1	0						
		5	0	0	1						
		6	1	0	1						
		7	0	1	1						
		8	1	1	1						
2-13	NOT USED	1	0	0	x	1	1	0	1		
		2	1	0	x						
		3	0	1	x						
		4	1	1	x						
		5	x	x	0						
		6	x	x	1						
2-14	NOT USED					1	1	1	0		--
2-15	NOT USED					1	1	1	1		--

5911

Table A-3. Power Supply On/Off Commands (Command Type #3)

x	-	-	-	-	-	-	-	0	1	1	x	x	x	x	x	
1	2	3	4	5	6	7	8	9	10	11	12	13	14	15	16	BIT TIME

Function Word Number	Variable	State	Bit Number 2	3	4	5	6	7	8	Function	Value
3-0	NEUTRALIZER KEEPER SUPPLY (I_{NK})	1	0	x	x	x	x	x	0	P.S. #7	Off
		2	1	x	x	x	x	x	0	P.S. #7	On
	DISCHARGE KEEPER SUPPLY (I_{DK})	3	x	0	x	x	x	x	0	P.S. #8	Off
		4	x	1	x	x	x	x	0	P.S. #8	On
	NOT USED	5	x	x	0	x	x	x	0	P.S. #12	Off
		6	x	x	1	x	x	x	0	P.S. #12	On
	DISCHARGE SUPPLY (I_D)	7	x	x	x	0	x	x	0	P.S. #9	Off
		8	x	x	x	1	x	x	0	P.S. #9	On
	SCREEN SUPPLY (I_S)	9	x	x	x	x	0	x	0	P.S. #11	Off
		10	x	x	x	x	1	x	0	P.S. #11	On
	ACCELERATOR SUPPLY (V_A)	11	x	x	x	x	x	0	0	P.S. #10	Off
		12	x	x	x	x	x	1	0	P.S. #10	On
3-1	NEUTRALIZER-CATHODE HEATER SUPPLY (I_{NH})	1	0	x	x	x	x	x	1	P.S. #5	Off
		2	1	x	x	x	x	x	1	P.S. #5	On
	DISCHARGE-CATHODE HEATER SUPPLY (I_{DH})	3	x	0	x	x	x	x	1	P.S. #3	Off
		4	x	1	x	x	x	x	1	P.S. #3	On
	NEUTRALIZER VAPORIZER SUPPLY (I_{NV})	5	x	x	0	x	x	x	1	P.S. #6	Off
		6	x	x	1	x	x	x	1	P.S. #6	On
	DISCHARGE VAPORIZER SUPPLY (I_{DV})	7	x	x	x	0	x	x	1	P.S. #2	Off
		8	x	x	x	1	x	x	1	P.S. #2	On
	NOT USED	9	x	x	x	x	0	x	1	P.S. #1	Off
		10	x	x	x	x	1	x	1	P.S. #1	On
	NOT USED	11	x	x	x	x	x	0	1	P.S. #4	Off
		12	x	x	x	x	x	1	1	P.S. #4	On

5911

Table A-4

REFERENCE WORD FOR NEUTRALIZER VAPORIZER HEATER LOOP
(COMMAND TYPE 4)

x	-	-	-	-	-	-	-	1	0	0	x	x	x	x	x	
1	2	3	4	5	6	7	8	9	10	11	12	13	14	15	16	BIT TIME

LSB — MSB

"VALUE" OF REFERENCE WORD AS A BINARY NUMBER TO LINEARLY REPRESENT V_{NK} VALUES BETWEEN 10 VOLTS AND 30 VOLTS

0	0	0	0	0	0	0	=	10 VOLTS
0	1	1	1	1	1	1	=	30 VOLTS
1	x	x	x	x	x	x	=	PROP. CONTROL

DISCHARGE CURRENT (I_D) REFERENCE WORD
(COMMAND TYPE 5)

x	-	-	-	-	-	-	-	1	0	1	x	x	x	x	x	
1	2	3	4	5	6	7	8	9	10	11	12	13	14	15	16	BIT TIME

LSB — MSB

"VALUE" OF REFERENCE WORD AS A BINARY NUMBER TO LINEARLY REPRESENT I_D VALUES BETWEEN 0.20 AMPS AND 1.00 AMPS

0	0	0	0	0	0	0	=	0.20 AMPS (MIN)
1	1	1	1	1	1	1	=	1.00 AMPS (MAX)

NOT USED REFERENCE WORD (COMMAND TYPE 6)

x	-	-	-	-	-	-	-	1	1	0	x	x	x	x	x	
1	2	3	4	5	6	7	8	9	10	11	12	13	14	15	16	BIT TIME

5911

Table A-5. Reference Word for Cathode Vaporizer Loop

x	-	-	-	-	-	-	-	1	1	1	x	x	x	x	x	
1	2	3	4	5	6	7	8	9	10	11	12	13	14	15	16	BIT TIME

LSB ... MSB

"VALUE" OF REFERENCE WORD AS A BINARY NUMBER TO LINEARLY REPRESENT ($V_D - V_{DK}$) VALUES BETWEEN 16 VOLTS AND 35 VOLTS

0 0 0 0 0 0 0 = 16 VOLTS (MIN)
1 1 1 1 1 1 1 = 35 VOLTS (MAX)

COMMAND USER FIELD, COMMON PPU ADDRESS DEFINITION
(INDIVIDUAL PPU ADDRESS DETERMINED BY COMMAND AND DIGITAL DATA CONNECTOR JUMPERS)

x	x	x	x	x	x	x	x	x	x	x	x	x	x	x	x
1	2	3	4	5	6	7	8	9	10	11	12	13	14	15	16

ALL PPU RESPOND: 1 0 1 0 1

5911

Table A-6. Telemetry Measurement Commands (Command Type 1)

x	-	-	-	-	-	-	-	0	0	1	x	x	x	x	x	
1	2	3	4	5	6	7	8	9	10	11	12	13	14	15	16	BIT TIME

Function Word Number	State	Bit Number 2	3	4	5	6	7	8	Parameter Measured
	1	1	0	0	0	0	0	0	I_B Beam Current (0 to 100 ma)
	2	1	1	0	0	0	0	0	V_B Net Accelerating Voltage (0 to 1200 volts)
	3	1	0	1	0	0	0	0	I_D Discharge Current (0 to 1 amp)
	4	1	1	1	0	0	0	0	V_D Discharge Voltage (0 to 50 volts)
	5	1	0	0	1	0	0	0	V_N Neutralizer Floating Potential (0 to 200 V)
	6	1	1	0	1	0	0	0	I_A Accelerator Current (0 to 5 ma)
	7	1	0	1	1	0	0	0	V_{NK} Neutralizer Keeper Voltage (0 to 50 volts)
	8	1	1	1	1	0	0	0	P_r Reservoir Pressure (0 to 50 psia)
	9	1	0	0	0	1	0	0	V_A Accelerator Voltage (0 to 300 volts)
	10	1	1	0	0	1	0	0	I_{NK} Neutralizer Keeper Current (0 to 1 amp)
	11	1	0	1	0	1	0	0	Not Used
	12	1	1	1	0	1	0	0	I_{IN} Total Thruster System Current (0 to 5 amps)
	13	1	0	0	1	1	0	0	Not Used
	14	1	1	0	1	1	0	0	T_{DV} Discharge Vaporizer Temperature (0 to 500 Ω)
	15	1	0	1	1	1	0	0	T_{NV} Neutralizer Vaporizer Temperature (0 to 500 Ω)
	16	1	1	1	1	1	0	0	T_{Hg} Propellant Temperature (0 to 500 Ω)
	17	1	0	0	0	0	1	0	T_{CK} Cathode Keeper Current (0 to 1 amp)
	18	1	1	0	0	0	1	0	V_{CK} Cathode Keeper Voltage (0 to 50 volts)
	19	1	0	1	0	0	1	0	I_{NH} Neutralizer-Cathode Tip Heater Current (0 to 4 amp)
	20	1	1	1	0	0	1	0	I_{DH} Discharge-Cathode Tip Heater Current (0 to 4 amp)
	21	1	0	0	1	0	1	0	Not used
	22	1	1	0	1	0	1	0	Not Used
	23	1	0	1	1	0	1	0	Not Used
	24	1	1	1	1	0	1	0	Not Used
1-0	1	0	0	0	0	0	0	0	Interrupt Status Word
	2	0	1	0	0	0	0	0	General Status Words (Bits TBD)
	3	0	0	1	0	0	0	0	Not Used
	4	0	1	1	0	0	0	0	Recycle Count Register

5911

TABLE A-7

6704-25

EXAMPLE 1

COMMAND DATA LINE INPUT (MEASURE V_A) (PPU 01001)

0	1	0	0	0	1	0	0	0	0	1	0	1	0	0	1	Bit Time
1	2	3	4	5	6	7	8	9	10	11	12	13	14	15	16	

PPU DIGITAL DATA LINE RESPONSE TO COMMAND DATA LINE INPUT

0	1	0	0	0	1	0	0	0	0	1	0	1	0	0	1	1	0	1	1	1	1	1	1	Bit Time
1	2	3	4	5	6	7	8	9	10	11	12	13	14	15	16	17	18	19	20	21	22	23	24	

ECHO BACK OF COMMAND LINE INPUT

VALUE OF V_A (SCALED, 63/10)

VERIFY BIT = 1

EXAMPLE 2

COMMAND DATA LINE INPUT (SET J_F TO 63, SCALED)

1	1	1	1	1	1	1	0	1	0	1	0	1	0	0	1	Bit Time
1	2	3	4	5	6	7	8	9	10	11	12	13	14	15	16	

PPU DIGITAL DATA LINE RESPONSE TO COMMAND DATA LINE INPUT

1	1	1	1	1	1	1	0	0	0	1	0	1	0	0	1	0	1	X	X	X	X	X	X	Bit Time
1	2	3	4	5	6	7	8	9	10	11	12	13	14	15	16	17	18	19	20	21	22	23	24	

ECHO BACK OF COMMAND LINE INPUT

VERIFY BIT = 0

COMMAND FLAG BIT = 1

EXECUTE COMMAND AT THIS TIME

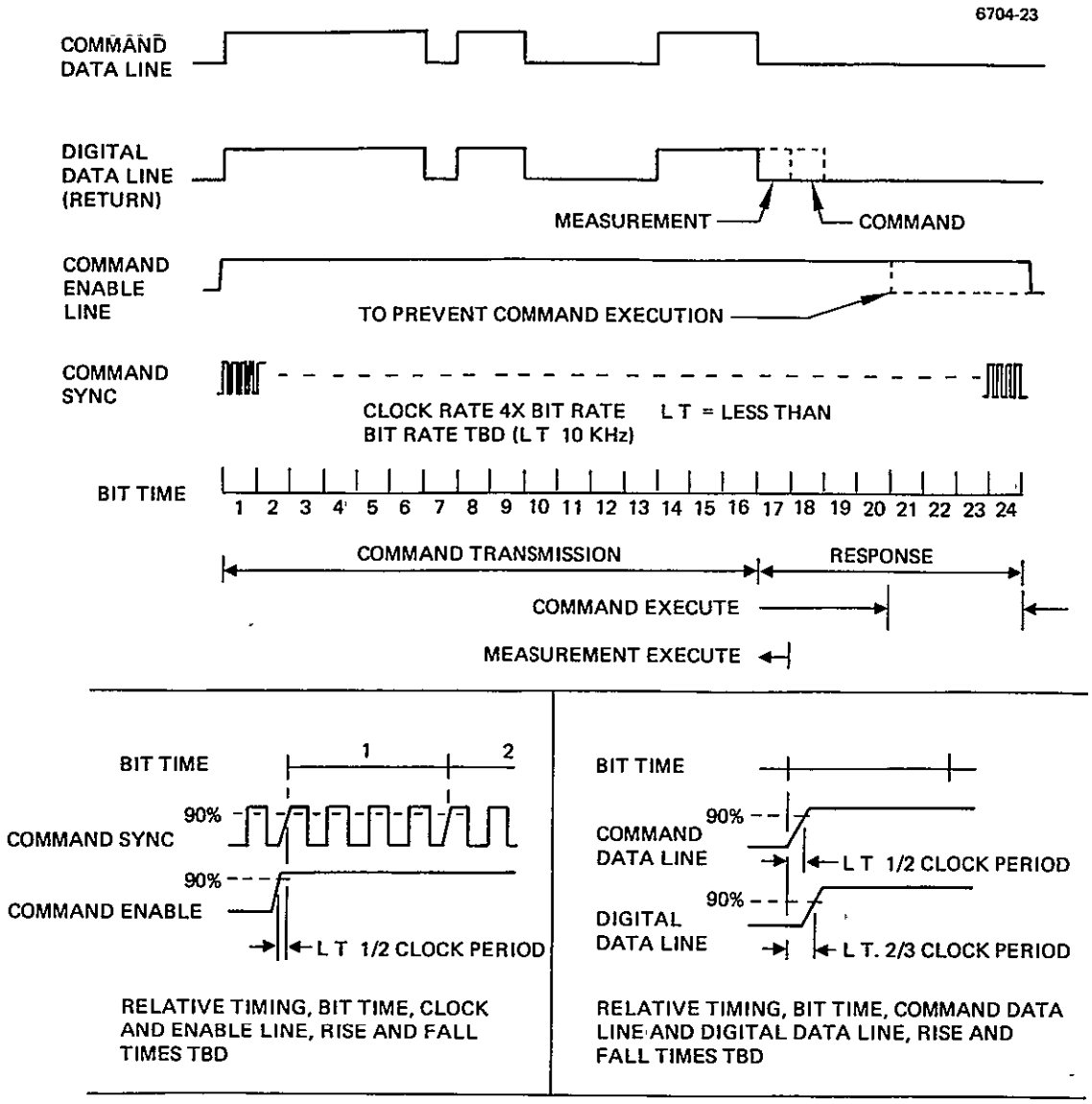

Figure A-1. Timing limits command data bus and digital data line, exact values.

6704-24R1

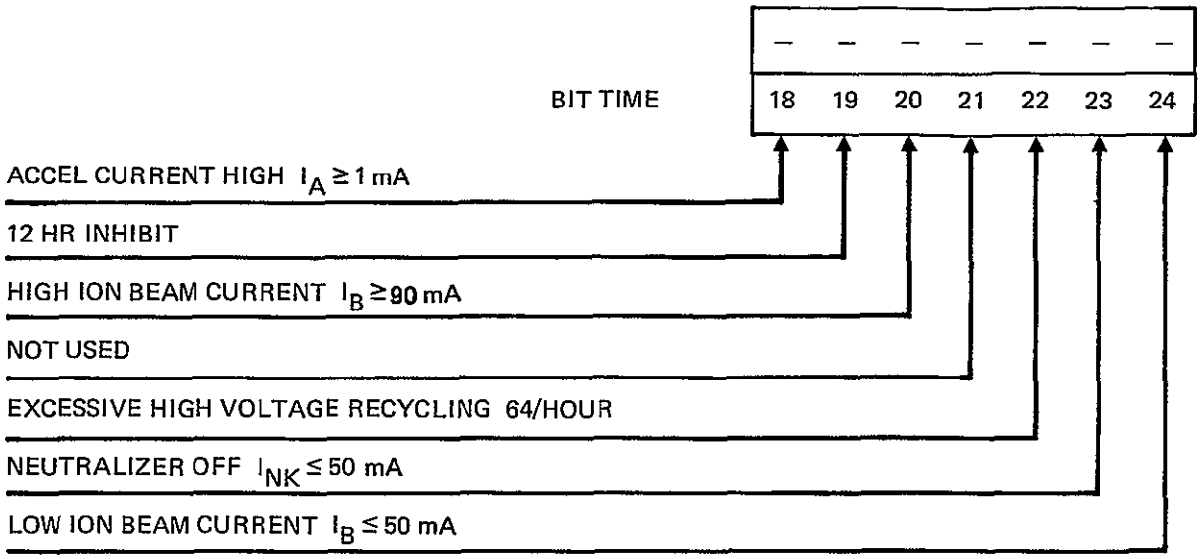

INTERRUPT IS OFF OR IN NORMAL STATE WHEN BIT = 0. WHEN ANY BIT = 1, THEN THE INTERRUPT OCCURS THE OFF-NORMAL CONDITIONS INDICATED CAUSE THE SPECIFIED BIT TO GO TO THE 1 STATE, CAUSING AN INTERRUPT. THE COMPUTER CAN THEN INTERROGATE THE STATUS WORD TO FIX THE CAUSE BY USING THE COMMAND TYPE CODE OF 001 IN BITS 9 THROUGH 11 (A MEASUREMENT REQUEST) WITH A MESSAGE DATA FIELD CODE OF 0000000 IN BITS 2 THROUGH 8 (THE ADDRESS OF THE FIRST STATUS WORD, WHICH SHALL BE THE INTERRUPT STATUS WORD) THE INTERRUPT STATUS WORD IS THEN RETURNED AS BITS 18 THROUGH 24

MEASUREMENT COMMAND, RESPONSE DEFINITION
(COMMAND TYPE 1)

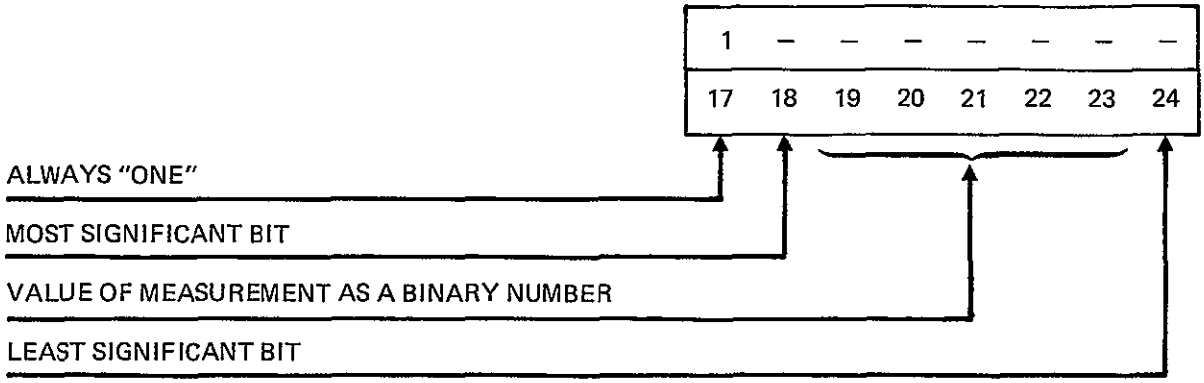

Figure A-2. Interrupt status word, bit definition.

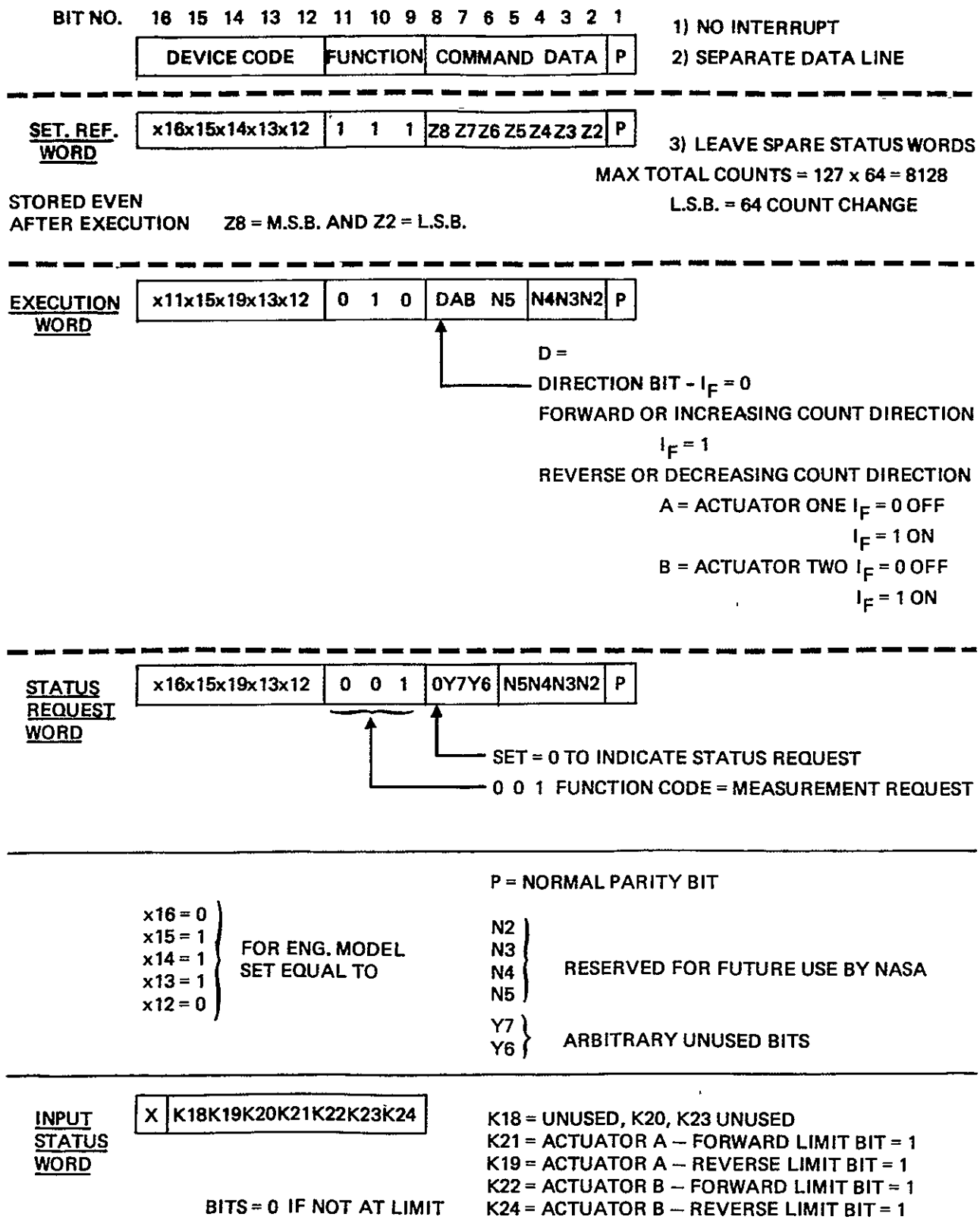

Figure A-3. Command code dictionary for vector Gimbal.

APPENDIX B

SATELLITE CONTROL ION THRUSTER

- Wiring Diagram
- Formulae for Calculating Performance
- Derivation of Equations

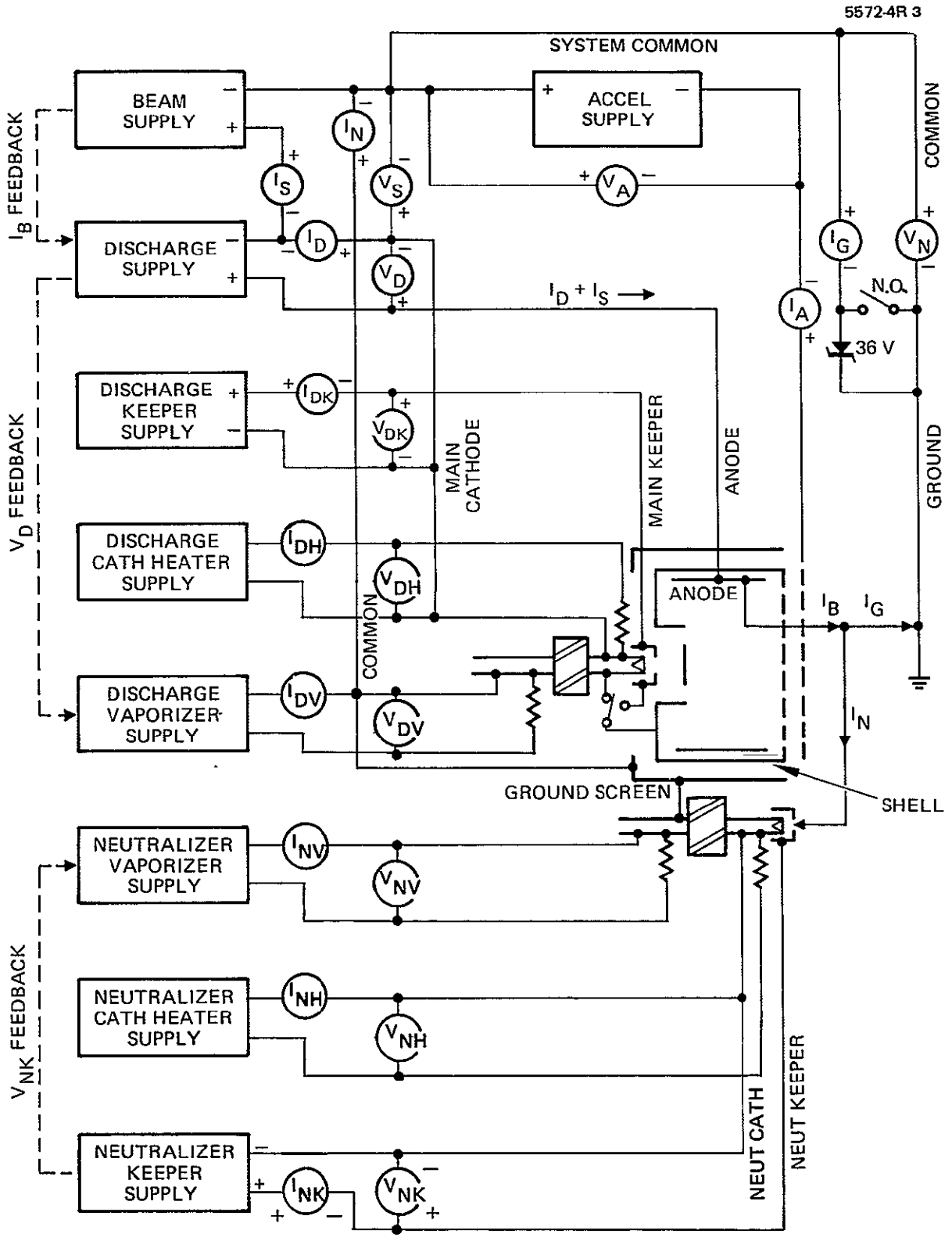

Figure B-1. Wiring diagram for mercury bombardment satellite control ion thrusters.

Table B-1. Formulae for Calculating Thruster Performance Parameters (SI Units)

Thrust, $T\ (N) = 2.0391 \times 10^{-3}\ I_S \sqrt{V_B}\ \gamma$

Specific Impulse (effective), $I_{sp}\ (sec) = 100.02\ \eta_{Hg} \sqrt{V_B}\ \gamma$

Exhaust Velocity (effective), $V_{||}\ (m\ sec^{-1}) = 980.82\ \eta_{Hg} \sqrt{V_B}\ \gamma$

Total Input Power, $P_T(W) = I_S V_S + I_A V_A + (I_S + I_D)\ V_D + I_{DK}\ V_{DK} + I_{DH} V_{DH} + I_{DV}\ V_{DV}$
(All inputs are positive) $+ I_{NK} V_{NK} + I_{NH} V_{NH} + I_{NV} V_{NV} + \text{Others}$

Output Beam Power, $P_B(W) = I_S\ V_B$

Power Balance, $P\ (W) = \dfrac{T\ I_{sp}\ g_o}{2\ \eta}$

Total Thrust Efficiency, $\eta = \eta_E\ \eta_{Hg} \gamma^2$

Electrical Efficiency, $\eta_E = \dfrac{I_S\ V_B}{P_T}$

Propellant Utilization Efficiency, $\tilde{\eta}_{Hg} = \dfrac{I_S}{I_{Hg}}$
(Uncorrected for doubly charged ions)

Discharge Propellant Utilization Efficiency, $\tilde{\eta}'_{Hg} = \dfrac{I_S}{I_{DHg}}$
(Uncorrected for doubly charged ions)

Total Propellant Flowrate Equivalent, $I_{Hg}\ (A) = I_{DHg} + I_{NHg}$

True Propellant Utilization Efficiency, $\eta_{Hg} = \left[\dfrac{1+\beta}{1+2\beta}\right] \tilde{\eta}_{Hg}$
(Corrected for doubly charged ions)

True Discharge Propellant Utilization Efficiency, $\eta'_{Hg} = \left[\dfrac{1+\beta}{1+2\beta}\right] \tilde{\eta}'_{Hg}$
(Corrected for doubly charged ions)

Discharge Power, $P_D(W) = I_D\ V_D$

Ion Generation Energy, $\epsilon_I(eV/ion) = (I_D\ V_D + I_{DK}\ V_{DK})/I_S$

Accelerator Drain Power, $P_A(W) = I_A \left(|V_A| + |V_N|\right)$

Neutralizer Coupling Power, $P_N(W) = \left(|I_S| - |I_A|\right) |V_N|$

$\gamma = \alpha f_{||}$, $\alpha = \dfrac{1 + 1.414\beta}{1 + 2\beta}$, $\beta = \dfrac{m_B^{++}}{m_B^{+}} = \dfrac{I_B^{++}}{2I_B^{+}}$ $I_B = (1 + 2\beta)\ I_B^{+}$

$I_B \equiv I_S$, $F_T = \dfrac{\int_0^{\theta max} T(\theta) \cos\theta\ d\theta}{\int_0^{\theta max} T(\theta)\ d\theta}$

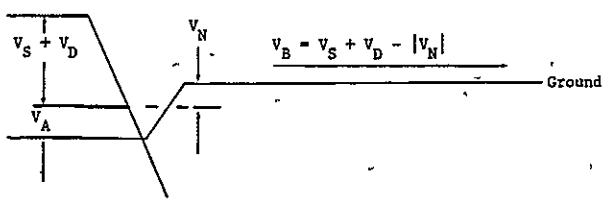

5911

Table B-2. Derivation of Thruster Characterization Equations

Mass Flowrate

$I_{Hg} = I_{DHg} + I_{NHg}$ In Amperes Equivalent

$\dot{m} = \frac{m}{e} I_{Hg}$ In Kilograms per Second

$\dot{m} = \dot{m}^{o} + \dot{m}^{+} + \dot{m}^{++}$

$1 = \frac{\dot{m}^{o}}{\dot{m}} + \frac{\dot{m}^{+}}{\dot{m}} + \frac{\dot{m}^{++}}{\dot{m}}$

$\eta_o = \frac{\dot{m}^{o}}{\dot{m}}$; $\eta_1 = \frac{\dot{m}^{+}}{\dot{m}}$; $\eta_2 = \frac{\dot{m}^{++}}{\dot{m}}$

$I_S = (\eta_1 + 2\eta_2) I_{Hg} = \tilde{\eta}_{Hg} I_{Hg}$

$\dot{m} = \frac{I_S m}{(\eta_1 + 2\eta_2) e}$

Thrust

$T = \sum_{\alpha} \dot{m}_\alpha v_{\alpha||} = \langle \dot{m} v_{||} \rangle$

$T = \dot{m}^{o} v^{o} + \dot{m}^{+} v^{+}_{||} + \dot{m}^{++} v^{++}_{||}$

$T = \dot{m} \left[\eta_1 + \sqrt{2}\, \eta_2 \right] \left(\frac{2eV_B}{m} \right)^{1/2} F_{||}$

$T = I_S (V_B)^{1/2} \left(\frac{2m}{e} \right)^{1/2} \left(\frac{\eta_1 + \sqrt{2}\, \eta_2}{\eta_1 + 2\, \eta_2} \right) F_{||}$

$T = I_S (V_B)^{1/2} \left(\frac{2m}{e} \right)^{1/2} \gamma$

Table B-2. Derivation of Thruster Characterization Equations (Continued)

Beam Exhaust Velocity (Singly Charged ions)

$$v_B = \left(\frac{2e\ V_B}{m}\right)^{1/2}$$

Exhaust Velocity (Effective)

$$v_{||} = \frac{\sum_\alpha \dot{m}_\alpha\ v_{\alpha||}}{\sum_\alpha \dot{m}_\alpha}$$

$$v_{||} = \frac{T}{\dot{m}} = \frac{I_S\ (V_B)^{1/2} \left(\frac{2m}{e}\right)^{1/2} \gamma}{\frac{I_S}{\eta_1 + 2\eta_2}\ \frac{m}{e}}$$

$$v_{||} = \left(\frac{2e}{m}\right)^{1/2} (\eta_1 + 2\eta_2)\ (V_B)^{1/2}\ \gamma$$

$$v_{||} = \left(\frac{2e}{m}\right)^{1/2} \tilde{\eta}_{Hg}\ (V_B)^{1/2}\ \gamma$$

Specific Impulse (Effective)

$$I_{sp} = \frac{v_{||}}{g_o}\ ; \qquad \begin{aligned} m &= 3.3309 \times 10^{-27}\ \text{kg} \\ e &= 1.6022 \times 10^{-19}\ \text{C} \\ g_o &= 9.8067\ \text{ms}^{-1} \end{aligned}$$

$$I_{sp} = \left(\frac{2e}{m}\right)^{1/2} \frac{\tilde{\eta}_{Hg}}{g_o}\ (V_B)^{1/2}\ \gamma$$

5911